OPTIMIZATION OF MISSION DESIGN FOR CONSTRAINED LIBRATION POINT SPACE MISSIONS

A DISSERTATION
SUBMITTED TO THE DEPARTMENT OF
AERONAUTICS AND ASTRONAUTICS
AND THE COMMITTEE ON GRADUATE STUDIES
OF STANFORD UNIVERSITY
IN PARTIAL FULFILLMENT OF THE REQUIREMENTS
FOR THE DEGREE OF
DOCTOR OF PHILOSOPHY

Samantha I. Infeld
December 2005
Revision Date: December 16, 2005

I certify that I have read this dissertation and that, in my opinion, it is fully adequate in scope and quality as a dissertation for the degree of Doctor of Philosophy.

Walter Murray
(Principal Advisor)

I certify that I have read this dissertation and that, in my opinion, it is fully adequate in scope and quality as a dissertation for the degree of Doctor of Philosophy.

Christopher Cassell

I certify that I have read this dissertation and that, in my opinion, it is fully adequate in scope and quality as a dissertation for the degree of Doctor of Philosophy.

Sanjay Lall

I certify that I have read this dissertation and that, in my opinion, it is fully adequate in scope and quality as a dissertation for the degree of Doctor of Philosophy.

Per Enge

Approved for the University Committee on Graduate Studies:

Abstract

Designing space missions to remain in the vicinity of an equilibrium point in a three-body system is both useful and more difficult than for a two-body system. Earth orbits are the most common two-body trajectory (the spacecraft being the second body). In a three-body system we are considering a spacecraft near two large masses rotating around their center of mass.

Because of the rotation of the system, there is not just one point of equilibrium, but rather five points where the gravitational and centripetal accelerations exactly cancel; three where the satellite is collinear with the other masses and two points where the satellite forms in-plane equilateral triangles with the other masses. These points are called libration points (L1-L5), or Lagrange points since it was Lagrange who obtained the first solutions of the three-body problem. This work chooses the Earth-Sun L2 point at which to apply the developed mission design approach because of current proposals for telescope missions at that point, but is equally applicable to any libration point in any three-body system.

The chosen point is behind the Earth from the Sun and is useful for a telescope mission because it is outside Earth's atmosphere and magnetosphere (beyond the moon's orbit), but close enough for fast communications and possibly human maintenance missions. Also the telescope can point away from the light and heat interference of the Sun, Earth, and Moon simultaneously. The collinear points (L1-L3,) although useful locations, are unstable equilibriums[1], which makes trajectories near them quite sensitive to differences in velocity or force perturbations by the full space environment (e.g. solar radiation pressure).

Trajectory and control history design about the unstable Sun-Earth L2 point will become increasingly complex as additional mechanical and scheduling constraints accompany scientific observation missions. Satisfying such constraints in designing a station-keeping plan may be viewed as an optimization problem, with the objective of maximizing the mission goals. It then adds little further complexity to minimize fuel usage as part of the objective, which is always a goal in space mission planning. Solving this design problem is an illustration of the power and ease of this alternative multiple-body mission design approach, which is based on optimization of the whole trajectory and control design. In this thesis, the formulation of such an optimization problem is explained in several steps using increasingly complex dynamical and mission constraint models, and some resulting solutions for these steps are presented and discussed. The continuous time problem is first discretized using a pseudospectral method, and the resulting finite dimensional problem is solved using a sequential quadratic programming algorithm. This approach is implemented by the software package DIDO, which calls the sparse nonlinear optimization software SNOPT. The design approach is discussed as a general mission optimization process, which can easily be used further into the design process and for more types of missions than the examples here, by applying it to a more realistically modeled and more highly constrained libration-point mission design.

Acknowledgments

Acknowledgments go here.

Contents

Tables, Figures, and Algorithms

Tables

Figures

Chapter 1

Introduction

The problem of mission design for a spacecraft at the Sun-Earth L2 point has been studied and accomplished in past missions. Farquhar first explored trajectory design strategies in the regions of libration points, taking into account periodic disturbances, eccentricity correction, gravitational perturbations and solar radiation pressure.[2] In these recent libration point missions, the spacecraft describes a Lissajous path about the libration point, which is usually corrected by engine burns at the crossing of the Earth-Sun line to ensure that the spacecraft will not escape the vicinity in the next few orbits. (A Lissajous path, named after the nineteenth century mathematician, is defined as the path of a point each of whose coordinates is under not necessarily related harmonic motion, so it stays within a certain area over time but does not repeat its path.) Several methods to compute trajectory control strategies have been developed, for example the Target Point Method[3], and the Floquet Mode method[4], which incorporates the idea of invariant manifold tubes from dynamical systems theory. This type of mission design, taking advantage of these tubes associated with libration point orbits, was used on the recent Genesis mission[5]. These methods target a trajectory control strategy based on a good estimate from the theory of an orbit that remains about the libration point only in a simple model, and they may optimize maneuvers individually from this strategy. They do not optimize the design because they do not search the whole acceptable design space. These missions do not require that the spacecraft remain in some specific orbit that exists only with a simple theoretical model, but the recent design methods do not consider acceptable paths other than the reference orbit. This outside space of alternate paths then are very likely to contain a path with a lower associated fuel expenditure, when considering a more accurate modeling of the forces and errors. Thus, the approach presented here will necessarily result in mission designs with lower fuel costs than mission designs based on reference orbits (as well as being a simpler and more direct design approach).

Future missions will carry more complicated and sensitive spacecraft structure and on-board instruments, and consequently will require more constraints on the station-keeping plan. As an example, consider the problem of an astronomical mission during which the cryogenic optics must be pointed away from the Sun, such as the James Webb Telescope or the Terrestrial Planet Finder. Such constraints limit the thrust direction. To keep light away from the instrument side of the spacecraft, there must be a large sun shield, and the spacecraft must be oriented such that the shield is completely protecting the instruments. Any blast of light (visible and IR) from the Sun, Earth, or Moon will destroy the cryogenic instrument, and even infrared radiated from the spacecraft will overwhelm the very faint astronomical signals. This sun shield will produce extra forces and torques due to the solar radiation pressure on the surface area of the shield[6]. The Earth-Sun L2 point provides a location where the sources of heat are all coming from the same general direction, and is far enough from the Earth to avoid major atmospheric and electrical field interference, but close enough to avoid the large antenna power requirements of interplanetary missions.

Proposals of more highly constrained missions necessitates the ability to create mission design plans that not only keep the spacecraft in the libration points vicinity, but also optimize for minimum fuel usage and other mission goals (e.g. least interference with scientific goals). The design approach presented in this thesis introduces an alternative direction in the development of more sophisticated processes for space mission design. The direction is that of concurrent engineering to incorporate optimization from the beginning of the design process, resulting in lower fuel requirements because of elimination of unnecessary assumptions about the orbit or control design (fuel-burning maneuvers to maintain planned orbit). In fact, other design approaches which make these assumptions, and design the trajectory and control design in series are unable to find fuel-optimal designs. Further, a concurrent design approach that does take the entire mission design process as one optimal control problem as is done here, but without taking advantage of sophisticated numerical methods, also leads to unsolvable problems.

The design of a control plan and corresponding trajectory (which together we call the 'mission design') is posed here as a single optimization problem that finds the optimum maneuver schedule to minimize fuel, achieve or maximize mission goals, and meet the mechanical and scheduling constraints. This optimization problem would be recognized from the controls point of view as an optimal control problem, which simply means we are searching for a control vector that when applied to a dynamical system results in optimum behavior as modeled by an objective function[7]. Optimizing the design of a space mission almost always implies minimizing fuel use. This minimizes the percentage of the spacecraft's mass taken by fuel, and maximizes the mass available for operations equipment. In the work presented here, it has been assumed that minimizing fuel use is the primary goal. We do not necessarily propose to control a particular orbit shape in minimum fuel; rather, we propose that the more fundamental problem is to explore the mission-length trajectory design space (e.g. by varying initial estimates as the optimization algorithm's starting point) to find minimum-fuel solutions. Thus it is part of the method to find many locally optimal solutions, rather than looking for the one local optimal solution closest to an estimate of a particular orbit shape. These solutions can then be evaluated for use in specific missions by adding appropriate position, attitude, and timing constraints and using the solutions as starting points for another iteration of the optimization algorithm. This approach, of telling an object what to do, rather than how to do it, has been successfully applied for the design and control of a variety of Earth-orbiting formations[8, 9] and libration-point formations [10]. This thesis looks briefly at formations, but the approach is mostly applied to a single spacecraft system design space with no restrictions on the orbit shape. The first step uses a simple force model. The optimal trajectories found in this space have zero cost (no fuel use needed), and are therefore global optimizers. Then some perturbations and mission constraints are added to the problem formulation. The next step in the development of this method is to iterate these trajectories in a design space with a complex (full) force model, to get an accurate minimum fuel solution for the set of chosen constraints.

This systems engineering approach of concurrently choosing the orbit and satisfying the mission constraints; concurrent design and optimization; results in ease of application. It is easy, and trivial to the solving of the problem, to change mission constraints, spacecraft or force models, or even location of the mission, because these are all simple inputs into a single encompassing optimization problem. This is a flexible approach in that the search space for minimum-fuel trajectories is not confined to be close to a reference orbit. Rather, the algorithm can search any combination of positions, velocities, and thrust at each time step, with the equations of motion in the region as a feasibility requirement rather than a requirement at each step in the algorithm, and the characteristics of the orbit restricted only by this feasibility through the laws of physics and a requirement that the spacecraft not have drifted too far by the end of the mission lifetime. The example mission used here illustrates how the concurrent approach opens the design space to allow total mission optimization, and the ease of altering the details of the problem formulation in order to guide the mission design process. This ease in formulation translates to use of this approach for any type of space mission design.

The mission design problem approached in this way is a single optimal control problem; a dynamic system that is affected by some chosen 'controls' is solved for it's behavior over a time period to find the set of controls that minimize a particular measure of the 'cost' of the behavior [11, 7]. The controls in this case are the accelerations added to spacecraft from burning the engines, where the magnitude and direction over time are the ‘control variables’ that are free to be chosen. The first formulation of any optimal control problem involves equations describing the dynamics of the system, the cost to be minimized, and any constraints which must be met to consider a solution valid. If the variables in these equations are continuous functions (e.g. an object’s position over time), the number of variables being considered in the optimal control problem is infinite, since each continuous variable is actually a variable at all points in time, an infinite set. Optimal control problems can rarely be solved analytically, which implies that we need to use numerical methods. The first step is to discretize the problem, which is to define the system at discrete points rather than with continuous functions. This results in a finite number of variables because the system variables are only defined at the discrete points. The number of variables for the optimal control problem is then the number of variables in the system times the number of discretization points. The consequence of discretizing the optimal control problem explored here is a nonlinearly constrained optimization problem. The unstable dynamics of the L2 vicinity require a more accurate representation of the trajectory to solve the problem than two-body mission design problems. Because the paths are not simple to describe mathematically and similar paths can diverge enormously over the long timescale of these mission, the grid representing the position, velocity (state variables), and added acceleration (control variables) at a finite number of time values in the discretized problem must be very fine or very well-designed to enable a numerical solution.

Methods of optimizing mission design using existing commercial software packages work well enough for libration point mission design optimization if the design is sequential; first finding a reference trajectory that will work and then optimizing the maneuver (controls) history to maintain this given constraints and perturbations. Using the concurrent trajectory control design and open design space described above, the standard methods would result in a discrete problem too large computationally to be of use during a mission, and may not even be solvable.

There is interest in spacecraft formation missions at libration points, which would multiply the computational workload with standard methods, but is greatly reduced in computation time and formulation complexity using the method introduced here (see Chapter 4). In this work, once the concurrent design problem framework is set up, the optimal control problem is solved by a Legendre pseudospectral method[12, 13, 14]. The entire Legendre pseudospectral procedure is automated in a Matlab code called DIDO[15] that is fully integrated with SNOPT[16], a sparse nonlinear programming solver through the Tomlab[17] interface.

1.1 Preliminary Investigation

This trajectory and control design problem is a hard problem because of the unstable dynamics of the region. It is a place of balance of large forces, which means that paths are very sensitive to perturbations. Small addition accelerations do not cause a constant or even slowly growing offset from the original path, they cause a very different new path. This is due to the unstable nature of the equilibrium of forces at the libration point. When the system is modeled with point masses and circular orbits, there exist paths that look like orbits because they are periodic in all axes; some forming a repeating round path around the line connecting the bodies and the libration point. These orbits exist because of the equilibrium nature of the vicinity. With any added complexity to the force model, these paths diverge from periodic and become an orbit about one of the two bodies within an orbit or two. In practice it takes a relatively small added acceleration (thrust from the a spacecraft's engine) to return to a similar path, if it is added at just the right place and direction. To find a path, looking beyond just correcting to these theoretical 'orbits', in which the required additional forces are a minimum (a fuel-optimal path) is even harder because changing the path a small amount to conduct the search may change the fuel required by a large amount, again due to the sensitivity of the problem.

Solar radiation pressure imposes a significant force on a spacecraft with a large surface area, such as a solar shield, and thus will impact the control plan as the force varies with the spacecrafts attitude. The attitude for a scientific observation mission is determined at most times by the object of observation. During maneuvers, the attitude is determined by the direction of thrust required. As described earlier, the direction is limited for these types of missions to keep the instruments from pointing too close to the Sun. The constraint on the attitude then is both very important and an increase in complexity of the problem. As this consideration along with mission requirements on the allowable timing of maneuvers will tend to increase the fuel needed, optimization of fuel use becomes even more important.

The Astrogator and Visualization Option tools, in the Satellite Tool Kit[18], were used for a preliminary investigation of the effect of solar radiation pressure on a spacecraft with large surface area in a traditional halo orbit within a complex model of all forces. Given a non-divergent orbit about L2, with the addition of a changing force along the Sun-Earth-L2 line, showed that the orbit diverges from the vicinity as a result. This confirmed the large influence of the solar radiation pressure on the spacecrafts sensitive trajectory about L2. Experimentation with a much simpler model in Matlab illustrated the useful but non-intuitive influence of the exact magnitude and timing of one impulse on the total Δv needed to keep the trajectory from diverging in the next orbit[19].

This preliminary work confirmed that the mechanics of the spacecraft and the constraints of the mission easily cause stationkeeping complications. It also showed that decreasing the fuel usage was possible with the burn schedule as control variables, while still satisfying constraints. This justified the further work of posing the mission planning as an optimization problem.

The next preliminary work was to find a method of discretizing the continuous optimization problem to form the matrices describing the cost and constraint functions at discrete points that are input into the optimization routine. The discretization method must capture the complex dynamics of the problem well enough with as few total variables as possible. With a simple, equal-length timestep discretization, the optimization problem could not be solved. The discrete problem was too inaccurate for all the constraints describing the motion to hold, and the optimization routine could not find a feasible point.

Another commonly used discretization method, direct collocation, implemented with the use of commercial software, worked with this optimization problem in situations too limited for this design approach. Optimal trajectories and control plans were found when the number of timesteps was below fifty, which limited the mission length to about one year, and when the input (guess) trajectory was very close to an optimal trajectory. This requires too much preparation work before the design optimization begins, while also limiting the design space to designs already known, as the optimal trajectories necessarily stay close to the input near-optimal trajectories.

The pseudospectral discretization method was chosen because it required a relatively smaller discretized problem in order to capture enough of the complex dynamics. It was found to provide a discrete formulation for which the optimization routine could find solutions, given correct scaling of the problem, for any type of input trajectory and control plan, not just those close to a known optimal trajectory. This method then is used for all the results presented in Chapter 4 and 5. All the discretization methods explored, and the optimization method, are described in Chapter 3.

1.2 Thesis Outline

The problem formulation is described at the end of Chapter 2, first in general and then its specific form when applied to a libration point space mission. This follows the Chapter 2 discussion of libration point missions including the framework for mission design and past approaches to designing these missions.

The methods used to solve the mission design optimization problem once it is formulated are presented in Chapter 3. The choice of a direct method to solve the optimal control problem is discussed. As direct methods first discretize the problem and then apply an optimization algorithm, the choice of these methods are discussed, and those implemented are further described.

The results of applying this approach to an example libration point mission are presented in Chapter 4. A brief comparison to the reference orbit approach follows five examples of specific problem formulations and solutions. The examples are repeated two more times after proving the expected results in the case of a simple gravitational model with no mission constraints, to show the effect of adding perturbations to the model and mission constraints to the problem formulation.

The ability to apply this to a second libration mission example is explored in Chapter 5. Here the problem of libration point spacecraft formation is solved using this mission design optimization approach for a few different sets of mission requirements.

Conclusions and possibilities expanding this approach to mission design in the future are found in Chapter 6.

Chapter 2

Libration Point Missions

This chapter first introduces the dynamical space in which libration point space missions are designed. Then past work on libration mission design is described, together with a summary of the methods used to compute the trajectories. This includes how optimization has been used during the design process for libration point missions. Prior to the work here, optimization had not been used for overall design. A review of traditional methods of incorporating optimization into space mission design in general is presented.

Space missions are designed in a multi-body space for several reasons. Traditionally, interplanetary trajectories were designed as patched conic paths. This means the trajectory is divided into several arcs during which only two bodies at a time are considered. This method is a very good approximation for most type of interplanetary missions, and can be used until the very final stages of planning. However, more time or fuel efficient trajectory options can be produced by considering all the bodies simultaneously, and these savings can make a difference for a spacecraft using low-thrust engines or visiting several moons of a planet. The rotation of bodies in the solar system produces dynamics that are observed in the multi-body space and can be taken advantage of to find very efficient paths for transferring between bodies or for stationing at a place near but not orbiting a body. These efficient paths can be seen as moving through or remaining near libration points. Libration points are where the gravitational forces of two massive bodies are exactly balanced with the centripetal force needed to rotate with them about the collective center of mass of the system, such that a third body of negligible mass could remain at that point in the rotating system. (Note: these equilibrium points are only static given the assumption of circular orbits of the masses.) Libration point missions are those that take advantage of the local dynamics to spend some or all of their mission in the vicinity of such a point. The advantage to this location for a spacecraft is to be close to a planet without having to orbit it. This can be used for a research, construction, or communication station for example at an Earth-Moon libration point because it is an easy transfer to orbit either body. A data-relay satellite at Earth-Moon L2 was proposed in 1966 and considered for Apollo 17. It can also be useful for scientific observation missions. Libration points are far enough away from the bodies to which they belong to have full perspective of their surface, and be outside atmospheric and magnetic influence on the instruments. This lack of interference also results in clearer astronomical observations. The most popular type of libration point mission currently being planned is astronomical observation at the Sun-Earth libration point that remains on the dark side of the Earth. This location makes it easy to block the radiation from the Earth, Moon, and Sun at once, while staying in relatively easy communication range and is close enough to allow maintenance.

Preliminary design work for a libration point mission is done in the context of the circular restricted three-body problem, as that is the framework in which the libration points are stationary. This problem is described below, and illustrated for the Sun-Earth-spacecraft case.

2.1 The Three Body Problem

The circular restricted three-body problem (CR3BP) is defined as a system of two bodies in circular orbits about their barycenter, and a third body of negligible mass. The equations of motion are solved for the third body. The stationary solutions of this problem are the five libration points. The equations are most simply and therefore most often expressed in the rotating barycentric frame (as they will be here). In this frame, the barycenter of the two masses is the origin. The x axis is the line through the center of the two large bodies. The frame rotates about the z axis with the angular velocity ω of the two large bodies about each other. This angular velocity is then 2π radians divided by the period of the two mass system. The two bodies here are the Sun and the Earth, so the period is one year.

The equations of motion for this problem are derived in many places, for example Battin's astrodynamics textbook [1], but is derived here for completeness and to establish terminology. With the goal of expressing the acceleration of the third body, we start by taking the second derivative with respect to time (in the inertial frame) of the position vector of the third body, $\vec{r}$.

$$\ddot{\vec{r}}_{/I} = \ddot{\vec{r}} \, + \, \dot{\vec{\omega}} \times r \, + \, \vec{\omega} \times (\vec{\omega} \times \vec{r}) \, + \, 2\vec{\omega} \times \dot{\vec{r}} \, + \, \ddot{\vec{r}}_B.$$

The vector $\vec{r}_B$ is the position vector with respect to the body frame, whose origin is at the center of the third body in the three-body system. Since the point whose motion we wish to know is the center of the third body, the position vector has zero

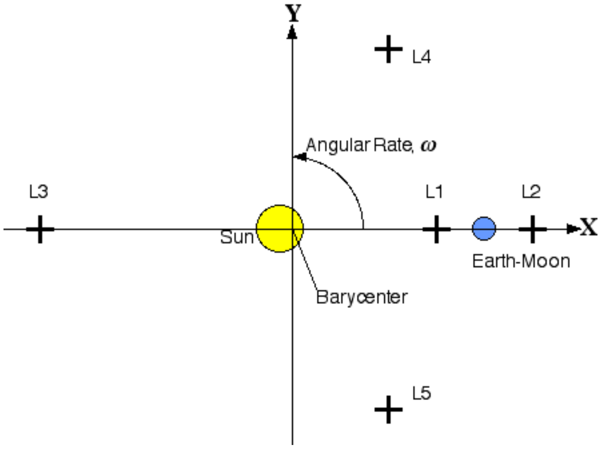

FIGURE 2.1 *Coordinate system for the restricted three-body problem*

length since it points from the origin of the body frame to the point in question (i.e. the same point). In evaluating this equation, we note then that $\ddot{\vec{r}}_B = 0$. We also have $\dot{\vec{\omega}} = 0$ because of the circular orbit assumption. It is important to be clear that the derivatives of $\vec{r}$ are with respect to the rotating barycentric frame since $\vec{r}$ is defined in that frame. Eventually, we want an expression for the acceleration of the position vector with respect to the rotating barycentric frame, so that we can describe the third body's motion in this frame. Since the angular velocity is about the z axis, the cross products with ω have simple expressions as seen in the following simplification of the above equation.

$$\ddot{\vec{r}}_{/I} = \ddot{\vec{r}} \; - \; \omega^2(x\hat{\imath} + y\hat{\jmath}) \; + \; 2\omega(\dot{y}\hat{\imath} - \dot{x}\hat{\jmath}). \tag{2.1}$$

We know the acceleration of the position vector in the inertial frame, $\ddot{\vec{r}}_{/I}$, because it is the acceleration on any point in the system due to the gravity of the two large bodies. The force potential at a certain point due to the gravity of body 1 is μ_1/r_{1p} in the direction of body 1, where $\mu_1 = Gm_1$, and r_1p is the distance between body 1 and the point p; G is the universal gravitation constant, and m_1 is the mass of body 1. We can express $\ddot{\vec{r}}_{/I}$ as the gradient of the total gravitational force potential. First define $\vec{r_{13}}$ as the vector from body 1 to body 3 (the third body whose motion we are deriving), with the plain r_{13} as the distance between the bodies. The same holds for body 2. Now we can write

$$\ddot{\vec{r}}_{/I} = \nabla(-\frac{\mu_1}{r_{13}}\vec{r_{13}} - \frac{\mu_2}{r_{23}}\vec{r_{23}}). \tag{2.2}$$

Combining (2.1) and (2.2) gives

$$\ddot{\vec{r}} \; - \; \omega^2(x\hat{i}+y\hat{j}) \; + \; 2\omega(\dot{y}\hat{i}-\dot{x}\hat{j}) = \nabla(-\frac{\mu_1}{r_{13}}\vec{r_{13}} - \frac{\mu_2}{r_{23}}\vec{r_{23}}).$$

Separating this equation into the components x,y,z, in the rotating frame gives

$$\begin{aligned}
\ddot{x} - \omega^2 x - 2\omega\dot{y} &= \frac{\partial}{\partial x}(-\frac{\mu_1}{r_{13}}\vec{r_{13}} - \frac{\mu_2}{r_{23}}\vec{r_{23}}) \\
\ddot{y} - \omega^2 y + 2\omega\dot{x} &= \frac{\partial}{\partial y}(-\frac{\mu_1}{r_{13}}\vec{r_{13}} - \frac{\mu_2}{r_{23}}\vec{r_{23}}) \\
\ddot{z} &= \frac{\partial}{\partial z}(-\frac{\mu_1}{r_{13}}\vec{r_{13}} - \frac{\mu_2}{r_{23}}\vec{r_{23}}).
\end{aligned}$$

Since $r_{13} = \sqrt{(x-r_1)^2+y^2+z^2}$ and $r_{23} = \sqrt{(x+r_2)^2+y^2+z^2}$, where r_j is the distance from the origin (barycenter) to body j, evaluating the differentiation on the right hand sides gives the equations of motion,

$$\begin{aligned}
\ddot{x} - \omega^2 x - 2\omega\dot{y} &= -\frac{\mu_1(x-r_1)}{r_{13}^3} - \frac{\mu_2(x+r_2)}{r_{23}^3} && (2.3) \\
\ddot{y} - \omega^2 y + 2\omega\dot{x} &= -\frac{\mu_1 y}{r_{13}^3} - \frac{\mu_2 y}{r_{23}^3} && (2.4) \\
\ddot{z} &= -\frac{\mu_1 z}{r_{13}^3} - \frac{\mu_2 z}{r_{23}^3}. && (2.5)
\end{aligned}$$

The non-dimensional units chosen here are TU for time units, DU for distance units, and MU for mass units, $\omega = 1$ radian/TU, $m_1 + m_2 = 1$ MU , and $r_{12} = 1$ DU. Defining unsubscripted μ as the mass ratio, equal to $\frac{m_2}{m_1+m_2}$ in any units (2 is always the smaller mass), then in nondimensional units body 1 is also μ DU from the origin and body 2 is $1-\mu$ DU from the origin.

In nondimensional units, r_{13} and r_{23} are

$$r_{13} = \sqrt{(x-\mu)^2+y^2+z^2} \text{ and } r_{23} = \sqrt{(x+1-\mu)^2+y^2+z^2}.$$

Evaluating the partial differentials in (2.3-2.5) using the above definitions gives the nondimensional equations of motion,

$$
\begin{aligned}
\ddot{x} - 2\dot{y} - x &= -\frac{(1-\mu)(x-\mu)}{r_{13}^3} - \frac{\mu(x+1-\mu)}{r_{23}^3} \\
\ddot{y} + 2\dot{x} - y &= -\frac{(1-\mu)y}{r_{13}^3} - \frac{\mu y}{r_{23}^3} \\
\ddot{z} &= -\frac{(1-\mu)z}{r_{13}^3} - \frac{\mu z}{r_{23}^3}.
\end{aligned}
$$

When using the equations of motion to design a spacecraft trajectory, we must include the force of the engine burning fuel. We may also include other forces that perturb the simplified three-body system, such as solar radiation pressure and the moon's gravity (without rewriting the equations in terms of a 4-body problem). All of these outside forces are incorporated in the variable F to finally express the acceleration of the spacecraft (third body) in each direction as follows:

$$
\begin{aligned}
\ddot{x} &= 2\dot{y} + x - \frac{(1-\mu)(x-\mu)}{r_{13}^3} - \frac{\mu(x+1-\mu)}{r_{23}^3} + F_x/m && (2.6) \\
\ddot{y} &= -2\dot{x} + y - \frac{(1-\mu)y}{r_{13}^3} - \frac{\mu y}{r_{23}^3} + F_y/m && (2.7) \\
\ddot{z} &= -\frac{(1-\mu)z}{r_{13}^3} - \frac{\mu z}{r_{23}^3} + F_z/m, && (2.8)
\end{aligned}
$$

where F_i is the component of the sum of the outside forces along the ith axis, and m is the current mass of the spacecraft.

2.2 Past Mission Trajectory Design and Control

The equations of motion described above are solved for a control plan (component of F applied with the engine as a function on time), and the resulting trajectory (x, y, z position as functions of time), within defined mission constraints. This is the solution to the mission design problem. The work presented here is an approach to solving the mission design problem that takes into account the difficulty of solving the problem in the unstable dynamics of a multi-body system, and the desired complexity of mission constraints for future space missions. Therefore, this approach is elaborated and applied in the context of a constrained libration point space mission, using a particular mission currently in the planning stages as a reference for spacecraft model and constraints. Following is an overview of past libration point mission planning work, with more attention paid to the mission used as a reference. These spacecraft were all put in Lissajous paths

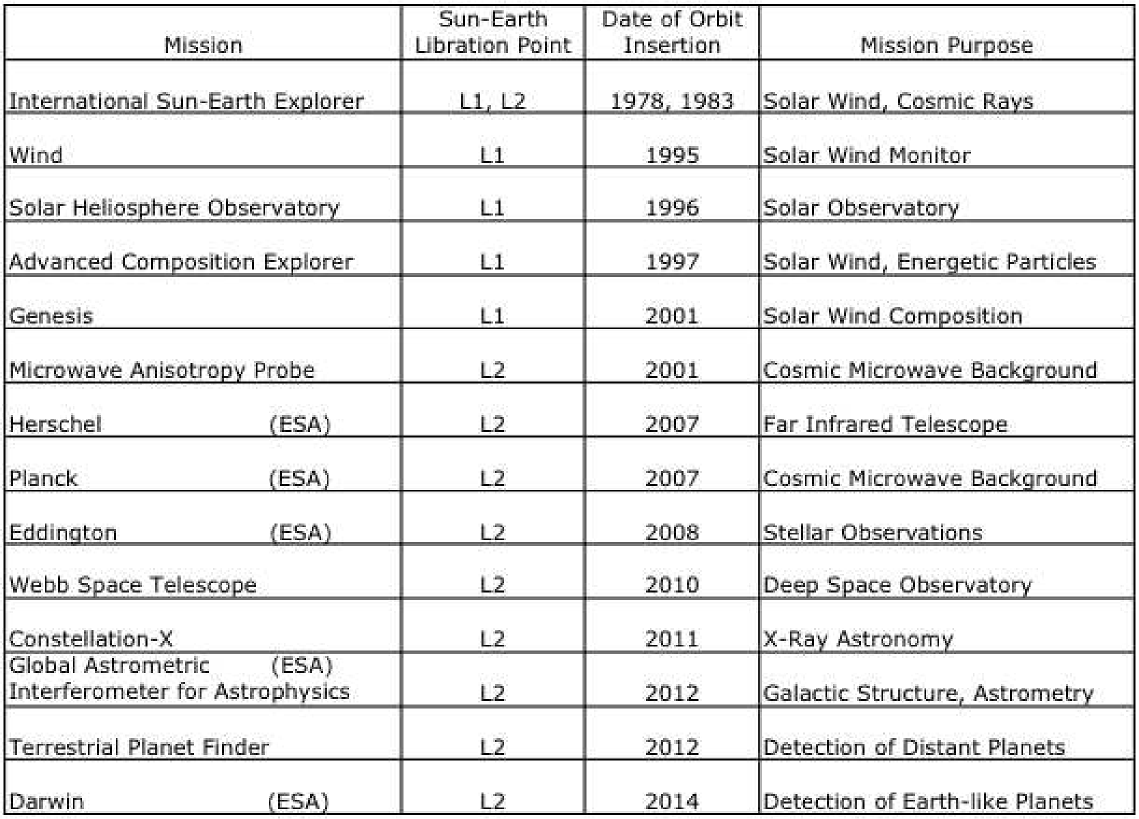

Mission	Sun-Earth Libration Point	Date of Orbit Insertion	Mission Purpose
International Sun-Earth Explorer	L1, L2	1978, 1983	Solar Wind, Cosmic Rays
Wind	L1	1995	Solar Wind Monitor
Solar Heliosphere Observatory	L1	1996	Solar Observatory
Advanced Composition Explorer	L1	1997	Solar Wind, Energetic Particles
Genesis	L1	2001	Solar Wind Composition
Microwave Anisotropy Probe	L2	2001	Cosmic Microwave Background
Herschel (ESA)	L2	2007	Far Infrared Telescope
Planck (ESA)	L2	2007	Cosmic Microwave Background
Eddington (ESA)	L2	2008	Stellar Observations
Webb Space Telescope	L2	2010	Deep Space Observatory
Constellation-X	L2	2011	X-Ray Astronomy
Global Astrometric (ESA) Interferometer for Astrophysics	L2	2012	Galactic Structure, Astrometry
Terrestrial Planet Finder	L2	2012	Detection of Distant Planets
Darwin (ESA)	L2	2014	Detection of Earth-like Planets

FIGURE 2.2 *Past and Planned Libration Point Missions*

(coordinates under harmonic motion) with matching periods in the x and y coordinates (sometimes called 'quasi-periodic' as they fill a torus). Some had preliminary designs as 'halo' orbits, which are Lissajous paths for which the x and y period align with the z period to form a perfectly periodic orbit. Halo orbits are solutions to the CR3BP (and do not exist without velocity corrections in more complex models), which can only be found with large enough amplitudes in the x and y coordinates and correct choice of z amplitude such that the resulting period matches the x and y periods. The amplitudes and periods resulting in a halo orbit in the CR3BP cannot be found analytically, but must be computed numerically.[20]

Several space missions have been accomplished at the Sun-Earth L1 point to study the Sun (Earth study at this point has been designed but not yet completed). There is currently one mission at the Sun-Earth L2 point, and most current proposals also choose this point. The International Sun-Earth Explorer (ISEE-3) and Solar Heliosphere Observatory (SOHO) were launched into large halo orbits about L1 in 1978 and 1996 respectively. ISEE-3 went into orbit around L2 in 1983 to study cosmic rays. The actual cost of maintaining the orbit were reduced from 7.5 meters/second per year for

ISEE-3 to 2.3 meters/second per year for SOHO [21]. This is because ISEE-3 was controlled to exactly maintain the halo orbit using thrust along all axes, while SOHO used thrust only in the x direction as it crossed the x-z plane about every 90 days, resulting in a Lissajous trajectory that approximated the nominal halo orbit. It was found that not having a precise halo orbit did not affect common types of mission design requirements motivated by the scientific mission goals. The solar wind observer WIND was stationed both at L1 in a Lissajous orbit starting in 1995. The Advanced Composition Explorer (ACE) was put into a small Lissajous orbit about L1 in 1997, and the Microwave Anisotropy Probe (MAP) was placed into a small Lissajous about L2 in 2001. Map performs station-keeping maneuvers about every 3 months. Genesis, a solar sample return mission, went into a large Lissajous orbit about L1 in 2001. The James Webb Space Telescope (JWST) will be put into a large Lissajous orbit about L2. All of these trajectories were designed with a process of a preliminary reference orbit based on the circular restricted three-body problem, and then used various means to use this as a guess for a more complex numerical calculation of the trajectory and the required control scheme to add velocity with engine maneuvers to maintain the reference trajectory calculated with the simple model. Other steps at this point were designing the transfer trajectory from Earth to the long-term halo or Lissajous orbit, and calculating the extra velocity needed for ‘station-keeping’, i.e. correcting for errors in position measurement or true maneuver application to keep the spacecraft along the reference orbit. Here we look only at the design of the trajectory and control scheme step.

For Genesis, the mission planning was in three stages. First a Lissajous trajectory with a center at the libration point was found that remains bounded over the mission lifetime in a model that includes ephemeris data for the Sun, Earth and Moon. This is computed using the Richardson and Cary [24] expansion as an initial guess, and then applying a differential correction algorithm that causes the velocity at the next x-z plane crossing to have zero magnitude in along the x axis [25]. The initial guess chosen to be computed is an application of dynamical systems theory. A path along an invariant manifold is chosen since this is known to remain in the libration point vicinity permanently in the CR3BP, and will remain bounded for a few years in a model including ephemeris information. Next, multi-conic techniques improved the estimated trajectory by propagating about a single body, and switching that body between the Earth and the Sun, with the inclusion of the effects of other gravitational forces and solar radiation pressure. This step allows mission constraints to be included while preserving the characteristics of the initial estimate. Differential correction is used on the position and velocity to force continuity. Finally numerical integration created a full trajectory,

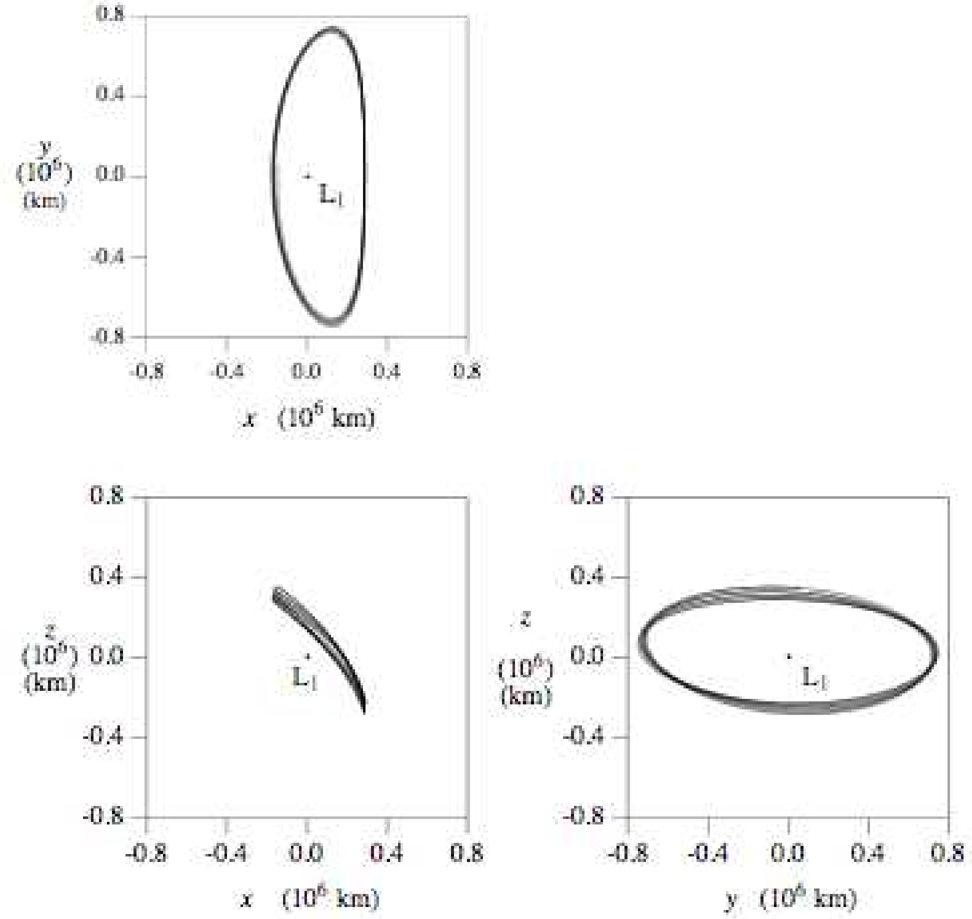

FIGURE 2.3 *Lissajous reference orbit for Genesis mission[22]*

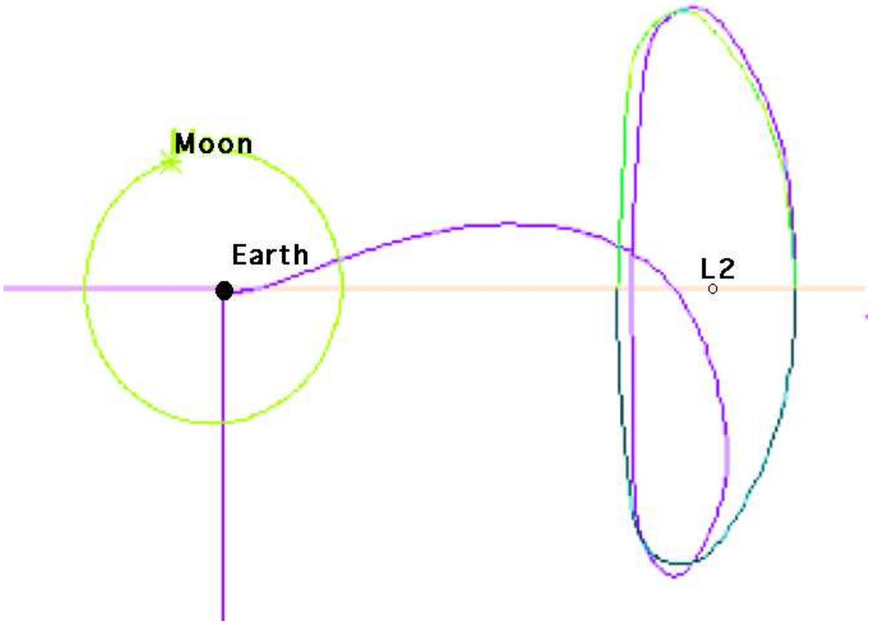

FIGURE 2.4 *Halo orbit from early JWST planning.[23] Note size in comparison to Moon's orbit around Earth.*

turning patched velocity discontinuities in the full force model into finite maneuvers [22]. The maneuvers were calculated using a targeting process to ensure that the nominal orbit would be matched until the next maneuver, within an estimate of measurement and maneuver execution errors, and position error due to the effects of solar radiation pressure. This calculated and targeted Lissajous orbit is most likely very close to the minimum fuel trajectory during mission operations because it requires no maneuvers during its lifetime in the theoretical realm without errors, and the effects due to the solar radiation pressure are small. The error-correcting maneuvers will stay as small as possible because they are not restricted in time or direction, so they are executed at the most efficient point in the most efficient direction for this type of orbit.

For a spacecraft with a large surface area, the solar radiation pressure will affect the path significantly. Combine this with mission goals that restrict the maneuvers to as infrequently as possible, and in a constrained direction, and it is quite likely that the methods used for mission design on Genesis are not close to the minimum fuel trajectory. The JWST mission is a good example of a large-surface area spacecraft for a mission with more constrained maneuvers (as are most of the libration point telescope missions being planned). It is was originally planned for a 2010 launch (as see in Fig. 2.2), but is currently in development for a mission starting no earlier than 2013. While these more complex requirements have been taken into account, the mission design is still based on a nominal halo orbit. There is no optimization done on the total mission design, or even on the control design (maneuvers plan). Mission design work at NASA Goddard has gone as follows (based on the version completed in 2004). Preliminary analysis on the station-keeping plan to maintain a periodic or quasi-periodic orbit while including a number of perturbation produced a maneuver framework. A nominal perturbation-free mission was created in Satellite Tool Kit Astrogator[18]. Then perturbations including orbit determination knowledge error, thruster performance error, predicted attitude due to solar radiation pressure error, error due to unknown added velocity from momentum unloads, and error in venting were added to the modeling. The reference orbit was chosen out of invariant manifolds that met selected size requirements to have minimum insertion cost into that orbit. Then Astrogator was used to target the trajectory (direct shooting method) within a complex model until it fit requirements. This perturbation analysis led to the conclusion that maneuvers should be performed as often as possible to prevent large magnitudes of thrust being needed to correct error. The ability to do accurate orbit determination is limited by a requirement of 21 days after a manuever to plan the next maneuver, so the recommended maneuver timing for JWST is every 22 days. The maneuvers were generally more expensive along the y axis than the x axis. (It is typical to plan only x-axis maneuvers rather than finding the optimum direction.) For this current planning, the optimum direction is calculated and planned for each maneuver separately. If it violated the constraint limiting the thrust direction to keep the telescope from pointing sunward, the nearest acceptable direction is used for that maneuver.[26]

2.3 Optimization in Mission Design

In the design of the libration point missions above, optimization was employed to find the best launch window to minimize the transfer trajectory from Earth, often including lunar swingbys, into the selected reference orbit at the libration point. Targeting, but not optimization, was used in increasingly sophisticated ways over time in order to design the control strategy to maintain the selected reference orbit about the libration point. Astrogator's numerical targeting is the current choice for preliminary control design. The Genesis mission and libration mission design work afterward at JPL uses their software LTool, which includes algorithms to compute Lissajous trajectories in a model that included ephemerides for selected bodies and uses a differential corrector to target estimated trajectories to a continuous orbit in the full model [27].

Looking at mission design outside of libration point missions, we see a similar use (or lack of use)of optimization. Optimal transfer trajectories (usually maximizing final mass) are computed with simple models as a start to the whole mission design process (such as a path from leaving Earth orbit to intersecting Mars orbit), but orbits that remain in some vicinity or around a body are just chosen according to some stable known orbit. More recent missions have used Dynamical Systems Theory to estimate trajectories that are more complicated than an orbit about a single body[20]. The maneuvers to control these orbits are designed by targeting techniques. For example, the Jupiter Icy Moons Orbitor (JIMO) mission proposal was designed (in 2003) using JPL's Mystic software [28]. The Static/Dynamic Control algorithm was used to optimize the trajectory in parts. The approach in this software could handle multi-body equations of motion and the varying physical scales, but not the complexity of the trajectory as a whole. This more recent approach, however, finds much lower-cost solutions than by calculating the optimum arc in a patched two-body approach that were used in past interplanetary missions.

2.4 Mission Design Optimal Control Problem

This section lays out the formulation of the total mission design continuous optimization problem in general form and then in more detail. The choices of the cost function, control variables, and constraint structure are explained for the different formulations described. The basic formulation describes the equations used in all the example cases whose results are shown in Chapter 4 and 5. The complex formulations describe the additional equations and terms that are included in different combinations to each example to create their unique detailed problem formulation.

The results chapter is divided into sections of examples all using the same mission models. The force model is defined by the equations of motion (seen as just more constraints by the optimization algorithm). The equations of motion in the Basic Formulation below describe the three-body forces under the circular restricted assumptions. The mission model that includes only these forces in the equations of motion and has no constraints on the attitude will be called the **Simple Model**. The mission model that includes terms in the equations of motion to model the force perturbations of the solar radiation pressure (SRP) and the lunar gravity, but also has no attitude constraints, will be called the **Perturbed Model**. The final mission model adds the mission-level constraint that will be required for telescope missions of bounding the angle of the attitude with respect to the sun. This is accomplished, as stated earlier, through constraints applied to the control variables rather than by introducing a new attitude variable to the state vector. This mission model will be called the **Perturbed Mission Con-**

strained Model. The Complex Formulations part of this section will outline which different additions are added to which examples in each of these mission model sections in Chapter 4, and then present the additional terms or equations.

TABLE 2.1
Mission Models (Sections of Results, Ch.4)

Simple Model	CR3BP
Perturbed Model	CR3BP + SRP/lunar perturbations
Perturbed Mission Constrained Model	CR3BP + perturbations + attitude constraint

2.4.1 Basic Formulation

The simply constrained set of problems presented here have the following general form: find the state and control variables at each time step over a given time period, such that a function of the control variables is minimized. The state variables are the position and velocity along the axes, and the mass of the spacecraft, which can be seen as a seven-dimensional state vector. To keep the formulations simpler, the attitude is never used as an independent variable, but is constrained in terms of the control variables in the final set of examples. The control variables are the thrust along the axes, which can be seen as a three-dimensional control vector. Minimizing the function of the control variables then corresponds to minimizing the use of fuel, which allows the launched mass to be minimized as well as opening the possibility for minimizing the time used for stationkeeping maneuvers that can inhibit payload use. The objective function for all examples shown here is the L1 norm of the control vector integrated over the set time period. This optimization is constrained by the equations of motion (see above), which govern the relationship of the position and velocity. We also impose a bound on the distance from the final position to the libration point, and the constraint of the rocket equation, which governs the relationship between the mass and thrust:

$$\frac{\partial m}{\partial t} = \frac{-T}{Isp * g},$$

where m = mass, t = time, T = total magnitude of thrust, Isp = specific impulse of the engine, and g = gravitational constant.

The final position distance bound (which necessarily occurs at the final timestep) ensures the whole trajectory is bounded to meet the stationkeeping goal of remaining in the vicinity of L2. There are a few more bounds applied to these problems to achieve realistic solutions. In every example formulation solved here, the following bounds are applied: the thrust magnitude has a maximum, the x position is restricted away from the Earth at each timestep, and the mass has a non-zero minimum to restrict the solution from a spacecraft consisting entirely of fuel.

The mathematical form of the basic continuous problem is the following optimal control problem: Determine the state-control function pair, $\mathbf{s}(t), \mathbf{u}(t)$ over $[t_0, t_f]$ that minimize the cost functional,

$$J[\mathbf{s}, \mathbf{u}] = \int_{t_0}^{t_f} F(\mathbf{s}(t), \mathbf{u}(t))dt, \tag{2.9}$$

subject to

$$\begin{aligned} &\textit{equations of motion} && f(\mathbf{s}(t), \mathbf{u}(t)) - \dot{s}(t) = 0 && (2.10)\\ &\textit{boundary constraints} && b(\mathbf{s}(t_0), \mathbf{s}(t_f)) = 0 && (2.11)\\ &\textit{path constraints} && h(\mathbf{s}(t), \mathbf{u}(t)) \leq 0. && (2.12) \end{aligned}$$

In the calculus of variations method of solving continuous optimal control problems, the cost functional takes a second form in terms of the adjoint variables. The Hamiltonian function is defined for ease of framing and solving the problem as a two point boundary problem[11]. It takes the following form:

$$H(t) = F(\mathbf{s}(t), \mathbf{u}(t)) + \lambda^T(t) f(\mathbf{s}(t), \mathbf{u}(t)), \tag{2.13}$$

where $\lambda(t)$ are the adjoint variables. Because the cost and dynamics equations do not depend explicitly on time, the derivative of the Hamiltonian with respect to time is

$$\dot{H} = \frac{\partial F}{\partial t} + \lambda^T \frac{\partial f}{\partial t} + \frac{\partial H}{\partial t}\dot{u} = \frac{\partial H}{\partial t}\dot{u}.$$

At an optimal solution, the cost functional is at a minimum, so $\mathbf{u}$ is stationary, and $\frac{\partial H}{\partial t} = 0$. This means that at a solution $\dot{H} = 0$. *The Hamiltonian function is zero at the optimal state-control function pair.* This fact will be used later to check the optimality of the results.

To frame the current optimal space mission design problem more specifically, the general optimal control problem (Equations 2.9-2.12) can be expanded to the following statement. Find the state vector $\mathbf{s}(t)$ with elements

$$\mathbf{s} = (x(t),\ y(t),\ z(t),\ v_x(t),\ v_y(t),\ v_z(t),\ m(t)),$$

and $\mathbf{u}(t)$, the control vector with elements

$$\mathbf{u} = (u_x,\, u_y,\, u_z),$$

which minimize the cost

$$J = \int_{t_0}^{t_f} \|\mathbf{u}(t)\|_1 \, dt.$$

This is subject to the equations of motion (with μ as the ratio of the Earth-moon systems mass (1) to the Suns mass (2)),

$$\begin{aligned}
\dot{x}(t) - v_x(t) &= 0 \\
\dot{y}(t) - v_y(t) &= 0 \\
\dot{z}(t) - v_z(t) &= 0 \\
\dot{v}_x(t) - 2v_y(t) - x(t) + \frac{(1-\mu)(x(t)-\mu)}{r_{13}(t)^3} + \frac{\mu(x(t)+1-\mu)}{r_{23}(t)^3} - \frac{u_x(t)}{m(t)} &= 0 \\
\dot{v}_y(t) + 2v_x(t) - y(t) + \frac{(1-\mu)y(t)}{r_{13}(t)^3} + \frac{\mu y(t)}{r_{23}(t)^3} - \frac{u_y(t)}{m(t)} &= 0 \\
\dot{v}_z(t) + \frac{(1-\mu)z(t)}{r_{13}(t)^3} + \frac{\mu z(t)}{r_{23}(t)^3} - \frac{u_z(t)}{m(t)} &= 0 \\
\dot{m}(t) + \frac{\|\mathbf{u(t)}\|_1}{Isp * g} &= 0,
\end{aligned}$$

for all $t : [t_0, t_f]$,(see section 2.1 for definition of r_{ik}). The minimization is further subject to the boundary condition,

$$(x(t_f) - (1 - \mu - r_{2-L2}))^2 + y(t_f)^2 + z(t_f)^2 \leq (\alpha L)^2,$$

where $0 \leq \alpha \leq 1$ and L is the distance between the Earth/Moon and L2; and the path constraints,

$$\begin{aligned}
x(t) \geq 1 - \mu + \text{margin, (1 - } \mu \text{ is position of Earth)} \\
-T_{max} \leq \mathbf{u}(t) \leq T_{max} \\
0.01 \leq m(t) \leq 1,
\end{aligned}$$

where T_{max} is the chosen maximum thrust acceleration.

The equations of motion are expressed in seven equations, with each one describing the change in one of the state variables. The state vector includes the velocity of each position variable in order for the equations of motions to be only first order differential equations. Compare the acceleration equations, $\dot{v}_i$..., to the equations derived in Chapter

2, (Equations 2.6-2.8) (note: $\dot{v_x} = \ddot{x}$). The boundary condition constrains the final distance from L2 to within some fraction of the distance to the Earth-Moon system. The mass is normalized to be equal to one at the start of the trajectory, which is $t = 0$ for these optimization problems. Practically, this point may be after a maneuver to insert it into the libration area trajectory from a launch or transfer trajectory. The mass is constrained to a minimum of 10% of the mass at start time, because this is reserved for the mass of the spacecraft itself, as opposed to expendable fuel. This is a conservative estimate for a spacecraft of the size modeled in examples here. The original design for the James Webb Telescope has a fuel to total mass ratio of six percent. For comparison, Genesis, in a three-year unconstrained orbit and ten times lighter, had a starting mass fuel that was 22 percent of its total mass. This constraint is not an issue for the few year simulation time of the problems solved here, but will become an important constraint for simulation times nearing ten years, and when using full force modeling and more complex constraints on the timing of the maneuvers.

The cost function used here is L^1 norm of the control, rather than the L^2 norm squared, which is often used as the familiar quadratic cost function, because L^1 measures fuel use whereas L^2 does not [29]. (Note: the L^p norm of $\mathbf{u}$ can be defined based on the l^2 norm as $||u||_{L^p} = (\int (\sqrt{u_x^2(t) + u_y^2(t) + u_z^2(t)})^p dt)^{1/p}$, or based on the l^1 norm as $||u||_{L^p} = (\int (|u_x(t)| + |u_y(t)| + |u_z(t)|)^p dt)^{1/p}$.) Using the l^2 based L^1 norm involves a square-root calculation, which causes difficulty because of the singularity when $\mathbf{u} = 0$. The l^1 based L^1 norm also looks difficult because its derivative is discontinuous at zero, but this was resolved (as explained below). The choice for the cost function formulation here then is the l^1 based L^1 norm, so that the optimization problem is seeking to minimize the sum of the thrust magnitudes in each direction. The control variables represent the way in which the spacecraft can control its trajectory by adding velocity in a certain direction to its motion. Velocity is added by burning the engine. This causes a thrust in the direction opposite to that in which the engine is pointed. The control vector then represents the thrust, with the components of the vector splitting the thrust magnitude along the axes of the rotating coordinate frame presented earlier. The actual control vector used in formulations here has six components, a positive and negative measure of the thrust along each of the axes (x, y, z). This was chosen to make the problem a reasonable one to solve with the optimization algorithm. The components are then all positive, with lower bound zero and upper bound T_{max}. The most important consequence of this form is the resolution of the l^1 difficulty: it makes the control variables' derivatives continuous. The lack of continuity would have considerably complicated solving the optimization problem. Because the magnitudes of these variables are to be minimized, and in further steps in the mission design process they will be forced to be zero except during planned maneuver times, we know that these variables over the mission lifetime will mostly be zero. Also, only the negative or positive part of the control in one direction can be non-zero at each point in time, in order to express a negative or positive component in that direction to the total thrust. This means that the control variables will be on their lower bound (zero) at most times, reducing the number of degrees of freedom in the problem, which makes the optimization problem easier to solve (despite the doubling of the number of control variables).

2.4.2 Complex Formulations

The above formulation is included in every example whose solutions are shown in Chapter 4 and 5. Increasing the complexity of the force models requires adding terms to the equations of motion constraint equation. Increasing complexity with mission constraints requires adding new constraint inequalities. This section presents the formulations of these additions. First the additions to the path and boundary constraint equations, and then the additions to the equations of motion for the first mission example (single spacecraft) are discussed, followed by a presentation of the additions to the basic formulation seen in the second mission example (two spacecraft in formation).

The basic formulation is the entirety of every example in the Simple Model section, except the first. The first includes a bound on the initial state (a boundary constraint) in order to produce a more common type of orbit. The Perturbed Model section examples all have bounds on the initial state (except the first because it has a much shorter simulation time). The full constraint formulation for the examples with these initial state bounds are under **Initial Position Bounded** below. In addition, some examples have path constraints bounding the position variables. The full constraint formulation for these examples are under **Initial Position and All Positions Bounded** below. The Perturbed Mission Constrained Model section further includes the restriction of the spacecraft's attitude, defined as a path constraint restricting the thrust direction; a function of the control variables. This addition to either of the complex formulations already named is seen under **Attitude Bounded** below. See the the introduction to the Perturbed Mission Constrained Model results (4.2.1) for a derivation of the attitude constraint equation. The three versions then of the constraint formulations beyond the basic constraint formulation of the previous section are as follows:

Initial Position Bounded

The boundary condition,

$$\begin{aligned} (x(t_f) - (1-\mu-r_{2-L2}))^2 + y(t_f)^2 + z(t_f)^2 &\leq (\alpha L)^2 \\ -L \leq x(t_0) &\leq L \\ -L \leq y(t_0) &\leq L \\ -L \leq z(t_0) &\leq L \end{aligned}$$

and the path constraints,

$$\begin{aligned} x(t) \geq 1-\mu + \text{margin, (1 - } \mu \text{ is position of Earth)} \\ -T_{max} \leq \mathbf{u}(t) \leq T_{max} \\ 0.01 \leq m(t) \leq 1. \end{aligned}$$

Initial Position and All Positions Bounded

The boundary condition,

$$\begin{aligned} (x(t_f) - (1-\mu-r_{2-L2}))^2 + y(t_f)^2 + z(t_f)^2 &\leq (\alpha L)^2 \\ -L \leq x(t_0) &\leq L \\ -L \leq y(t_0) &\leq L \\ -L \leq z(t_0) &\leq L, \end{aligned}$$

and the path constraints,

$$\begin{aligned} x(t) \geq 1-\mu + \text{margin, (1 - } \mu \text{ is position of Earth)} \\ -T_{max} \leq \mathbf{u}(t) \leq T_{max} \\ 0.01 \leq m(t) \leq 1 \\ -2L \leq x(t) \leq 2L \\ -2L \leq y(t) \leq 2L \\ -2L \leq z(t) \leq 2L. \end{aligned}$$

These position bounds are (like the margin from the Earth) in terms of L, the distance between the Earth and L2.

Attitude Bounded

The boundary and path constraints may look like either of the previous formulations, but added to the path constraints is

$$-u_x tan(a) \leq \sqrt{(u_y^2 + u_z^2)}.$$

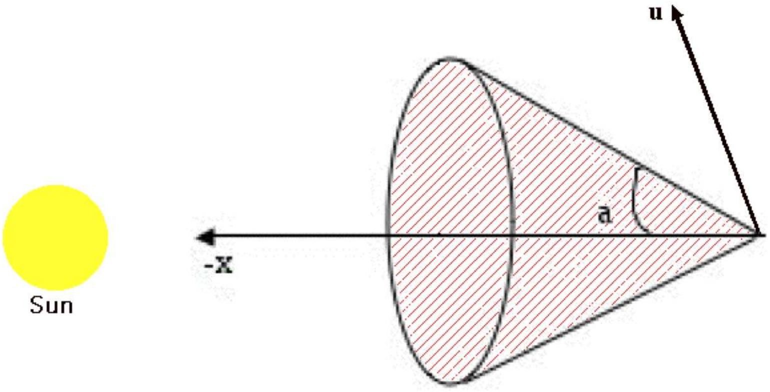

FIGURE 2.5 *The thrust direction* **u** *must stay out of the sun-view cone.*

The Perturbed Model (and the Perturbed Mission Constrained Model) include approximations to the force perturbations caused by the Moon's position varying from the rotating frame's x axis, and from the solar radiation pressure against the solar shield of the sample spacecraft. Including these perturbations alter only the three acceleration equations in the equations of motion section of the formulation. Following is the version of the equations of motion constraint for the perturbed model, **Perturbed Equations of Motion**. See the introduction of the perturbed model (4.1.3) for a derivation of the extra terms.

Perturbed Equations of Motion

$$\begin{aligned}
\dot{x}(t) - v_x(t) &= 0 \\
\dot{y}(t) - v_y(t) &= 0 \\
\dot{z}(t) - v_z(t) &= 0 \\
\dot{v}_x(t) - 2v_y(t) - x(t) + \frac{(1-\mu)(x(t)-\mu)}{r_{13}(t)^3} & \\
+\frac{\mu(x(t)+1-\mu)}{r_{23}(t)^3} - \frac{u_x(t)}{m(t)} - \frac{g_{moon}\ cos(\alpha(t))}{m} & \\
-\frac{.9\ SRP\ (surface\,area)\ cos(angle\,between\,shield\,normal\,and\ -x\,vector)}{(distance\,from\,1\ AU)^2\ (m(t))} &= 0 \\
\dot{v}_y(t) + 2v_x(t) - y(t) + \frac{(1-\mu)y(t)}{r_{13}(t)^3} + \frac{\mu y(t)}{r_{23}(t)^3} - \frac{u_y(t)}{m(t)} - \frac{g_{moon}\ sin(\alpha(t))}{m(t)} &= 0 \\
\dot{v}_z(t) + \frac{(1-\mu)z(t)}{r_{13}(t)^3} + \frac{\mu z(t)}{r_{23}(t)^3} - \frac{u_z(t)}{m(t)} &= 0 \\
\dot{m}(t) + \frac{\|\mathbf{u}(\mathbf{t})\|_1}{Isp * g} &= 0,
\end{aligned}$$

for all $t : [t_0, t_f]$.

The secondary mission example (Chapter 5) uses the original force model, but has two spacecraft, and therefore some extra constraints. The cost function is still the sum of all the control variables, but these now include those for both spacecraft, so it represents the sum of fuel use for all spacecraft in the formation. There are twice as many variables because the states and controls are repeated for the second spacecraft. This means that the equations of motion are doubled; there is a repetition with the first set applying to spacecraft one and the second set applying to spacecraft two. Note, however, that for ease of comparison with previous work, the mass is not a state variable, so the controls are the pure accelerations at each time rather than the thrust force. The final distance constraint is only defined for one spacecraft since the formation distance constraint would cause other spacecraft to also end their path in the L2 vicinity. The added constraints are the distance between the two spacecraft and the requirement that the two spacecraft have similar fuel use. The examples here all use initial position bounds. Some of the examples further include a periodic constraint. The formulation for the formation examples follows.

Find the state vector $\mathbf{s}(t)$ with elements

$$\mathbf{s} = [x_1(t),\ y_1(t),\ z_1(t),\ v_{x1}(t),\ v_{y1}(t),\ v_{z1}(t),\ x_2(t),\ y_2(t),\ z_2(t),\ v_{x2}(t),\ v_{y2}(t),\ v_{z2}(t)]$$

with subscript 1 and 2 for spacecraft 1 and 2, and $\mathbf{u}(t)$, the control vector with elements

$$\mathbf{u} = [u_{x1}(t),\ u_{y1}(t),\ u_{z1}(t),\ u_{x2}(t),\ u_{y2}(t),\ u_{z2}(t)],$$

which minimize the cost

$$J = \sum_{i=1}^{N_s} J_i = \int_{t_0}^{t_f} \sum_{i=1}^{N_s} \left\|\mathbf{u}^i(t)\right\|_1 \, dt,$$

where $N_s = 2$. This is subject to

$$\begin{aligned}
\dot{x_1}(t) - v_{x1}(t) &= 0\\
\dot{y_1}(t) - v_{y1}(t) &= 0\\
\dot{z_1}(t) - v_{z1}(t) &= 0\\
\dot{v}_{x1}(t) - 2v_{y1}(t) - x_1(t) + \frac{(1-\mu)(x_1(t)-\mu)}{r_{1s1}(t)^3} + \frac{\mu(x_1(t)+1-\mu)}{r_{2s1}(t)^3} &\\
-u_{x1}(t) &= 0\\
\dot{v}_{y1}(t) + 2v_{x1}(t) - y_1(t) + \frac{(1-\mu)y_1(t)}{r_{1s1}(t)^3} + \frac{\mu y_1(t)}{r_{2s1}(t)^3} - u_{y1}(t) &= 0\\
\dot{v}_{z1}(t) + \frac{(1-\mu)z_1(t)}{r_{1s1}(t)^3} + \frac{\mu z_1(t)}{r_{2s1}(t)^3} - u_{z1}(t) &= 0\\
\dot{x_2}(t) - v_{x2}(t) &= 0\\
\dot{y_2}(t) - v_{y2}(t) &= 0\\
\dot{z_2}(t) - v_{z2}(t) &= 0\\
\dot{v}_{x2}(t) - 2v_{y2}(t) - x_2(t) + \frac{(1-\mu)(x_2(t)-\mu)}{r_{1s2}(t)^3} + \frac{\mu(x_2(t)+1-\mu)}{r_{2s2}(t)^3} &\\
-u_{x2}(t) &= 0\\
\dot{v}_{y2}(t) + 2v_{x2}(t) - y_2(t) + \frac{(1-\mu)y_2(t)}{r_{1s2}(t)^3} + \frac{\mu y_2(t)}{r_{2s2}(t)^3} - u_{y2}(t) &= 0\\
\dot{v}_{z2}(t) + \frac{(1-\mu)z_2(t)}{r_{1s2}(t)^3} + \frac{\mu z_2(t)}{r_{2s2}(t)^3} - u_{z2}(t) &= 0
\end{aligned}$$

for all $t : [t_0, t_f]$, where r_{isk} = distance from body i to spacecraft k; the boundary conditions,

$$\begin{aligned}
(x_1(t_f) - (1-\mu-r_{2-L2}))^2 + y_1(t_f)^2 + z_1(t_f)^2 &\leq (\alpha L)^2\\
J_1 &= J_2,
\end{aligned}$$

where $0 \leq \alpha \leq 1$ and L is the distance between the Earth/Moon and L2; and the path constraints,

$$\begin{aligned} x_1(t) \geq 1 - \mu + \text{margin, (1 - } \mu \text{ is position of Earth)} \\ -T_{max} \leq \mathbf{u}(t) \leq T_{max} \\ c_2^{1,2} - \delta_l^{1,2} \leq \left\| \mathbf{r}^1(t) - \mathbf{r}^2(t) \right\|_2 \leq c_2^{1,2} + \delta_u^{1,2} \qquad \forall\, t, i, j, \end{aligned}$$

where r^i is the position vector of spacecraft i, c is the constant inter-spacecraft distance required, and the δs are the margins on that distance.

Chapter 3

Solving the Optimal Control Problem

All but the simplest optimal control problem must be solved numerically. There are two basic approaches often termed direct and indirect. An indirect method utilizes the first-order conditions for optimality given by the Pontryagin's maximum principle[7]. To solve for the solution of these conditions requires solving a two point boundary value problem whose dimension is two times the number of state variables. It is simpler and easier computationally to discretize the optimal control problem (a direct method). However, the direct approach may not satisfy the optimality conditions in the limit. While the discretization will not be driven to the limit, it is important to consider the property of the limit because we would like to be able to state the error between the solution found and the true solution. This error is related to the size of the discretization. We can show that the solution obtained does satisfy this property for many of the optimality conditions and in particular the feasibility conditions. This is clearly important for the solution to be tenable. It then follows if we have not satisfied the full optimality conditions (although we often do) it may mean there is a better feasible control than the one we have found. How important it is to find a better control in that case depends on the size of that error from the true optimal solution relative to the errors that can be expected in the hardware implementation of the controls and navigation measurements. The acceptable error also depends on the stage of the design process for which the problem is being solved.

The resulting discrete problem is a nonlinear finite-dimensional optimization problem and may be solved numerically by standard algorithms for this problem. Inevitably the discretization process leads to large nonlinear programs. The optimization algorithm used here is a sequential quadratic programming (SQP) method, implemented in the software SNOPT (produced by the Stanford Systems Optimization Lab, see section 3.2.2 for details), which is explicitly designed to solve large problems.

There are a plethora of ways to discretize the optimal control problem[30]. The method of discretization leads to both different theoretical and numerical properties and to different sizes of discrete problem to obtain the same degree of approximation. The difference in size may be substantial. The discretization methods compared in the following section all use SNOPT to ensure it is only the discretization process that differs.

3.1 Discretization of the Optimal Control Problem

***diagram In this section, a general overview of discretization methods is given, followed by three in-depth discussions of particular methods. These were the methods explored for discretizing the optimal control problem presented in this thesis: user calculated divisions and finite differencing (3.1.1), direct collocation (3.1.2), and pseudospectral (3.1.3). The pseudospectral method was eventually chosen over a direct collocation method because of the need to look at optimality when using a new approach to an optimal control problem.

Shooting methods are a common way to discretize an optimal control problem. Shooting methods approximate the state equations by integrating the vector field. The time period may be divided into intervals. The state variables at the 'knots' between each interval are the variables for the discretized problem. The differential equations describing the dynamics of the system (called state equations because they define the relationship of the state derivatives to the state variables) are solved over each interval by numerical intergration; typically Euler or Runge Kutta. An explicit integration identifies the discretization as multiple shooting because it integrates over *multiple* time arcs, while an implicit integration is used in the collocation method. With the implicit integration, the state and controls are optimization variables at each point of the integration as well as at the knots. So if using an n-degree Runge Kutta formula, the collocation formulation has n times more variables than the multiple shooting formulation of the same problem which only puts optimization variables at the knots between shooting arcs. This does not make the collocation formulation a longer problem to solve however, and may make it faster because the first derivatives are easier to compute. Collocation is less accurate in terms of the state equations though because of the implicit integration. Direct collocation does not converge to the solution of the optimal control problem because an N_{th}-order integration scheme for the differential equations may not necessarily lead to an Nth-order approximation scheme for the dual variables[35]. The constraints Jacobian and objective function Hessian are sparse for both multiple shooting and collocation. There is also a single shooting method in which the control vector represents coefficients in a polynomial that approximates the control function. This function encompasses the state equations, eliminating the state variables. The components of the control vector are the variables, and the objective and constraint functions are formulated in terms of this vector. This creates a smaller but more dense problem. In the single shooting formulation, the objective function is very sensitive to the control variables, so it can require a larger number of timesteps, i.e. a finer grid, to be stable. A more detailed description of all these methods can be found in Ref.[31].

Another type of discretization approximates not just the states, but also the controls, and sometimes state derivatives as polynomials and interpolates to define the discrete states and controls. These methods can be called differentiation-based rather than integration-based[30]. The Hermite-Simpson method uses a Hermite interpolating polynomial over each interval based on the states and state derivatives at the end points. There is an equality constraint applied to the center of each interval that forces the values of the polynomial and its derivative to match the state equations, which express the relationship of the continuous state function to the continuous state derivatives. Pseudospectral methods use Lagrange interpolating polynomials to approximate the states. The expansion points where the discrete variables are defined are chosen as specific set of points. One example is the Legendre-Gauss-Lobatto (LGL) points used in the LGL pseudospectral method. This is the method of choice for the optimal control problem explored in this thesis, and is explained in more detail in Section 3.1.3.

3.1.1 Experiments with finite differencing and user differentiation

This formulation discretizes the equations of motion, including the impulsive ΔVs, into constraints; a set for each time step. This creates a large complicated problem, but allows the algorithm to proceed even if the current trajectory is physically infeasible as well as mission-wise infeasible (diverges from L2). Of course an optimal solution is by definition also a feasible solution, so the final trajectory will still follow the equations of motion (in their discretized form).

In this first formulation, the optimization problem formulation discretizes the ordinary differential equations of motion using a simple finite difference scheme[33]:

$$\frac{u(t+h)-u(t)}{h} = \dot{u}(t) + O(h),$$

where h = length of time step. The traditional state vector is the position and velocity at the current time step: $X = (x, y, z, \dot{x}, \dot{y}, \dot{z})$. The state vector for the optimization problem is the whole trajectory. Thus the state vector or trajectory for the current iteration in the optimization program is $Z = (X_1, X_2, ., X_N)$, where N is the number of timesteps. For the problem formulations done in this preliminary research, both h and N are determined by the Matlab differential equation solver when the program calls for the initial trajectory.

The discretization into time steps then results in three linear equations(e.g. $\dot{X}_1 = X_4$) and three nonlinear equations (e.g. $\dot{X}_4 = f(X_{1-6})$ for each time step. The nonlinear equations, although complicated as they depend on distances from the masses, are analytically differentiable. This means that the gradient of the nonlinear constraints can be calculated before the equations are discretized into finite differences. The nonlinear equations use finite differences to approximate the accelerations, or first derivatives of X_{4-6}. The linear equations use finite differences to approximate the velocities, or first derivatives of X_{1-3}.

It is quite valid to pose this as a finite optimization problem by having a certain number of timesteps, which requires that the maneuvers that add δv are modeled as impulses. This is because the dynamics and thus period of the orbit about a libration point are on a very large scale; in fact a scale proportional to the half period of the Sun-Earth frame rotation. Therefore, the period will be about six months, whereas the actual burn duration should not be more than a day, and is probably much less.

With an appropriate discretization formulation, SNOPTs feature of elastic nonlinear constraints is very helpful, and possibly essential, in finding a solution to this simplified model, and to more highly constrained models.

3.1.2 Direct Collocation Method

The simple model optimization problem was also solved by the package, GESOP[34], which uses a direct collocation discretization, and SNOPT to solve the discretized problem. However, the exploration of this method for solving the problem is presented in this section.

The examples here use the collocation code TROPIC (TRajectory OPtimization using dIrect Collocation), which was developed by DLR, Junsch(1990), Schnepper(1992). It is similar to that used in NASA's OTIS optimization software (which also uses SNOPT), but has automatic function and parameter scaling. TROPIC approximates the controls and states over time by third-order Hermite polynomial functions.

Inputs to GESOP include a guess of states and controls at the starting time, and of the final time, along with bounds. For this problem, the bounds on states are very wide, the bounds on the controls are the same as the original problem (zero lower bound and maximum thrust magnitude upper bound), the final time is set to a fixed value. GESOP then generates an initial guess using the equations of motion and timesteps as defined by the user. The integrator is a Runge-Kutta-Fehlberg integrator of fifth order, using Dormand and Prince formulae. There is a minimum step value to avoid the integrator getting stuck if the control estimate is not smooth. A discretization grid, defined by the user set the collocation nodes. To compare the main discretization method to traditional collocation, the nodes in GESOP are always chosen to be equally spaced in the examples shown here.

TROPIC applies a scaling transformation as follows. Given original function F, the scaled function $\bar{F} = DF$, where D is a positive constant. The scaling factors, D, are computed to keep the scaled collocation constraints at each node matching the scales states. For $x(i)$ at an interval beginning and $x(i+1)$ at an interval end (between collocation nodes), the scaled states are

$$y(i) = d(i)\ x(i) + c(i) \text{ and } y(i+1) = d(i+1)\ x(i+1) + c(i+1).$$

The scaling factors in this interval are then

$$D = (d(i) + d(i+1))/2.$$

If the state outside the interval is not optimized, only $d(i)$ or $d(i+1)$ is used.

Although this scaling is applied, GESOP could not find a feasible solution for the libration point mission design problem until the state scaling scheme used with the pseudospectral method (see Section 3.2.3) was additionally applied. For all GESOP runs, the final distance constraint was half the distance from L2 to Earth. It was observed that GESOP needs a fairly good input to find an optimal solution with a cost approximately zero (the cost of the known global optimal). Using the initial state of the large halo input, which is a feasible position but zero velocity values, the initial guess propagated by GESOP does not make an orbit shape, but breaks the final distance constraint fairly early. GESOP was unable to find a feasible solution with this input for any time period longer than when the distance constraint was broken.

Given the initial state of the sitting at L2 input, which is all zero for position and velocity, the initial guess propagated again immediately leaves the L2 vicinity, but at a slightly slower rate. For a time period of 5 TU (0.8 years), GESOP finds an optimal solution that starts away from L2 and forms a curve about the point. However, this solution also uses thrust more than half of the time period, so the cost is relatively large (1.4 DU/TU or 42 km/s). GESOP did not find one of the global optimals for this starting point. This guess of sitting at L2 yields widely varying results. When the time was increase to 5.5 TU (0.9 years), GESOP does find a (nearly) zero cost solution that has a halo orbit shape. With times of 6 and 7 TU, GESOP cannot get feasible, but when the optimal solution with 5.5 TU is loaded at the start of the optimization, the same optimal orbit is found with an exactly zero cost. With a good starting point, propagated from the initial state of the full halo input, GESOP can find a global optimal usually very close to the input, as long as the time period is not too long (less than about 7 TU). With time periods of 7 to 9 TU (1.1-1.4 years), global optimal solutions are found, but often as a smaller or larger halo-type or bean-shaped orbit. At 9 TU, with 35 nodes a local optimal is found with a similar orbit as the propagated input, but using bang-bang controls, such that the cost is 4.6. However, when this was changed to 10 nodes in the optimization, leaving 35 steps for simulations (propagation of initial state), a global optimal was found.

With larger time periods, the solutions for various numbers of nodes mostly are infeasible, and rarely are non-zero cost optimals. With the timelength of 4π TU (2 years), GESOP found an optimal for 15 nodes with 45 nodes for simulation. This solution had a cost of 0.1 because it had a positive z thrust over the first two nodes. It is likely that more nodes could help to enable GESOP to see the problem as feasible more often and so more likely to find a global optimal solution, but after about 50 nodes, there is not enough space to compute the problem, and up to 50 nodes, it was still unable to see the problem as feasible.

Starting with a nonzero controls guess for just the positive x control, GESOP is able to find an optimal solution quite close to the same input with a totally zero controls guess. With other nonzero guess controls, though, it cannot find an optimal, and is unable to compute a good enough search direction to get beyond the first iteration of the algorithm.

For starting points that did not propagate to 'good' guesses, but started reasonably near the L2 point, nearly zero cost optimal solutions were found for some cases with final times of 4 TU or less. For longer times, the problem was infeasible.

Using a direct collocation method limited the scope of formulations that could be solved for the optimal design and control of a libration point mission. This method was sometimes fast for very good input trajectories and relatively short mission simulations, but it either broke down computationally or had no feasible point when discretizing simulations longer than about 8 TU or 1.3 years. Some input trajectories that were infeasible due to their final distance worked to find an optimal solution if the time period was short and the starting state variables close to that of a halo orbit, but in general the set of inputs that work with this discretization method is limited and forces optimal trajectories to be halo-type orbits of the size suggested by the input. These results reflect the need for more knots when using third-order polynomials (as opposed to much larger orders using the pseduospectral method below) to represent the equations of motion accurately enough to match the discretized constraints. However, the number of knots needed is limited by memory availability, and was about 50 for this amount of variables (as described above). When compared to the PS method, direct collocation is harder to use and leaves less negotiation for minimum-fuel mission designs when including further constraints and force perturbations. It doesn't allow for the wide variety of input trajectories that is seen using the PS method, although it produces results a little faster with a good input (for this mission design problem).

Table 3.1
Limitations of direct collocation method

Speed	Fast for good input, stalled for poor input, or long sim. times
Input Variety	No feasible or optimal solution without near-optimal input
Output Variety	Only found halo-shaped optimals, when solution possible
No. Timesteps	Need larger number to capture dynamics, out of memory for$\geq$50
Sim. Time	Limited to a max. of 9 TU for very good input

3.1.3 Pseudospectral Method

The main advantage of pseudospectral discretization is that it chooses the optimal node placement in time to discretely represent the variables over time used in the optimization problem. The nodes are placed at the roots of the Legendre polynomial (called the Legendre-Gauss-Lobatto (LGL) quadrature nodes), taking advantage of the theory of Gaussian quadrature, which states that the optimal abscissas of the Gaussian quadrature formulas are exactly the roots of the orthogonal polynomial over the same interval and weighting function. Legendre-Gauss quadrature is limited to the interval $[-1, 1]$ and the weighting function $W(x) = 1$. The roots of the Legendre polynomials occur symmetrically about 0. That the Legendre polynomials are orthogonal is to say that the following relationship holds:

$$\int_{-1}^{1} P_m(t)P_n(t)dx = \delta_{mn}\frac{2}{2n+1},$$

where P_m and P_n are the polynomials and δ_{mn} is the Kronecker delta, which is 0 when $m \neq n$ and 1 when $m = n$. So we can also say of Legendre polynomials that

$$\int_{-1}^{1} [P_n(t)]^2 dx = \frac{2}{2n+1}.$$

This method succeeded where the previous methods failed in solving the problem discussed here without a good estimate of an optimal solution as a guess. It was implented with DIDO[15], a Matlab application package which discretizes an optimization problem from its continuous form and then calls SNOPT by way of Tomlab wrappers that provide an interface between Matlab and SNOPT. DIDO does a pseudospectral discretization[35] of the optimal control problem into a large nonlinear programming (NLP) problem which is a representation of the continuous (and thus infinite) optimal control problem as a finite-dimensional optimization problem.

In DIDO, the state and control functions are approximated by Nth degree polynomials; N+1 being the number of nodes. The discrete derivatives of the states and controls are the derivatives of these functions at each node. They are calculated by the differentiation matrix D, which itself is calculated using the Nth degree Legendre polynomial and is a function only of the number of nodes (so it is a constant). The original continuous problem ((2.9)-(2.12)) is translated to the discrete model, which poses the problem of finding the $(N+1)(N_s+N_u)$ vector $X = \mathbf{s}, \mathbf{u}$ that minimizes

$$J(X) = \frac{t_f - t_0}{2} \sum_{k=0}^{N} F(s_k, u_k) w_k,$$

where w_k are the LGL weights, a function of N and the Nth degree Legendre polynomial, and subject to the constraints

$$\begin{array}{rc} \textit{equations of motion} & \frac{t_f - t_0}{2} f(s_k, u_k) - \sum_{l=0}^{N} D_{kl} x_l = 0 \\ \textit{boundary constraints} & b(s_0, s_N) = 0 \\ \textit{path constraints} & h(s_k, u_k) \leq 0 \end{array}$$

for k=0,...,N. See the continuous problem for function definitions used in this work. The D matrix is a $(N+1)^2 \times (N+1)^2$ matrix with a block diagonal form, made up of submatrix $(N+1) \times (N+1)$ blocks $D_{kl} =$

$$\begin{array}{cl} \frac{L_N(t_k)}{L_N(t_l)} \frac{1}{t_k - t_l} & k \neq l \\ -\frac{N(N+1)}{4} & k = l = 0 \\ \frac{N(N+1)}{4} & k = l = N \\ 0 & otherwise. \end{array}$$

For example,

Table 3.2
Submatrix diagonal in D matrix for $N = 4$

-5.0	6.8	-2.7	1.4	-0.5
-1.2	0	1.7	-0.8	0.3
0.4	-1.3	0	1.3	-0.4
-0.3	0.8	-1.7	0	1.2
0.5	-1.4	2.7	-6.8	5.0 .

These submatrices are each rank deficient by one. The optimization algorithm can deal with this however because in choosing N independent columns from the Lagrangian function, it can take some from the Jacobian of the constraints as well as this differentiation matrix.

The state and control vectors, which were functions of time in the continuous model, consist of N discrete values in this model; evaluating the value of the function at the time represented by each of the N nodes during each iteration of the optimization algorithm. It is important to note that the discretized input trajectory is already different than exactly what is calculated (as described in the Optimization Formulation section) as a good input because of the choice of nodes. The optimization algorithm starts with the input trajectory, composed of state and control variables at N nodes. These variables are the values calculated by estimating state and control functions based on the states and controls at given times, and then evaluating these functions at the LGL nodes.

The number of nodes chosen for DIDO to use to solve an optimal control problem is based on the complexity of the problem and length of time simulated. For the libration point mission design problem, a relatively large number of nodes are needed to capture the dynamics of the unstable region (although the PS method generally requires many fewer timesteps than other discretization methods). The large number of variables at each time as well as the complexity itself motivate limiting the number of nodes in order to limit the computation time to a reasonable length. The process is much faster if the input is the output from a previous run of DIDO, so a common practice in this work was to run DIDO with a small number of nodes - about 5-10 nodes per rotation of the Earth-Sun system or 2π TU. This first run was often (but not always) too rough of a grid to capture the dynamics and resulted in SNOPT being unable to find a feasible solution. This was then the input for a second run of the desired number of nodes - 20 to 80 nodes per system rotation, depending on the accuracy desired. The lower end is enough to produce a clear optimal solution, and the upper end will produce the same trajectory as a Runga-Kutta integration of the equations of motion with the optimal control history for at least 2π TU.

3.2 Solution of the Discretized Problem.

The discretized nonlinear programming problem is solved with a sequential quadratic programming (SQP) algortithm. The problem from the perspective of the optimization algorithm is formulated here, and the advantages of the implementation of the SQP for this particular problem are discussed.

3.2.1 Nonlinear Programming Problem

The optimization algorithm does not distinguish the nonlinear programming problem solved here as an optimal control problem. The variables consist of every state and control at every node (in time). These all make up the variable vector, X. The nonlinear programming problem is

$$\begin{aligned} &\text{find } X \text{ that minimizes } J(X) \\ \text{subject to } &B_L \leq (X, C(X), AX) \leq B_U, \end{aligned}$$

where B_L and B_U are lower and upper bounds, J must be smooth and scalar, $C(X)$ is a vector of smooth nonlinear constraint functions, and A is a sparse matrix such that AX are any linear constraints. The first and second derivatives of J and C are used in the optimization algorithm.

3.2.2 Algorithm Details

An SQP algorithm was implemented using the software SNOPT[16], licensed by the Systems Optimization Laboratory at Stanford University[32]. The algorithm routines in SNOPT are designed to handle large-scale problems, and take advantage of the sparsity in the matrices of the discretized problem that result from a small number of degrees of freedom. These qualities make SNOPT an efficient solver for trajectory design in a complex dynamical space. The degrees of freedom are limited by restriction that the trajectory satisfy some equations of motion, while the complexity requires representation at more points in time to adequately capture the dynamics. The amount of time points used results in thousands of variables and thousands of constraints in the discretized problem for which SNOPT is well-suited. The approach of exploring the design space by allowing any kind of input trajectory and control rather than a near-optimal reference orbit is also made possible by a characteristic of SNOPT. If the current QP subproblem is infeasible, it enters an 'elastic' mode which minimizes constraint violations while allowing the main optimization algorithm to continue into a feasible area. The optimization algorithm is complete when it finds a minimum in the cost function within a set optimization tolerance, that meets the constraint function within a set feasibility tolerance.

3.2.3 Implementation Analysis

Calling SNOPT from DIDO, the derivatives of functions are not defined, so the first derivatives are estimated with finite differences[33] by SNOPT. The approximation of the second derivatives in the form needed at each iteration is part of the algorithm, in its Hessian approximation.

SNOPT succeeds well in solving the discretized problem even with hundreds of nodes (this is also due to the form resulting from the PS discretization) despite the lack of accurate derivatives. It also takes a very reasonable amount of time (on the order of a few minutes for the largest formulations), but only if the variables are appropriately scaled. This means that the variables are multiplied by a factor (possibly a different number for each state and control) before being input into the optimization algorithm. The factor is usually one that puts their maximum value between 0.1 and 1, but in some cases, the factor needed to be one or two magnitudes larger. Without scaling the problems either took days to solve or could not find a feasible point.

Chapter 4

Results for an Example Mission

In this and the next chapter we report the results from testing the algorithms described on the problem of libration point mission design; the optimal control problem. The testing has several purposes. We first demonstrate that the Pseudospectral Method performs considerably better than the alternative methods of discretization. Only simple models were needed to reach these conclusions since the alternatives to the PS method performed poorly even on the simplest problem. Another purpose is to show that the mission design problem is in fact solvable without breaking it into several steps and making assumptions about the orbit, and it is in fact solvable for an optimal point without starting from a "good guess".

Although the approach we adopt can be applied to any libration point with similar results, we choose to design and control formations about the Sun-Earth $L2$ point because of the complicated constraints on some of the missions currently proposed at this location; thus, we have,

$$\begin{aligned} \mu &= 2.448 \times 10^{-6} \\ \mathbf{r}_L &= (1 - \mu + 0.01, 0, 0)\ DU \end{aligned}$$

in the barycentric frame, where DU is the distance unit equal to the astronomical unit, AU. The origin in these examples is shifted to $L2$ to improve variable scaling, so $\mathbf{r}_L = (0, 0, 0)$.

This chapter is divided into results of posing the simple problem: keep a spacecraft in the libration point area for a given time period, and the results of posing the more complex problem of adding the types of mission constraints that will be imposed on large telescope spacecraft. This approach allows those more complicated constraints to be considered during the initial design stage, which will allow a better final design. The next chapter contains the result of applying this approach to create a formation of several spacecraft in the Sun-Earth $L2$ vicinity.

4.1 Mission-Unconstrained Results

The following section describes the details of the inputs and constraints along with the results for cases in which mission constraints are not applied. The only constraints, aside from the equations of motion, are those which define the basic problem of a spacecraft with a set starting mass that is free to thrust in any direction at any (discrete) time with any magnitude within a set maximum in order to be within a certain radius of the Sun-Earth L2 point at a set ending time. The position of the spacecraft at times other than the final time is also bound in a few examples.

Mission constraints would be, for example, a requirement about when or in which direction the engine could produce thrust, a minimum or maximum distance from the Sun-Earth line, or a periodicity requirement. The result of applying a mission constraint within this framework will be seen in the next section.

4.1.1 Simple Model Definition

The simple model uses the equations of motion for the circular restricted three-body problem, without any perturbations, which was described in Section 2.1. As expected for this model, optimal trajectories are found for *zero cost* which remain in ‘orbit’ about L2.

4.1.2 Simple Model Solutions

For each of the following examples, the number of nodes to be used and the value of the final distance constraint, d_f are chosen. The other constraints remain the same, and their form can be seen in the previous section. In addition, an estimate of the solution is defined as a starting point for the optimization algorithm. The discretization and optimization software are run with this information, and output the states and controls at each node that are determined to be an optimal solution (resulting in a local minimum in the cost function). The estimate of the solution is also in the form of state variables and control variables, but are given at any list of timesteps, along with the value of these timesteps. We call this information the ‘input trajectory’.

The input trajectories for these examples are chosen to find different but similar optimal solutions, and to illustrate the ability of this method to find optimal solutions with different quality starting points. The input trajectories are halo-shaped orbits, with variations in velocity information, distance constraint values, and orbit size. There is also an input of just a few timesteps, all at the L2 point, as a low-quality estimate example.

Example 1

As expected for the circular restricted three-body problem, an optimal trajectory is found for *zero cost* which remains in ‘orbit’ about L2. In all examples here, we consider a fixed-horizon problem, and set $t_f = 4\pi\ timeunits(TU)$ (730 days). The time unit is equal to the period of the rotation system, which is the inverse of the frequency, 2π radians per year. The thrust acceleration magnitude constraint is, $u_{max} = 0.001\ DU/TU^2$, where TU, the time unit is $1/(2\pi)$ of the period of the of the primary system; i.e. a year for the Sun-Earth system. The maximum final distance d_f is .002 DU, 1/5 the distance between the Earth and L2 (call this distance L). The input states and controls (the starting point for the optimization algorithm) are the position coordinates of a halo orbit. The velocities and controls are zero, and the mass stays at the initial normalized mass of 1. This means the initial estimate of the solution is infeasible since the equations of motion do not hold. The input trajectory is produced with the equations,

$$\begin{aligned} x &= -Ax * cos(2 * t) \\ y &= Ay * sin(2 * t) \\ z &= Az * sin(2 * t + pi/4) \\ for\ t &= 0; .01; .02 ... 4\pi, \end{aligned}$$

where

$$Ax = 206,000\ km, Ay = 665,000\ km, Az = 110,000\ km.$$

The initial state of the input for this example is (in DU and DU/TU):

$$\begin{aligned} x(t_0) &= -1.377 \times 10^{-3}, & v_x(t_0) &= 0 \\ y(t_0) &= 0, & v_y(t_0) &= 0 \\ z(t_0) &= 0.520 \times 10^{-3}, & v_z(t_0) &= 0. \end{aligned}$$

To reduce the computation time, the initial state of the solution was bound to a box of 0.01 DU on either side of the about input initial state. In another technique to reduce computation time, the problem was first solved for 40 nodes, and the solution used as input to solve the problem with 200 nodes, which produced a clear solution. This solution was then used as an input to compute a 400 node solution in order to achieve the accuracy needed to make the comparison shown in Fig. 4.4.

As noted earlier, we used DIDO[15] with SNOPT[16] to solve the optimization problem. A solution to the problem for a choice of 400 nodes (roughly, a 399th-order Legendre polynomial) is shown in Fig. 4.1. This solution is clearly globally optimal because it has zero cost, i.e. $J = 0 \Leftrightarrow \mathbf{u} = \mathbf{0}$. The optimal controls are almost all zero at each node as shown in Fig. 4.2.

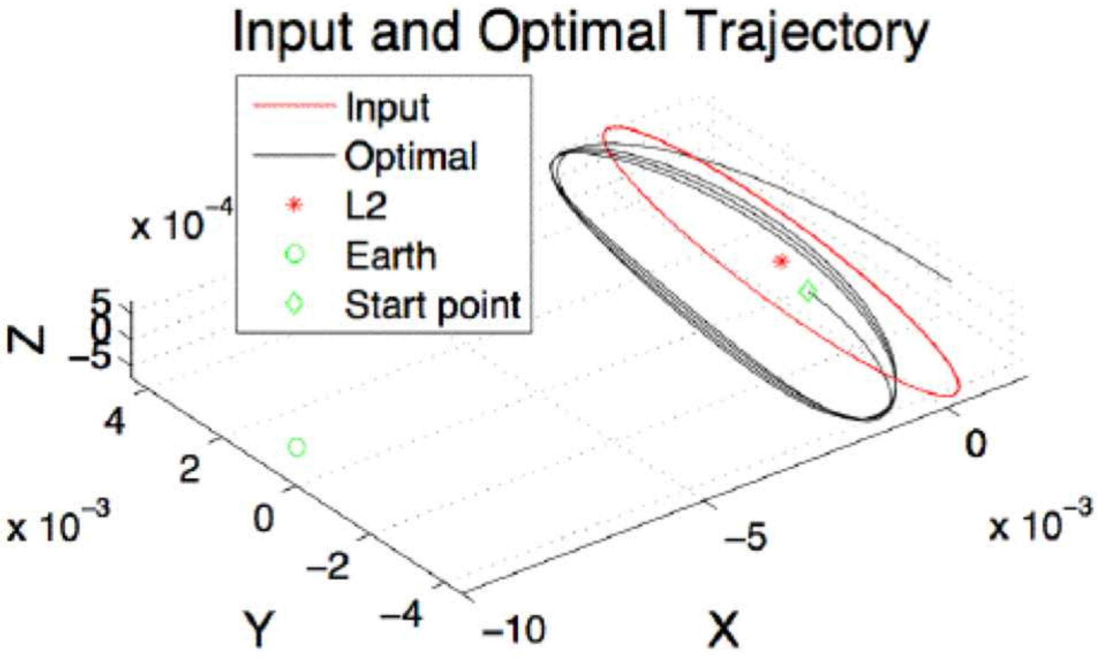

Input Trajectory and Initial Position:

$$
\begin{aligned}
x &= -Ax * cos(2*t) & x(t_0) &= -1.377 \times 10^{-3}, & v_x(t_0) &= 0\\
y &= Ay * sin(2*t) & y(t_0) &= 0, & v_y(t_0) &= 0\\
z &= Az * sin(2*t + pi/4) & z(t_0) &= 0.520 \times 10^{-3}, & v_z(t_0) &= 0.\\
for\ t &= 0; .01; .02 ... 4\pi, & & & &
\end{aligned}
$$

$Ax = 206,000\ km, Ay = 665,000\ km, Az = 110,000\ km.$

FIGURE 4.1 **Simple Model Example 1:** *An Optimal Trajectory for Large Halo Input*

Note that there is just one non-zero control variable, at the first node, and it is about $1 \times 10^{-8}\ DU/TU^2$, compared to the maximum allowed magnitude of 1×10^{-3}. This may be considered noise since it is smaller than the tolerances and the trajectory would be the same within these tolerances if this variable were exactly zero. So the cost

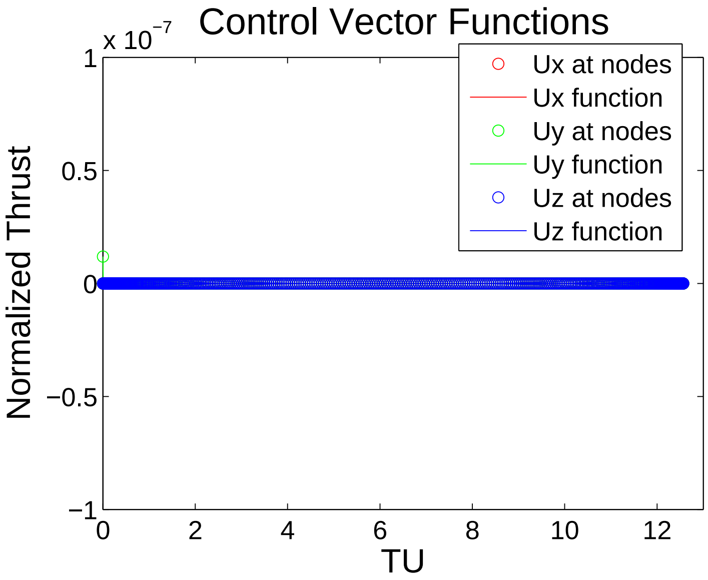

FIGURE 4.2 **Simple Model Example 1:** *Thrust over time*

can be considered zero.

The claim of optimality is based on several tests[15]. One of these tests is the approximate constancy of the Hamiltonian with an average value equal to zero.[13] The Hamiltonian was defined in Chapter 2 (Equation 2.13). For illustration of this test, the non-zero values of the Hamiltonian for this example are shown to be trivially small in Fig. 4.3. In order to practically demonstrate the convergence of the solution, we use the optimal initial conditions (in DU and DU/TU),

$$\begin{aligned} x(t_0) &= 0.24 \times 10^{-4}, & v_x(t_0) &= 5.27 \times 10^{-4} \\ y(t_0) &= -6.75 \times 10^{-4}, & v_y(t_0) &= -79.03 \times 10^{-4} \\ z(t_0) &= -2.67 \times 10^{-4}, & v_z(t_0) &= -9.57 \times 10^{-4} \end{aligned}$$

to propagate the solutions using ode45 in Matlab. Fig. 4.4 shows a comparison of the optimized velocity states to the propagated velocity states of one of the spacecraft up to the point of divergence. It is apparent that the propagated states track fairly well to the optimized ones up to π TU, indicating that it takes 400 nodes over this time period for a solution accurate enough for preliminary design considerations for one year in the current formulation. This is because the timestep at which the solution diverges

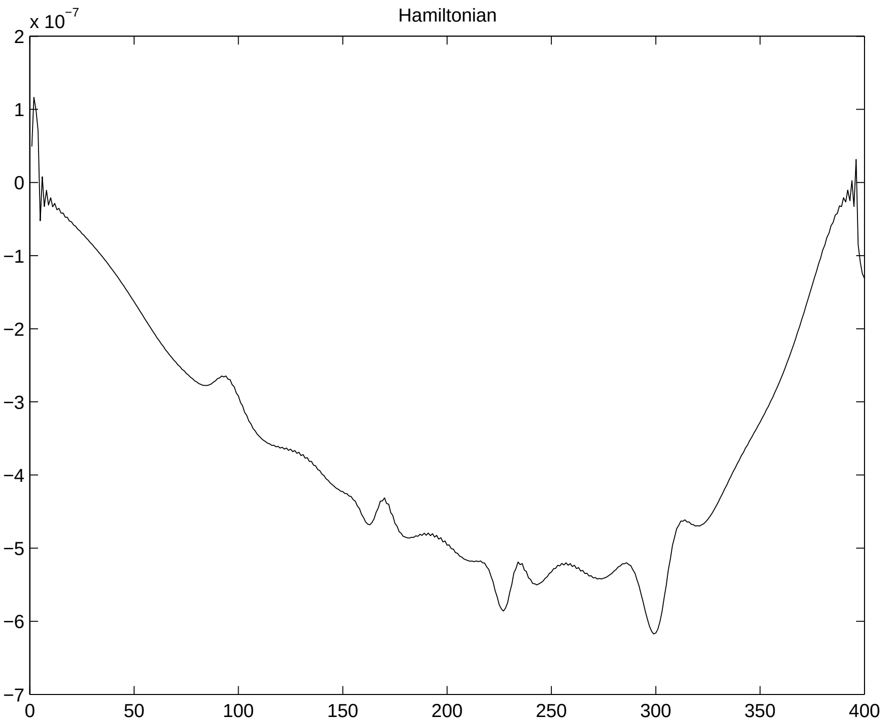

FIGURE 4.3 **Simple Model Example 1:** *Evolution of the Hamiltonian; note the scale on the ordinate*

from the propagated trajectory increases proportionally to the number of nodes. For the rest of the examples the number of nodes will be only large enough to produce a clear optimal solution, since solutions that more closely align with a differential equation solver solution can be easily found with an increase in the number of nodes.

Example 2

The input states and controls (the starting point for the optimization algorithm) are again the position coordinates of a halo orbit with the velocities and controls zero, but this orbit is only 10% of the size of the previous example's input. The input mass is again 1 at all nodes. There is no bound on the initial state, and the maximum final distance d_f is L, the distance between the Earth and L2. The input trajectory is produced with the equations,

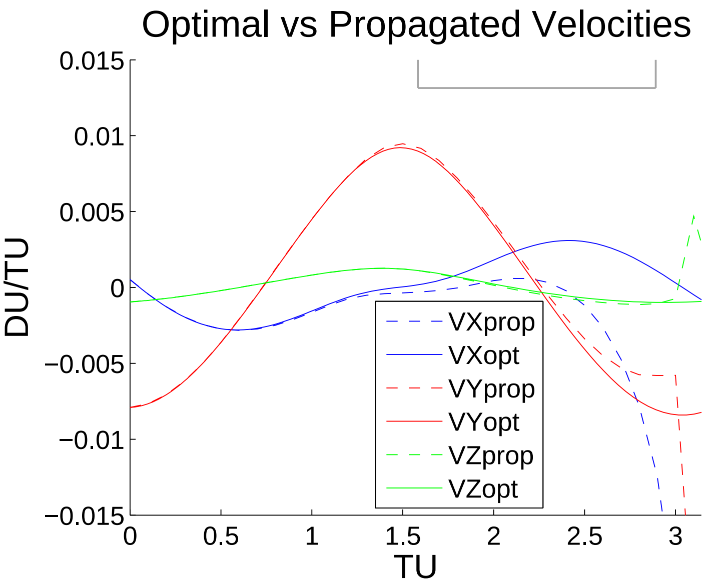

FIGURE 4.4 **Simple Model Example 1:** *Comparison of the velocity states to those propagated by ODE45 in Matlab (dotted)*

$$
\begin{aligned}
x &= -Ax * cos(2*t)\\
y &= Ay * sin(2*t)\\
z &= Az * sin(2*t + pi/4),
\end{aligned}
$$

where

$$Ax = 20,600\ km, Ay = 66,500\ km, Az = 11,000\ km.$$

The solution shown here was computed first for 25 nodes for which no feasible solution could be found, and then iterated for 125 nodes.

The optimal controls are all exactly zero at each node.

Example 3

The input states and controls are the same as the previous example's input. There is still no bound on the initial state, but the maximum final distance d_f has been reduced to .005 DU, or L/2. The input trajectory is produced with the equations,

$$\begin{aligned} x &= -Ax * cos(2 * t) \\ y &= Ay * sin(2 * t) \\ z &= Az * sin(2 * t + pi/4), \end{aligned}$$

where

$$Ax = 20,600\,km, Ay = 66,500\,km, Az = 11,000\,km$$

The solution shown here was computed first for 25 nodes for which an optimal but too coarse solution was found, and then iterated for 125 nodes.

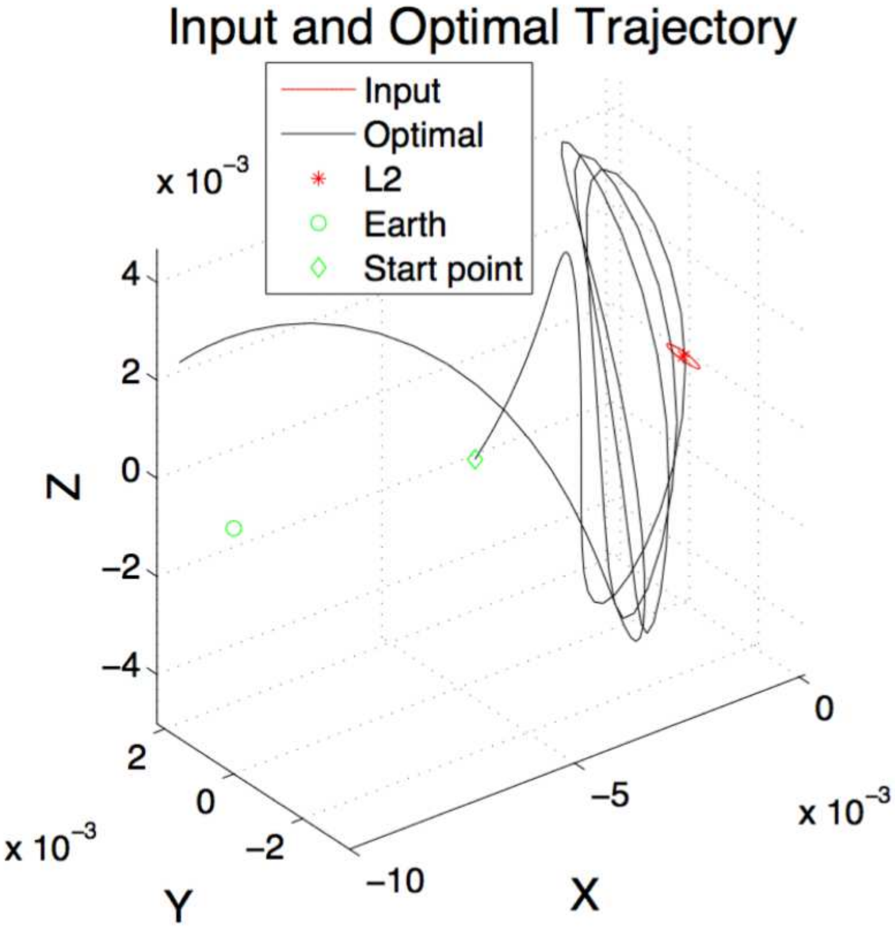

Input Trajectory and Initial Position:

$$
\begin{aligned}
x &= -Ax * cos(2*t) & x(t_0) &= -1.377 \times 10^{-3}, & v_x(t_0) &= 0\\
y &= Ay * sin(2*t) & y(t_0) &= 0, & v_y(t_0) &= 0\\
z &= Az * sin(2*t + pi/4) & z(t_0) &= 0.520 \times 10^{-3}, & v_z(t_0) &= 0.\\
for\ t &= 0; .01; .02 ... 4\pi, & & & &
\end{aligned}
$$

$Ax = 20,600\ km, Ay = 66,500\ km, Az = 11,000\ km.$

FIGURE 4.5 **Simple Model Example 2:** *An Optimal Trajectory for Small Halo Input, $d_f = D$*

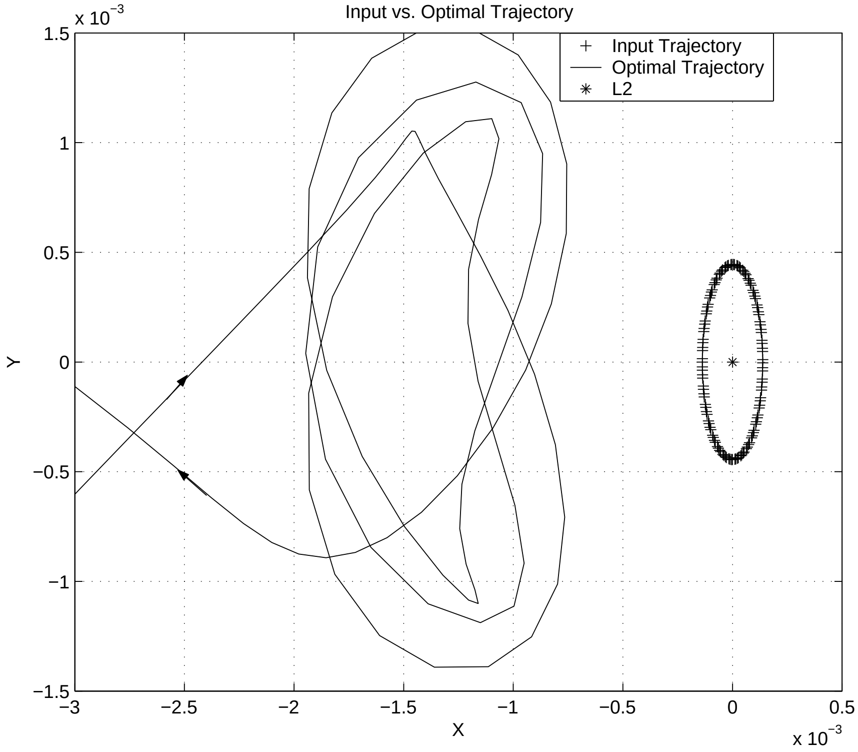

FIGURE 4.6 **Simple Model Example 2:** *A 2-D Zoomed View of the Optimal Trajectory*

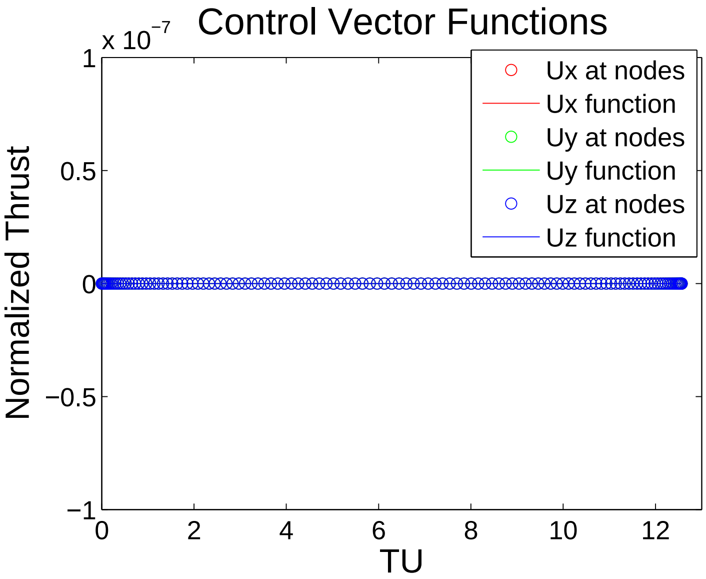

FIGURE 4.7 **Simple Model Example 2:** *Thrust over time*

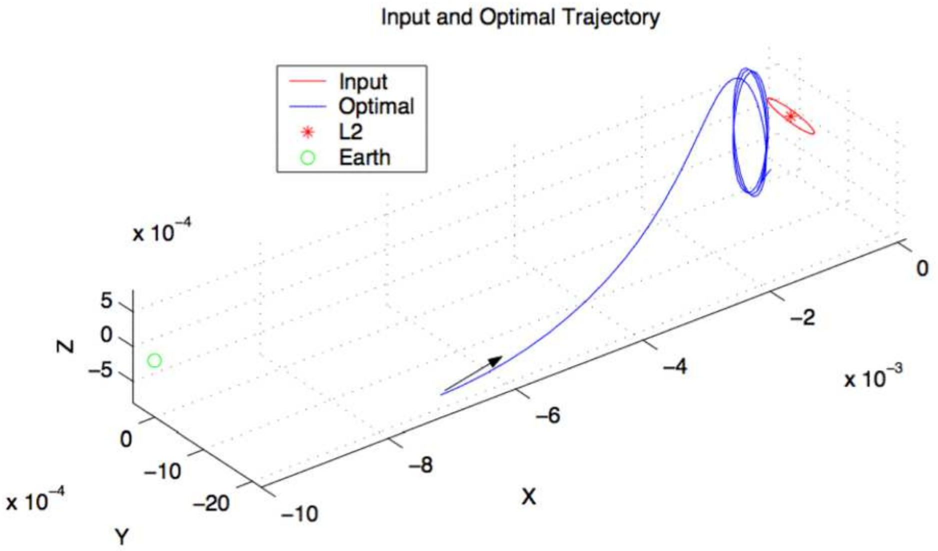

Input Trajectory and Initial Position:

$$\begin{array}{rcl} x & = & -Ax*cos(2*t) \\ y & = & Ay*sin(2*t) \\ z & = & Az*sin(2*t+pi/4) \\ for\ t & = & 0;.01;.02...4\pi, \end{array} \qquad \begin{array}{ll} x(t_0) = -1.377\times10^{-3}, & v_x(t_0)=0 \\ y(t_0) = 0, & v_y(t_0)=0 \\ z(t_0) = 0.520\times10^{-3}, & v_z(t_0)=0. \end{array}$$

$$Ax = 20,600\ km, Ay = 66,500\ km, Az = 11,000\ km.$$

FIGURE 4.8 **Simple Model Example 3:** *An Optimal Trajectory for Small Halo Input,* $d_f = D/2$

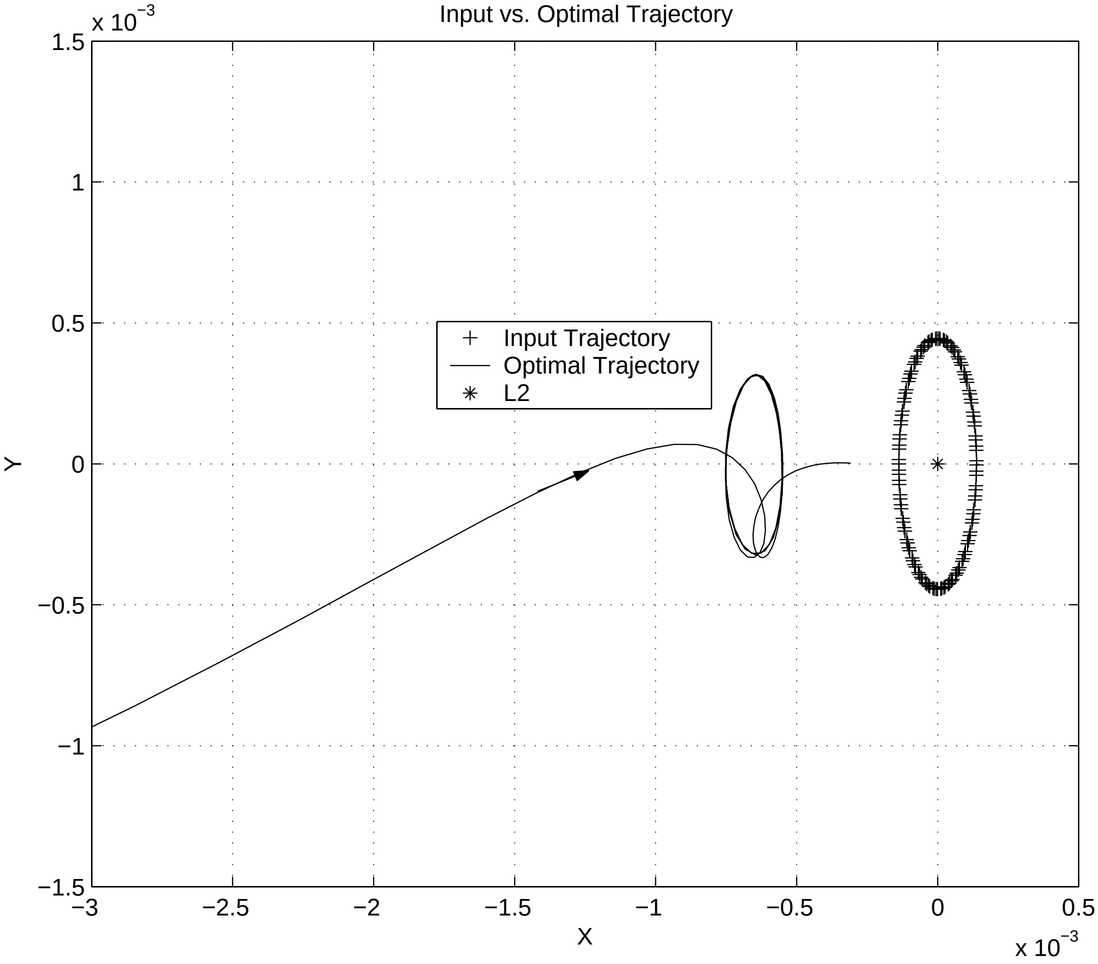

FIGURE 4.9 **Simple Model Example 3:** *A 2-D Zoomed View of the Optimal Trajectory*

The optimal controls are almost all zero at each node as shown in Fig. 4.10. Note that two non-zero control variables, at the first and second node, in the z direction at about 1×10^{-5} DU/TU^2, and then in the x direction at about 5×10^{-5} DU/TU^2, compared to the maximum allowed magnitude of 1×10^{-3}. This is larger noise than the first example, but is still small enough that it is most likely due to amplification because of placement of nodes, and would disappear with a larger number of nodes.

Example 4

The input states in this example are both positions and velocities of a sample halo orbit. The orbit is calculated using the same equations of motion that are a constraint in the optimization problem. The input trajectory calculator varies the starting velocities, targeting zero velocity in the y direction at the crossing of the x axis. This results in

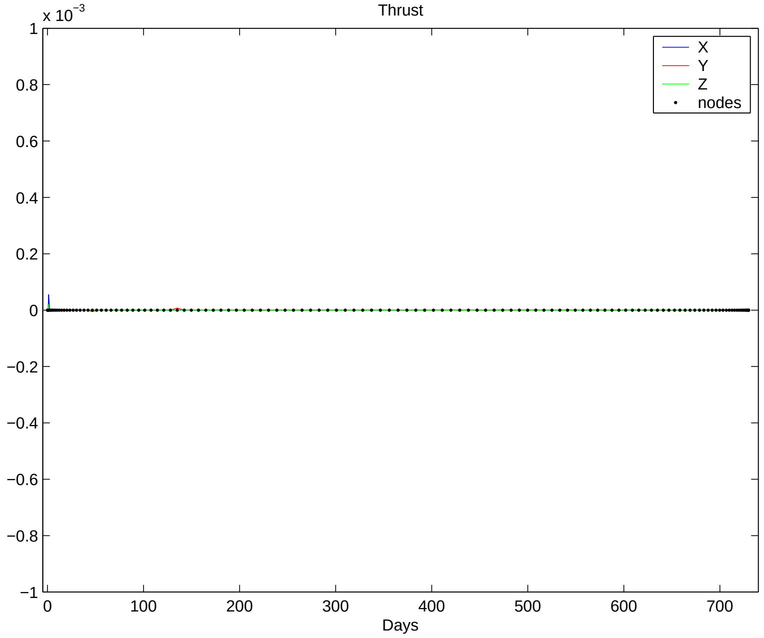

FIGURE 4.10 **Simple Model Example 3:** *Thrust over time*

an approximation of a natural halo orbit, so the input control variables are all zero. Like the previous examples, the mass component of the input state vector is always at the 'full' value, one instead of zero. There is no bound on the initial state, and the maximum final distance d_f is .005 DU, or L/2. This constraint is active as the optimal trajectory diverges from the almost repeating 'orbit' to end at this distance (toward Earth) on the final node. The resulting input trajectory starts at the same position as the previous examples, but with a velocity of about $0.0046 DU/TU$ in the y direction. Figures 4.11 and 4.12 show the optimal solution found with this more complete halo orbit as a starting point. It was computed first for 25 nodes for which an optimal but too coarse solution was found. This was the input for a 35 node solution which was optimal and zero cost but still somewhat course, which was then iterated into a 125 node solution for accuracy and consistency. The optimal controls are all exactly zero at each node, so the thrust over time plot is not shown.

Example 5

The input states and controls are zero, which means the input trajectory is stationary at L2. The mass component of the input state vector is one at all nodes. There is still no bound on the initial state, and the maximum final distance d_f is L. But this constraint is not active because the optimal trajectory starts closer to the Earth and orbit L2, ending close to the point; about 1% of the maximum final distance allowed by the distance constraint. The input trajectory is the following,

$$\begin{aligned}
\mathbf{x}(0) &= \mathbf{0}, \textit{except } m(0) &= 1 \\
\mathbf{x}(2\pi) &= \mathbf{0}, \textit{except } m(2\pi) &= 1 \\
\mathbf{x}(4\pi) &= \mathbf{0}, \textit{except } m(4\pi) &= 1.
\end{aligned}$$

As seen above, there are only 3 nodes for the input. The solution shown below (Fig. 4.13) was computed first for 35 nodes for which an optimal but too coarse solution was found, and then iterated for 125 nodes. The optimal controls are all exactly zero at each node (Fig. 4.14).

Table 4.1
Summary of Results: Simple Model

Ex.	Input Trajectory	d_f	$x(0)$ Bounds	Nodes	Optimal Control
1	large halo, x, y, z only	L/5	$\pm L$ box	400	10^{-8} at node 1
2	small halo, x, y, z only	L	none	125	all 0
3	small halo, x, y, z only	L/2	none	125	10^{-5} at node 1 & 2
4	halo with full state	L/2	none	125	all 0
5	3 nodes: stationary at L2	L	none	125	all 0

We have seen that increasing the number of nodes increases the accuracy of the solution. A larger number of nodes also means a longer processing time, so it is advisable to choose a number just large enough to capture the accuracy for the mission time-length being used, about 30 to 80 per year. (This informed the choice of 125 nodes in the above examples.) In order to quantify this performance of the discretization and optimization algorithms relative to number of nodes, an optimal solution with 25 nodes was chosen as an input to produce a few optimal solutions of more gradually increasing number of nodes. The CPU time was measured along with the accuracy, as measured by the magnitude of violation of the constraints (Fig. 4.15).

Because this experiment is based on a 25 node solution, the error in the optimal output for 25 nodes is significantly lower that it would be for a non-optimal input, or an optimal input of fewer nodes. The exponential decrease in error with increasing nodes can be seen in the remaining data points.

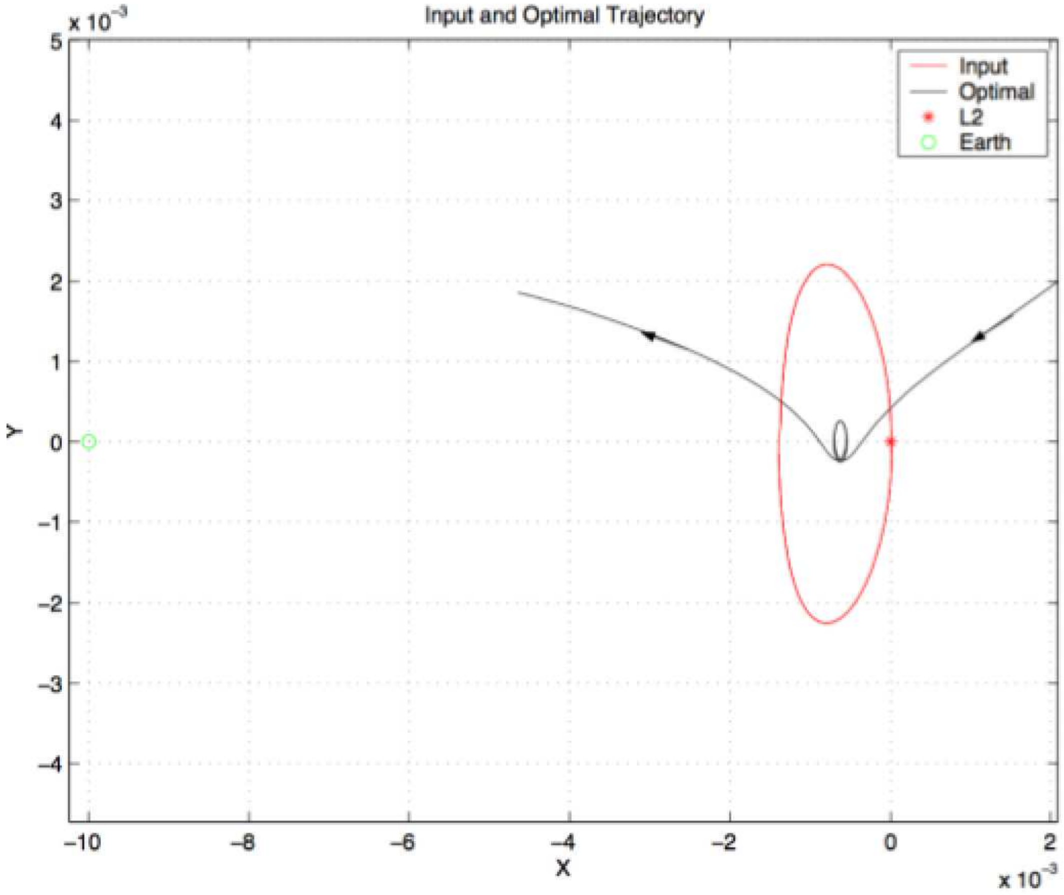

Initial position:

$$
\begin{aligned}
x(t_0) &= -1.377 \times 10^{-3}, & v_x(t_0) &= 0 \\
y(t_0) &= 0, & v_y(t_0) &= 4.600 \times 10^{-3} \\
z(t_0) &= 0.520 \times 10^{-3}, & v_z(t_0) &= 0.
\end{aligned}
$$

FIGURE 4.11 **Simple Model Example 4:** *An Optimal Trajectory for Full Halo Orbit Input,* $d_f = D/2$

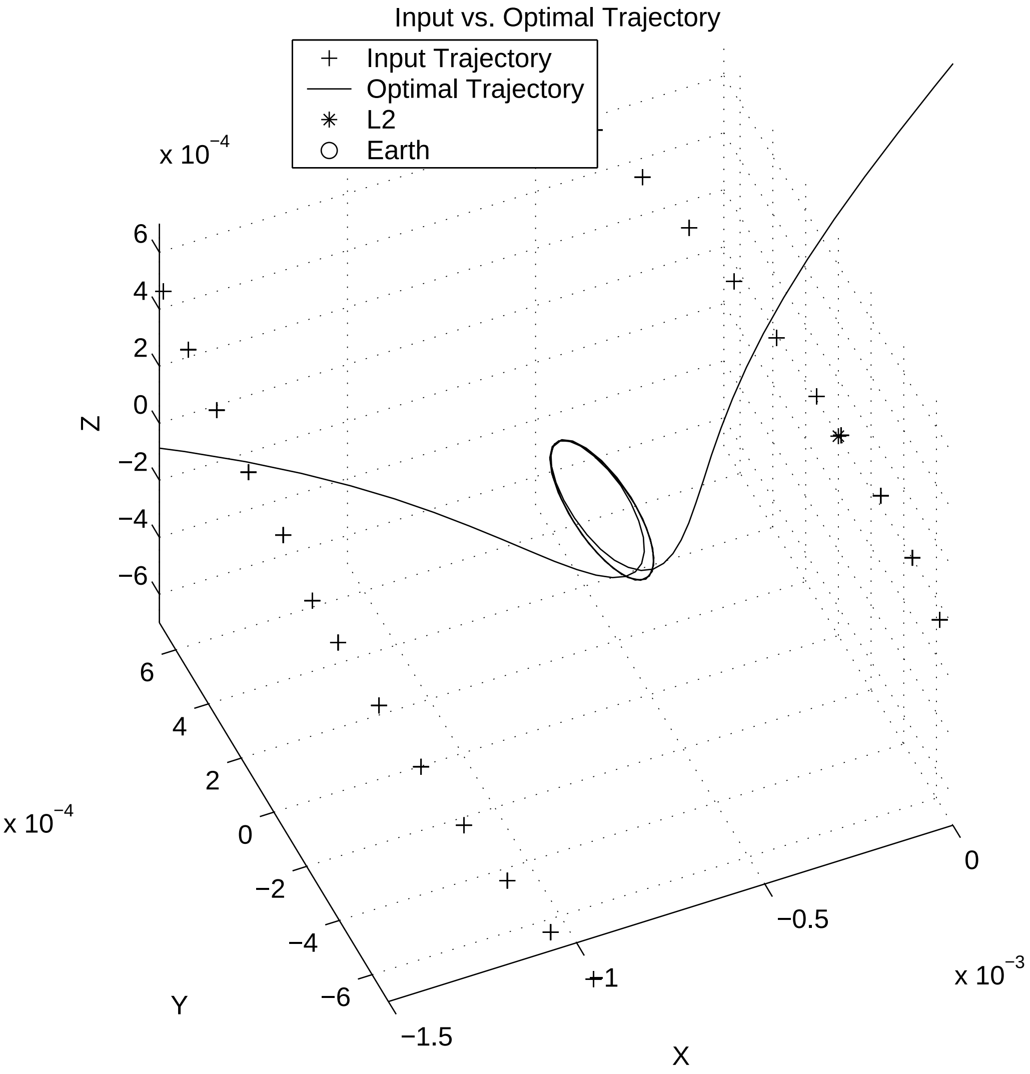

FIGURE 4.12 **Simple Model Example 4:** *A Zoomed View of the Optimal Trajectory,* $d_f = D/2$

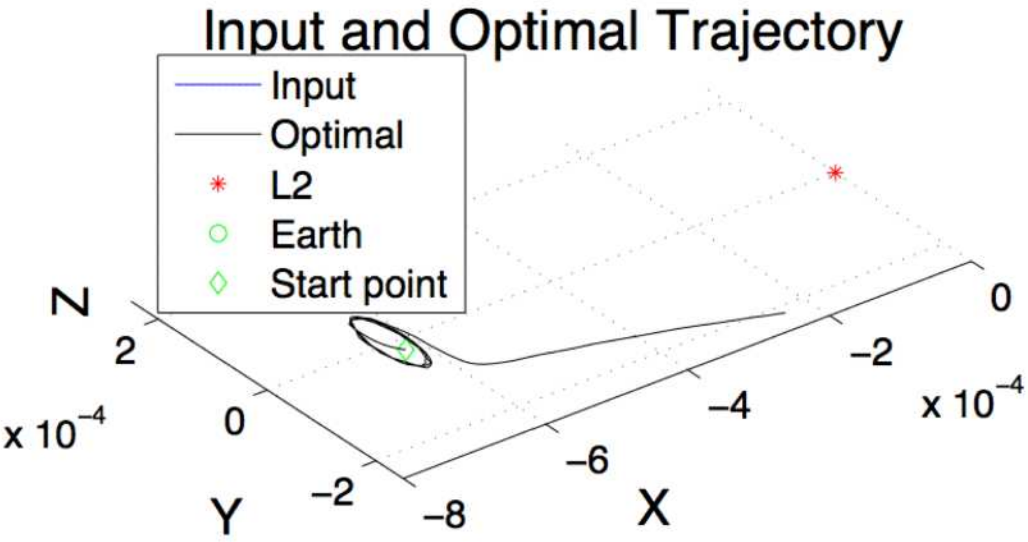

Input Trajectory:

$$
\begin{aligned}
\mathbf{x}(0) &= \mathbf{0}, \mathit{except}\ m(0) &&= 1 \\
\mathbf{x}(2\pi) &= \mathbf{0}, \mathit{except}\ m(2\pi) &&= 1 \\
\mathbf{x}(4\pi) &= \mathbf{0}, \mathit{except}\ m(4\pi) &&= 1.
\end{aligned}
$$

FIGURE 4.13 **Simple Model Example 5:** *An Optimal Trajectory for Stationary L2 Input, $d_f = D$*

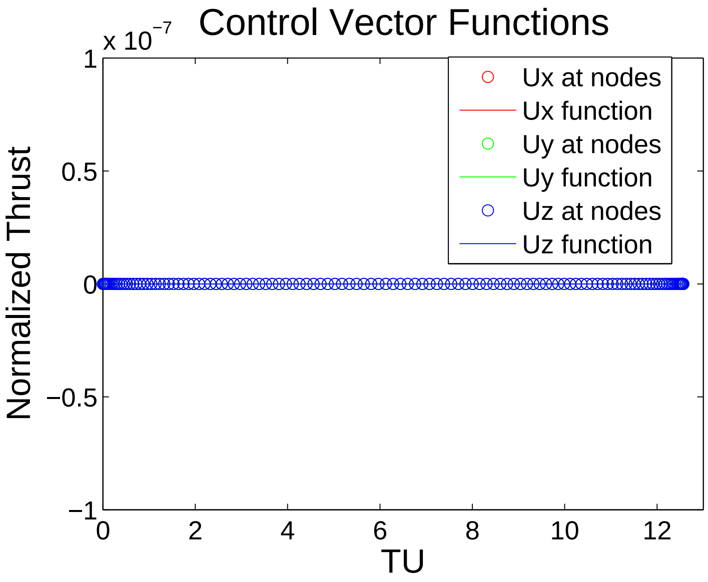

FIGURE 4.14 **Simple Model Example 5:** *Thrust over time*

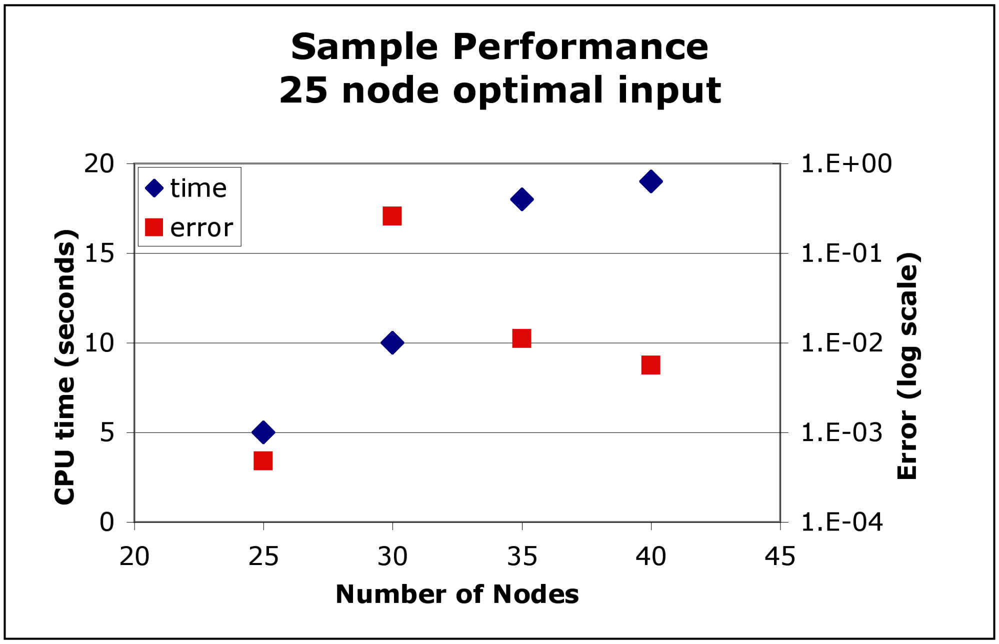

FIGURE 4.15 *Speed and Accuracy vs Number of Nodes*

4.1.3 Perturbed Model Definition

In the following examples the equations of motion include the solar radiation pressure and lunar gravity as perturbations on the force model. The solar radiation pressure is modeled as a force in the positive x direction which varies only with distance. The perturbation of the moon's gravity is modeled as a cyclical force within the x-y plane. It has a mostly negative x direction with a y component that varies over time between positive and negative. Below are the equations for the acceleration due to each which are added onto the acceleration equations in the differential equations of motion (e.g a_x = acceleration added to x acceleration equation).

Solar Radiation Pressure
SRP= $4.6 \times 10^{-6} N/m^2$at 1 AU
surface area = 260 m^2

$$a_x = \frac{.9\ SRP\ (surface\, area)\ cos(angle\, between\, shield\, normal\, and\, -x\, vector)}{(distance\, from\, 1\ AU)^2\ (mass)}$$

Lunar Gravity
P = period of the moon in rotating frame = 29.4 days
M = maximum angle between x axis and L2-moon line
= arctan(Moon-Earth line / L2-Earth line)
$\alpha = M$, time=0 at moon x-axis crossing
g_{moon} = gravitational acceleration of moon at L2 = $6 \times 10^{-6} km/s^2$

$$\begin{aligned} a_x &= \frac{g_{moon}\ cos(\alpha)}{mass} \\ a_y &= \frac{g_{moon}\ sin(\alpha)}{mass} \end{aligned}$$

4.1.4 Perturbed Model Solutions

All of the following results had a maximum thrust magnitude constraint of 1 and final distance constraint of L/2. These first set of three examples use as input the states describing a large halo orbit without velocity information. They vary in the amount of constraints on the position state variables.

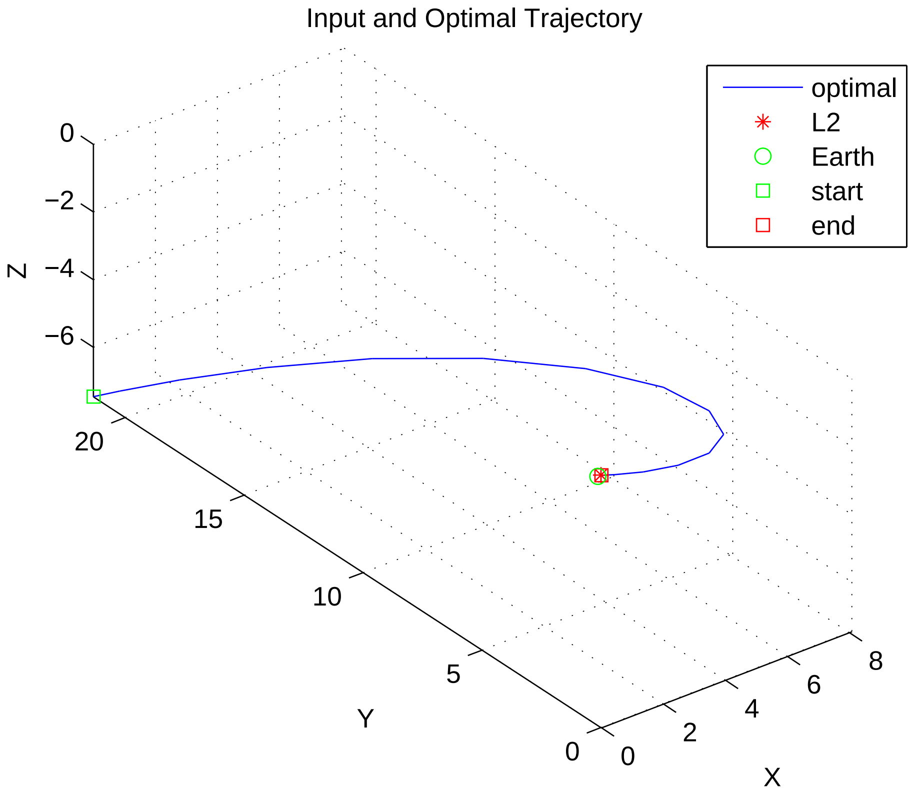

FIGURE 4.16 **Perturbed Model Example 1:** *Optimal trajectory with no bounds on states*

Example 1

With no bounds on the states, the optimal trajectory found starts far from the libration point and makes an arc to bring it within the final distance constraint. The longer the simulation time, the farther away it starts, so the example shown here (Fig. **??**) is for the short time period of $\pi/2$ TU or 3 months. This result is different than with the unperturbed model, where the optimization routine found an optimal closer in size to the input, staying relatively close to the libration point without any path constraints on the position to force that characteristic. This trajectory requires a large thrust profile (Fig. 4.18). This design may be desirable if the trajectory is coming from outside the Earth/Moon system. If this is not the case, we may use position constraints to eliminate trajectories such as this.

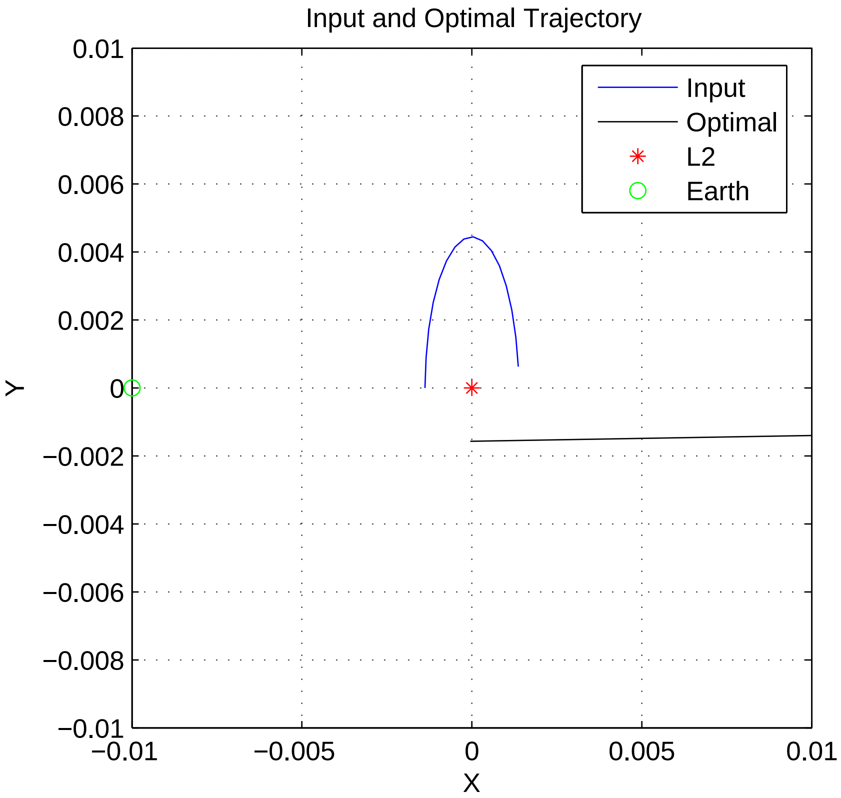

FIGURE 4.17 **Perturbed Model Example 1:** *Optimal trajectory with no bounds on states (zoomed)*

Example 2

Here, a boundary constraint bounds the positions at the starting time to $\pm L$ in each direction. This results in a starting and final position near the libration point, but the trajectory is still very large, making a circle that goes beyond the orbital path of Mars (Fig. 4.19). The control vector part of the solution again requires significant thrust at a few points, especially along the y axis (Fig 4.20). This also could be a useful trajectory shape, and could be further constrained to design a Mars cycler, for example. Also, if closer distance was not as important for a particular astronomical observation mission as it may be for solar power or data transfer, and this were a lower minimum in the cost function than other closer trajectories. (We will see though that in exploring the design space further we find an example of a lower minimum in a smaller orbit.) However, if it is more important to maintain a smaller communication delay or maximum solar power, we can use a path constrain to limit the position of the spacecraft at all times.

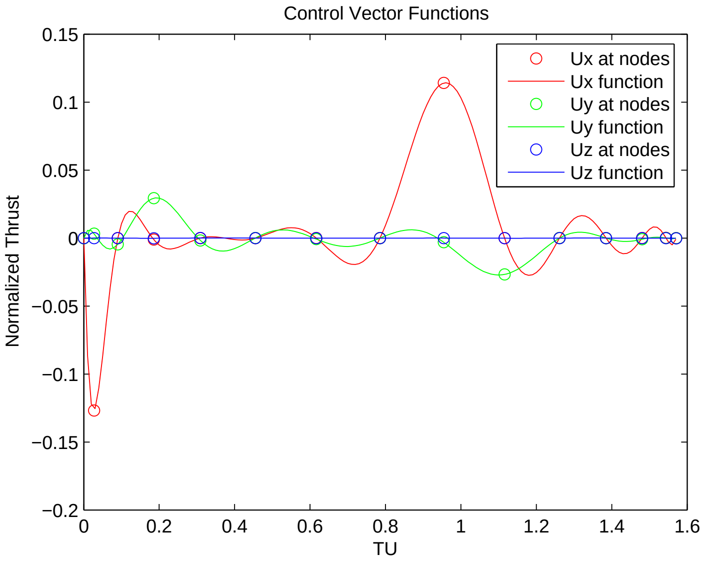

FIGURE 4.18 **Perturbed Model Example 1:** *Thrust over time with no bounds on states*

Example 3

In this last example in the set, in addition to the initial state bound, the positions at all times are bound to $\pm 2L$. This forces the optimization routine to find a minimum in the cost function that results in a trajectory of similar size to the input large halo orbit (Fig. 4.21). Increasing the constraints on the position has increased the amount of fuel needed. This example has a control vector that reaches maximum magnitude of thrust along all three axes at different nodes (Fig. 4.22). Also, it must use a curve rather than small periods of thrust between longer periods of zero thrust (engines off). This would not be acceptable for a telescope mission since the engines must be off for observations. Either further constraints on the controls would be needed, or selection of a different base minimum fuel trajectory found in the design space by varying the input.

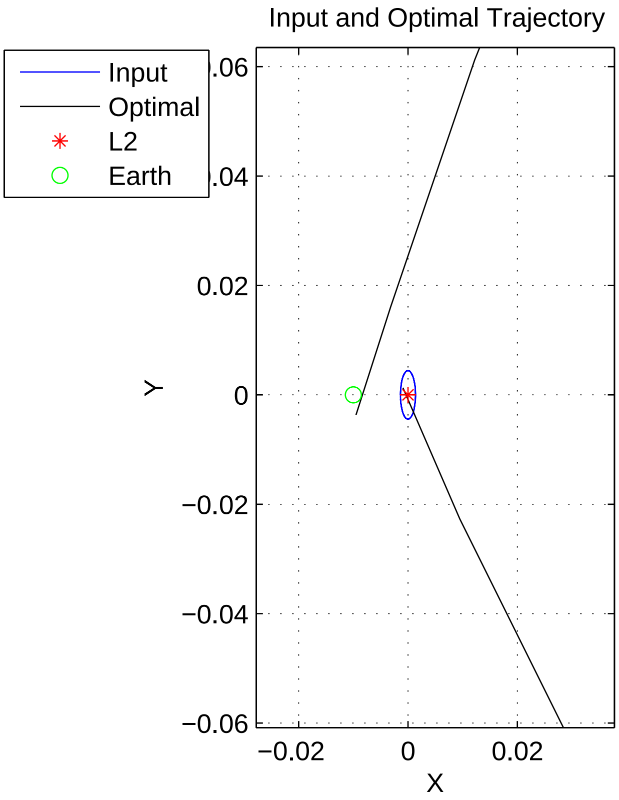

FIGURE 4.19 **Perturbed Model Example 2:** *Optimal trajectory with initial states bound*

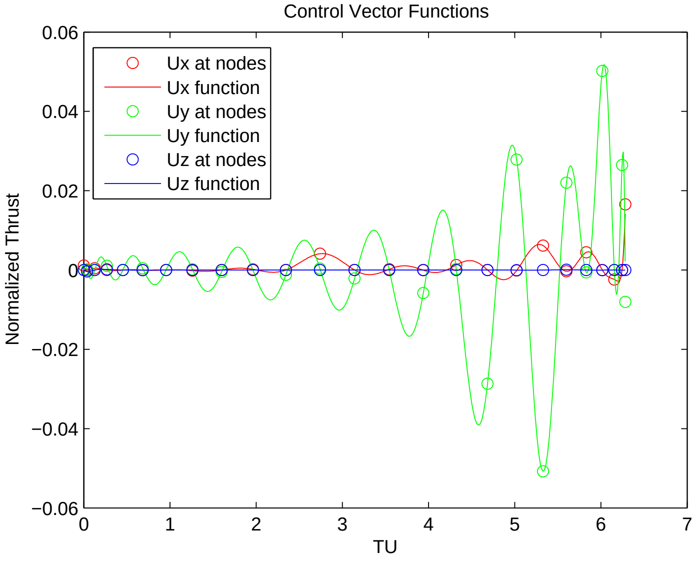

FIGURE 4.20 **Perturbed Model Example 2:** *Thrust over time with initial states bound*

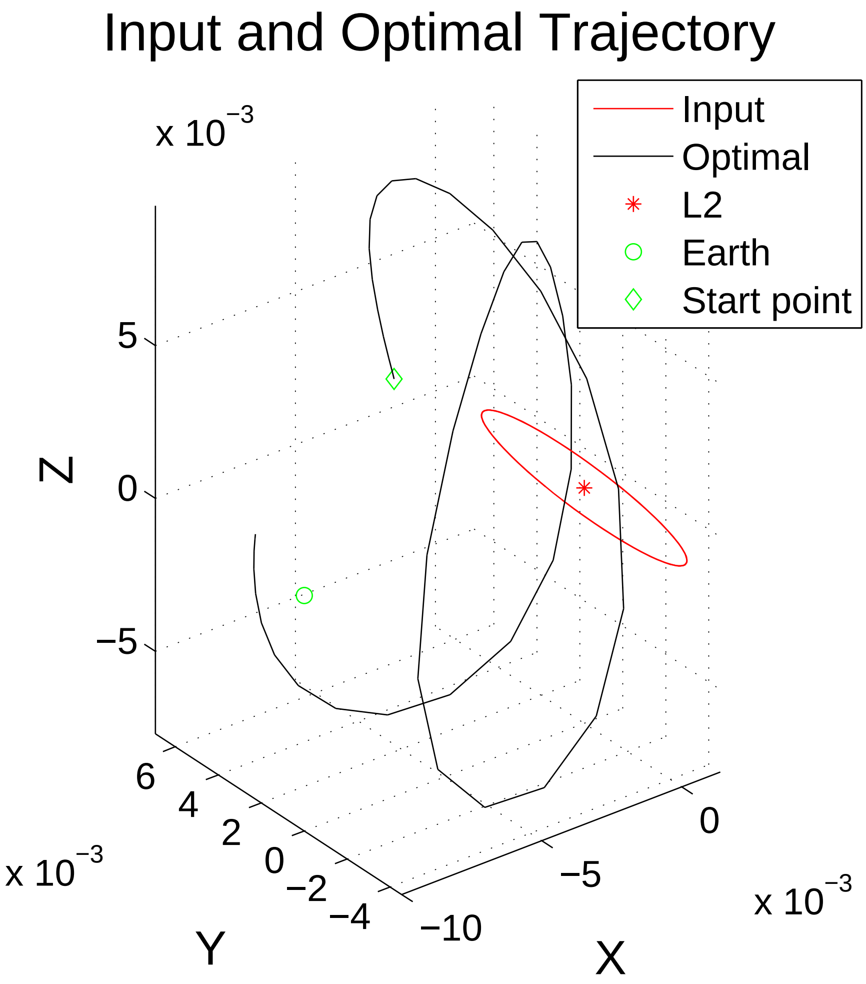

FIGURE 4.21 **Perturbed Model Example 3:** *Optimal trajectory with states bound*

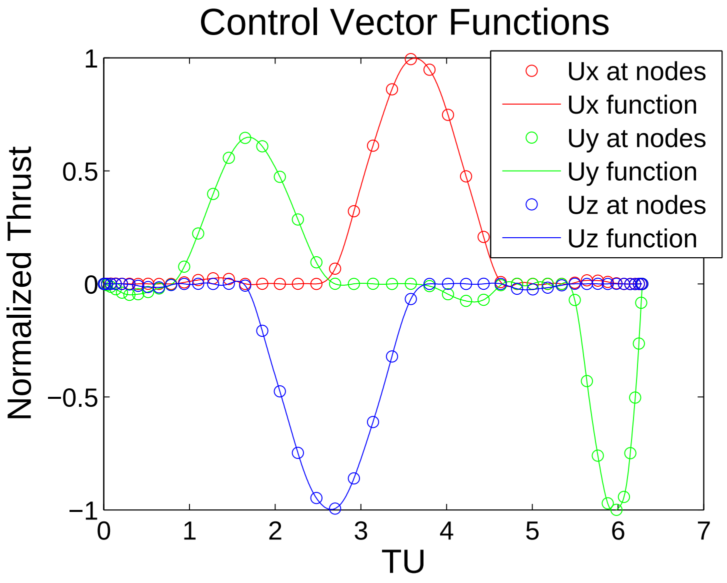

FIGURE 4.22 **Perturbed Model Example 3:** *Thrust over time with states bound*

The last two examples try some inputs very different from the large halo to find the illustrate the variety found by simple input changes. The states have the same boundary and path constraints as the previous example, so the solutions will be limited in size to ±$2L$ about the libration point (Fig. ??). The control vectors of the solution show that much smaller thrusts are required for these trajectories (Fig. ??). This next example uses the three points over time at L2 with no velocity as the input, i.e. all zero values in the state and control vector at three timesteps.

Example 4

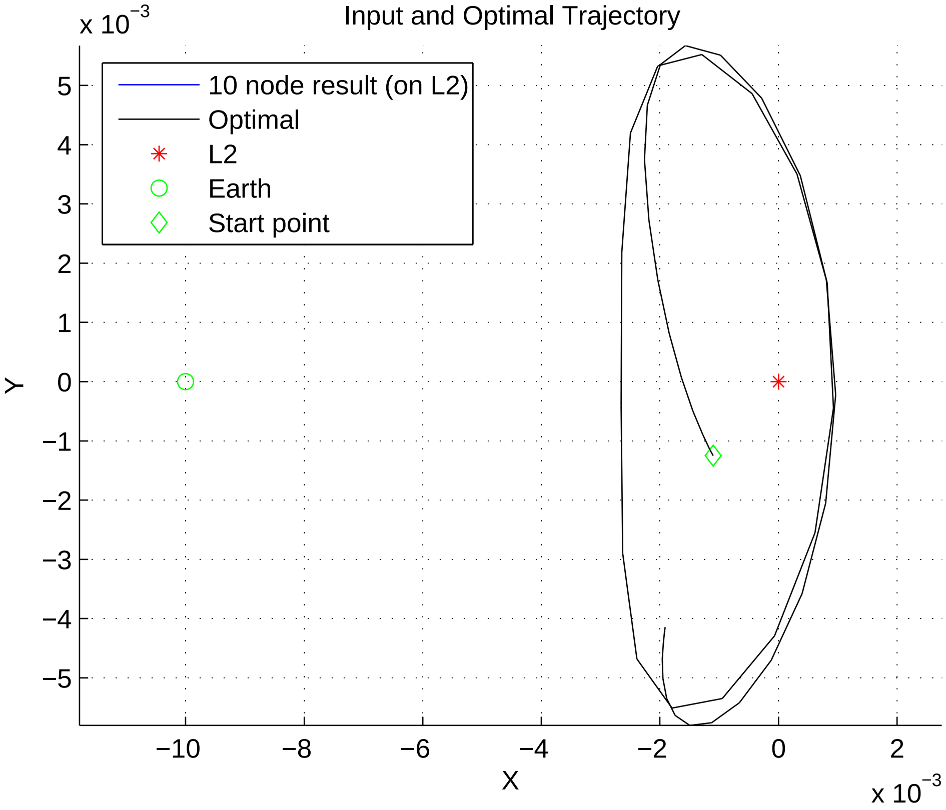

FIGURE 4.23 **Perturbed Model Example 4:** *Optimal trajectory with states bound*

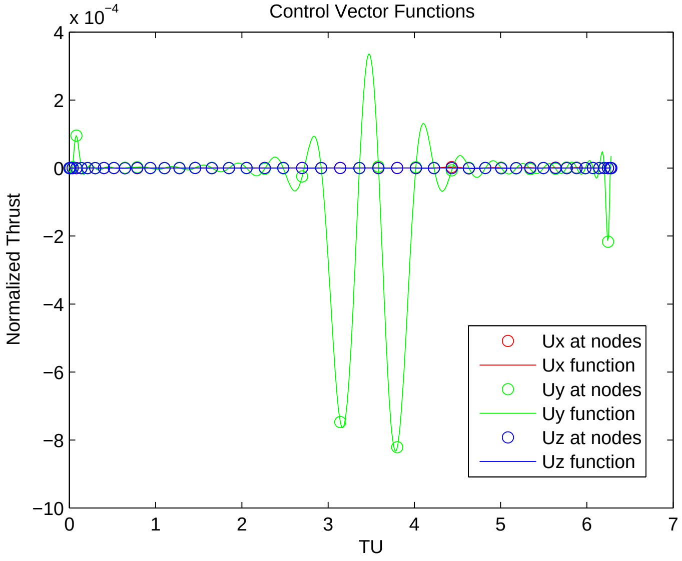

FIGURE 4.24 **Perturbed Model Example 4:** *Thrust over time with states bound*

The last example has an input much like the previous except it is sitting at the point halfway between Earth and L2.

Example 5

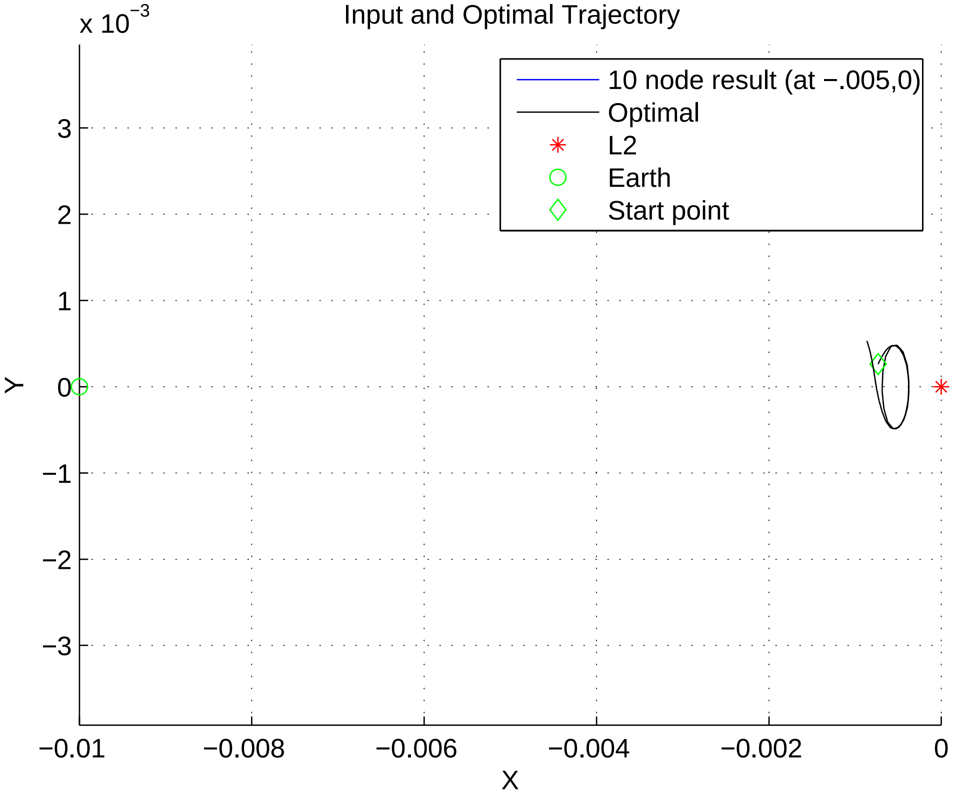

FIGURE 4.25 **Perturbed Model Example 5:** *Optimal trajectory with states bound*

The value of the cost function for the solutions found with the stationary point inputs are much lower minimums than those found with the large halo input, as is reflected by the smaller magnitudes of thrust in the control vectors. This shows the value of exploring the design space by using many types of input trajectories, not just those close to known optimal trajectories for the simplest model.

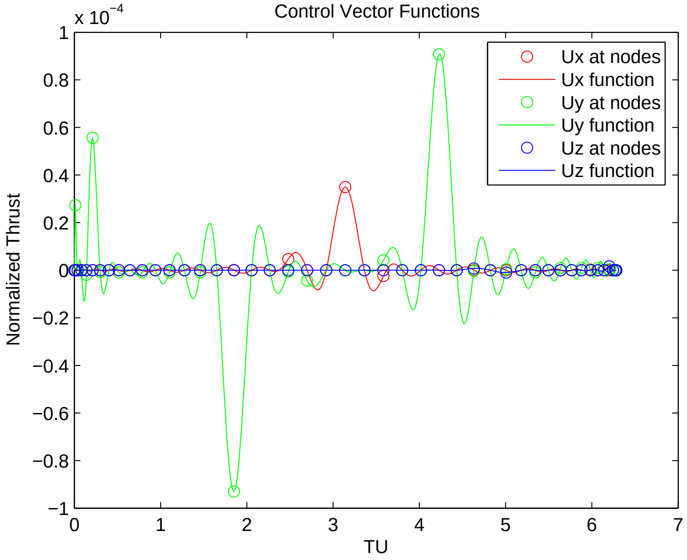

Figure 4.26 **Perturbed Model Example 5:** *Thrust over time with states bound*

Table 4.2

Summary of Results: Perturbed Model. t_f in TU, Cost in DU/TU and m/s

Ex.	Input Trajectory	t_f	State Bounds	Nodes	Cost	Cost
1	large halo, x, y, z only	$\pi/2$	none	15	0.0035	104
2	large halo, x, y, z only	2π	initial $\pm L$	25	0.006	179
3	large halo, x, y, z only	2π	all $\pm 2L$	45	0.36	10730
4	3 nodes: stationary, L2	2π	all $\pm 2L$	45	8.8×10^{-6}	0.26
5	3 nodes: stationary, $x = L/2$	2π	all $\pm 2L$	45	6.6×10^{-6}	0.20

4.2 Mission Constrained Results

These results are all based on the pertubed model, but also include an added constraints on the attitude.

4.2.1 Attitude Constraint Definition

If we assume that the thruster is exactly opposite the center pointing direction of the sensors and/or telescope, the thrust direction is where the sensors are pointed. (If the thrust is zero, we assume it will be pointed in some safe direction as non-thrusting times will be observation times, and observations are all done away from the sun.) So it is the angle between the thrust direction and the direction toward the sun that has a minimum allowed value. The thrust direction is the direction of the vector composed of the total control magnitude along each axis. The direction toward the sun is negative x. Define u_x, u_y, u_z as the total control magnitudes along each axis, and a is the minimum sun-sensor angle The constraint looks like a cone about the x axis with half angle a. It is the negative half of the cone we are concerned with since that is the direction of the sun. From this cone we see the relationship

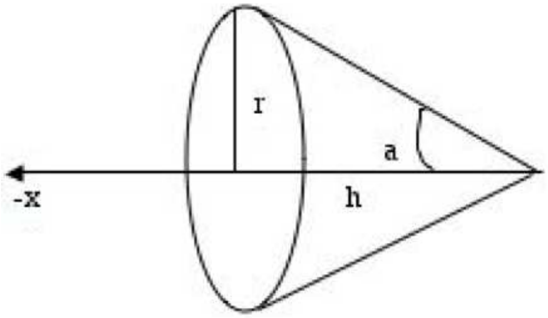

FIGURE 4.27 *The thrust direction (defined by the control vector) must stay out of the sun-view cone.*

$$tan(a) = r/h$$

If we look at the case where the thrust vector is at the boundary of the cone, we have

$$h = u_x, \; r = \sqrt{u_y^2 + u_z^2}$$

So this boundary can be defined with the equation

$$tan(a) = \frac{\sqrt{u_y^2 + u_z^2}}{u_x}$$

We rewrite this equation as

$$u_x tan(a) = \sqrt{u_y^2 + u_z^2}$$

to avoid dividing by zero.

Since we want to define an inequality constraint that holds when the thrust direction vector is **outside** the cone, we want the inequality to be broken when u_y and u_z are zero and u_x is negative. The inequality must also be true for any positive u_x. Since $tan(a)$ will always be greater than zero (a is the desired minimum sun-spacecraft angle between zero and 90 degrees), the inequality constraint describing the attitude restriction is

$$-u_x tan(a) \leq \sqrt{(u_y^2 + u_z^2)}.$$

4.2.2 Perturbed Mission Constrained Model Solutions

This first set of examples correspond to the first set in the Perturbed Model section, but these trajectories include the above constraint, with the maximum angle from the -x axis set to 40 degrees. The attitude over time for the previous and current section are then compared for each example. Since the attitude is not an actual variable but only defined as a constraint of the control vector, it is only valid when the control vector (thrust acceleration) is non-zero. The attitude plots shown here are calculated based on the control vector at each node, as the angle from the -x axis. When the control vector is zero (within tolerance), the attitude is defined as 90 degrees.

Example 1

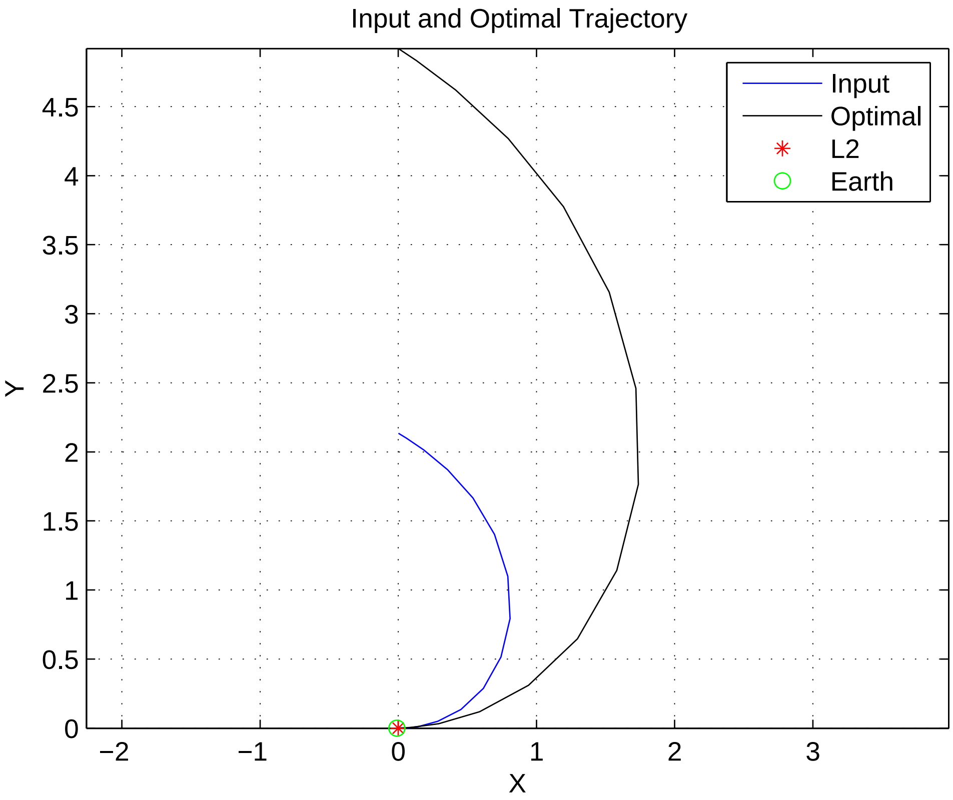

FIGURE 4.28 **Constrained Example 1:** *Optimal trajectory with attitude constraint and states not bound*

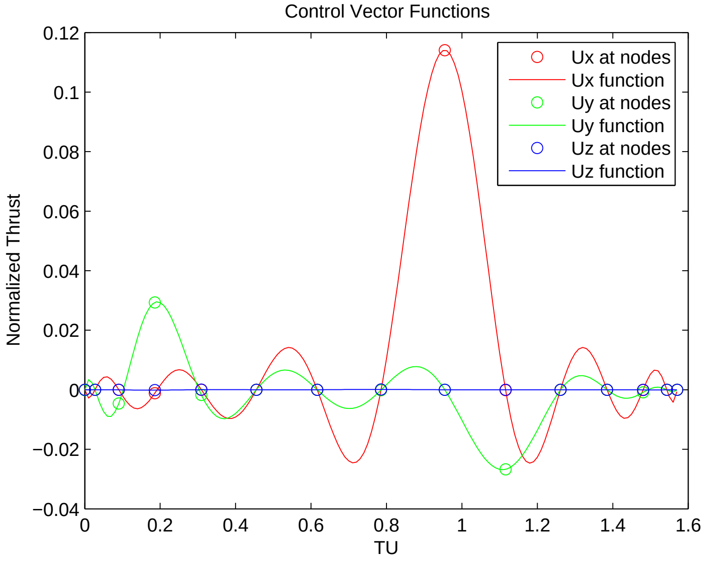

FIGURE 4.29 **Constrained Example 1:** *Thrust over time with attitude constraint and states not bound*

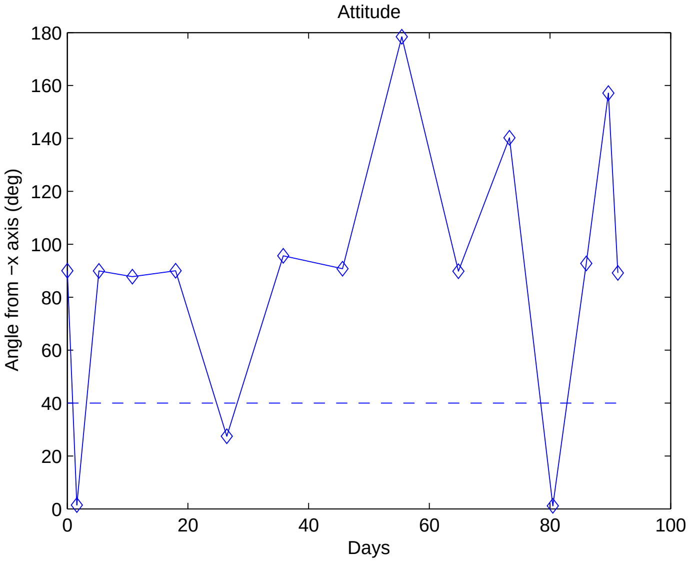

FIGURE 4.30 **Constrained Example 1:** *Attitude over time w/out constraint and states not bound*

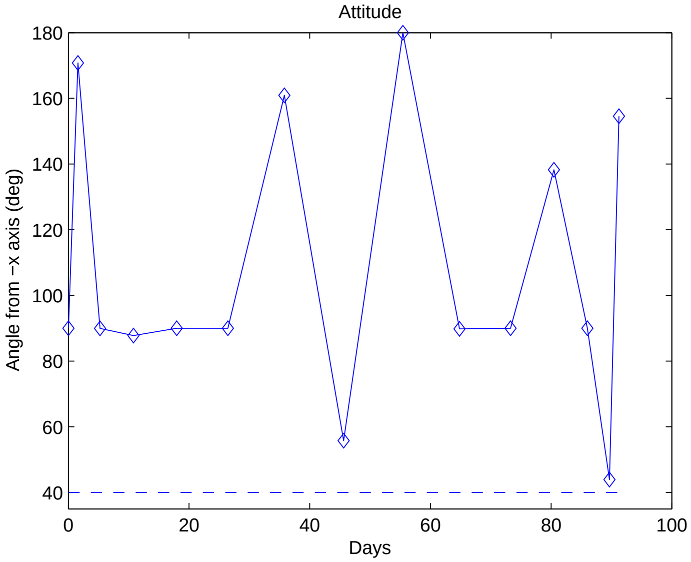

FIGURE 4.31 **Constrained Example 1:** *Attitude over time with constraint and states not bound*

Example 2

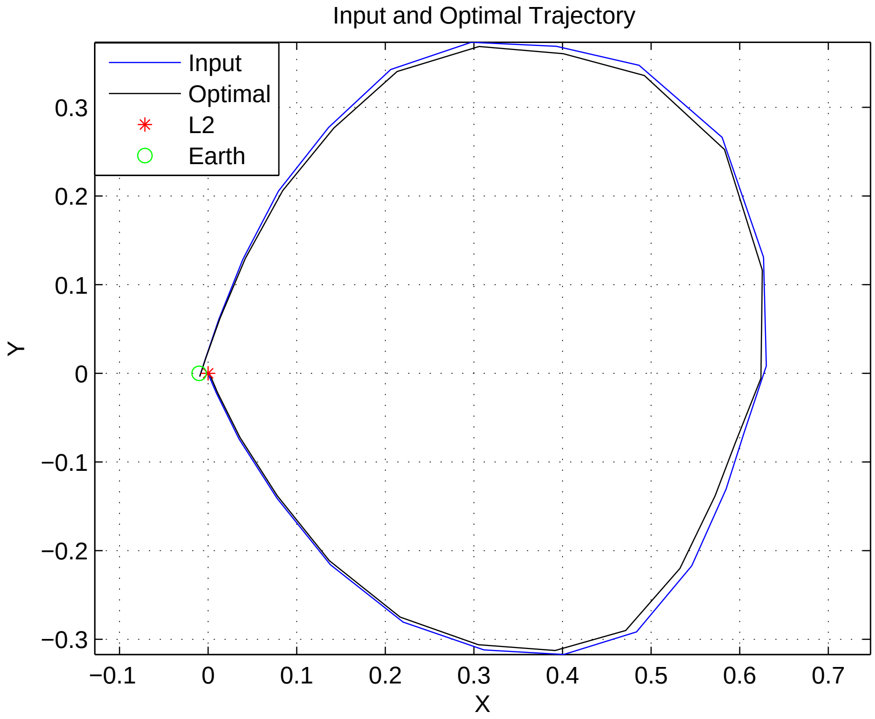

FIGURE 4.32 **Constrained Example 2:** *Optimal trajectory with constraint and initial states bound*

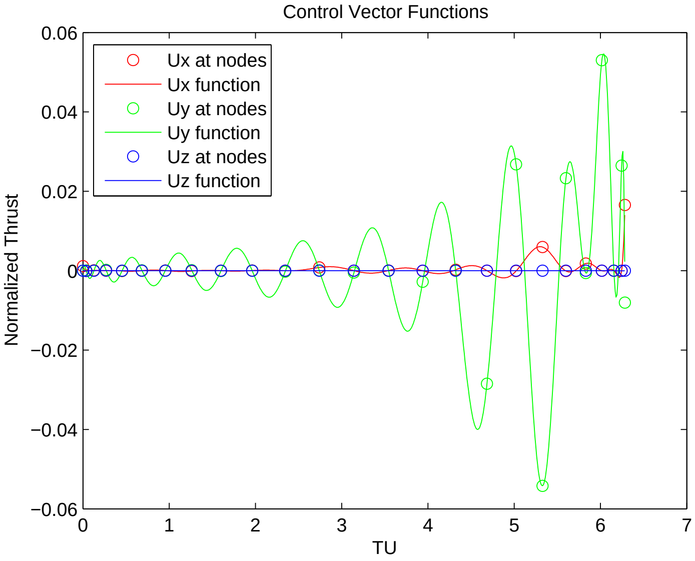

FIGURE 4.33 **Constrained Example 2:** *Thrust over time with attitude constraint and initial states bound*

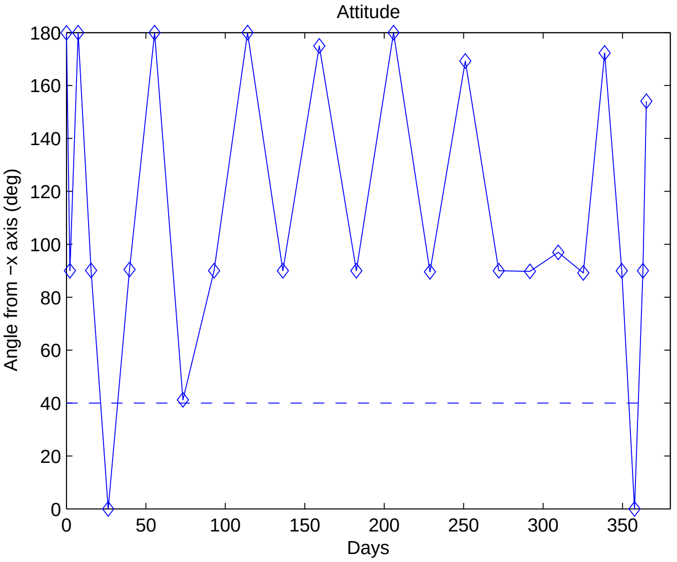

FIGURE 4.34 **Constrained Example 2:** *Attitude over time w/out constraint but initial states bound*

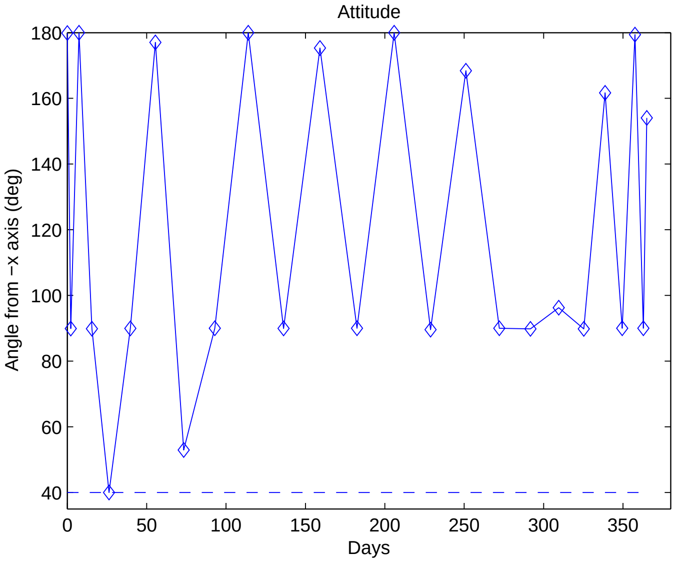

FIGURE 4.35 **Constrained Example 2:** *Attitude over time with constraint and initial states bound*

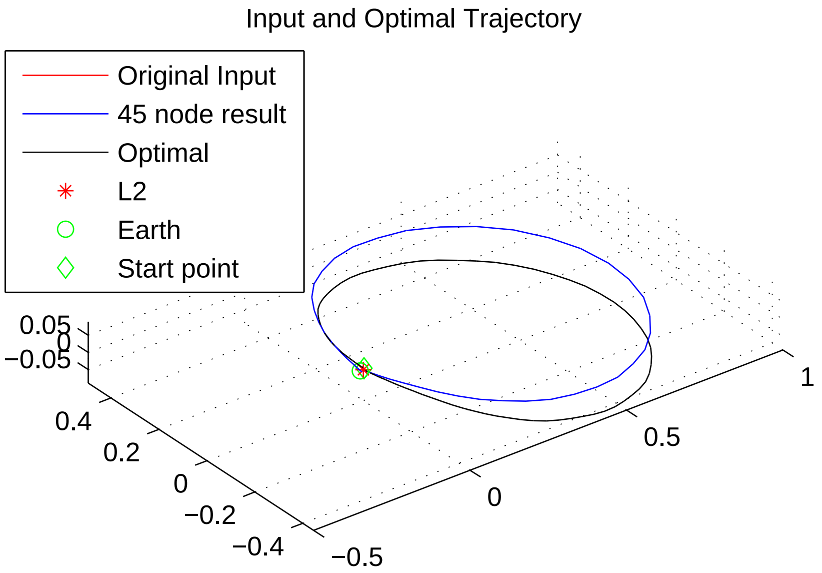

FIGURE 4.36 **Constrained Example 2:** *Optimal trajectory with constraint and initial states bound, twice as many nodes*

By doubling the number of nodes, the control can take advantage of more points to apply a small continuous thrust rather than a few larger maneuvers toward the end of the time period. This reduces the cost by 30%, but this control design would work better for a low-thrust transfer or station mission than for an observational mission which needs long periods with the engine off.

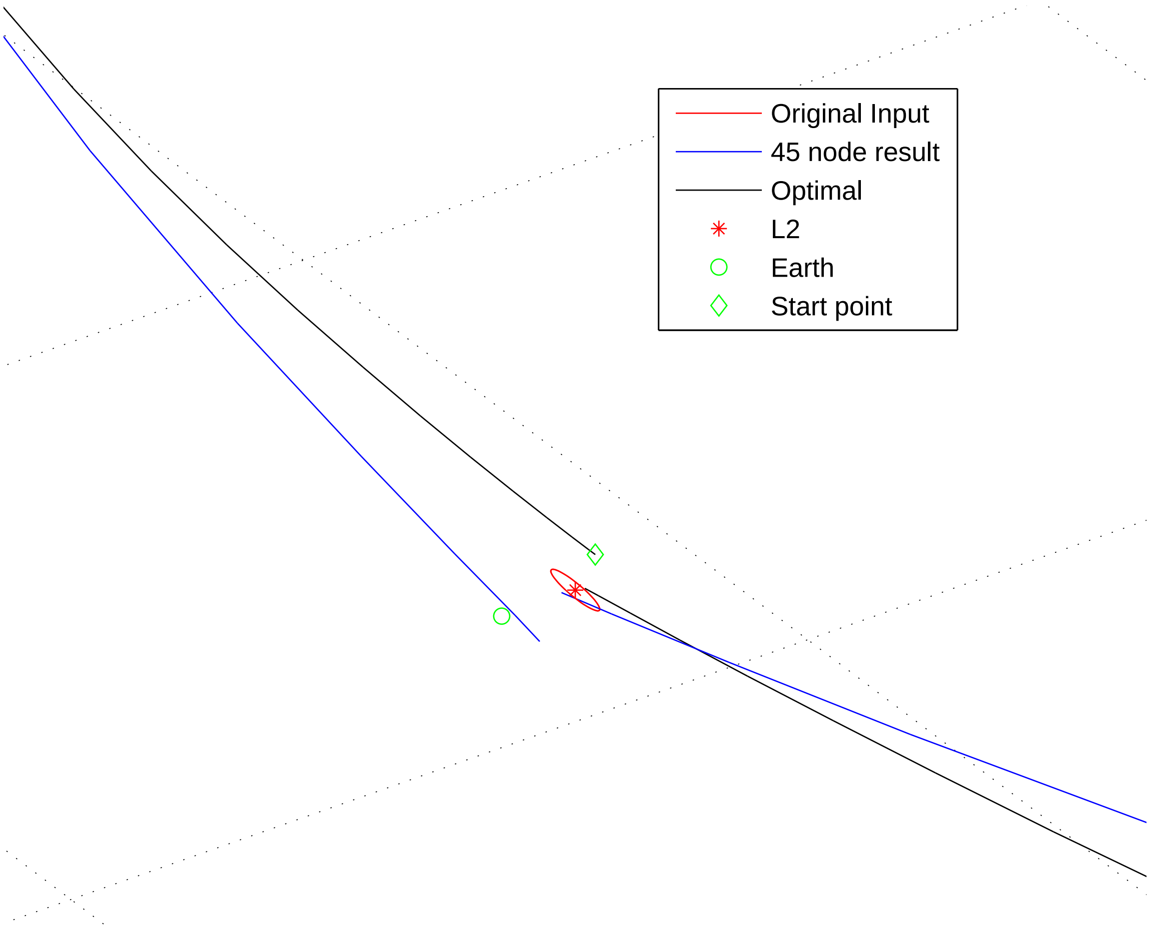

Figure 4.37 **Constrained Example 2:** *Optimal trajectory with constraint and initial states bound, twice as many nodes (zoomed)*

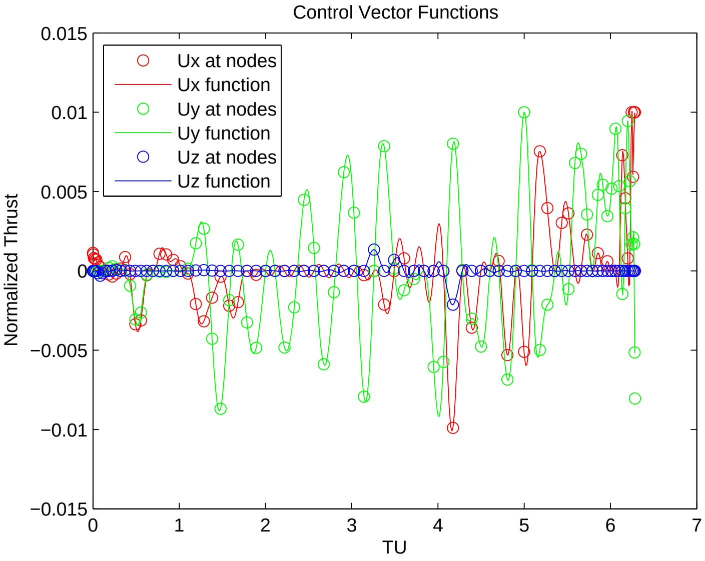

FIGURE 4.38 **Constrained Example 2:** *Thrust over time with constraint and initial states bound, twice as many nodes*

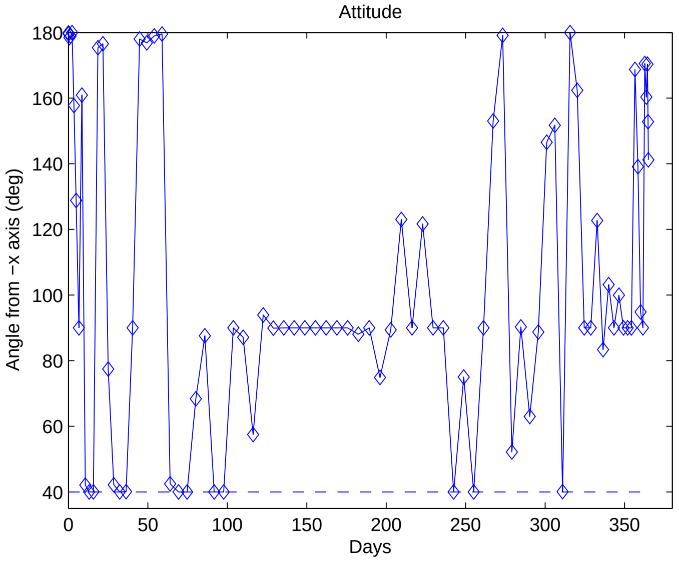

FIGURE 4.39 **Constrained Example 2:** *Attitude over time with constraint and initial states bound, twice as many nodes*

Example 3

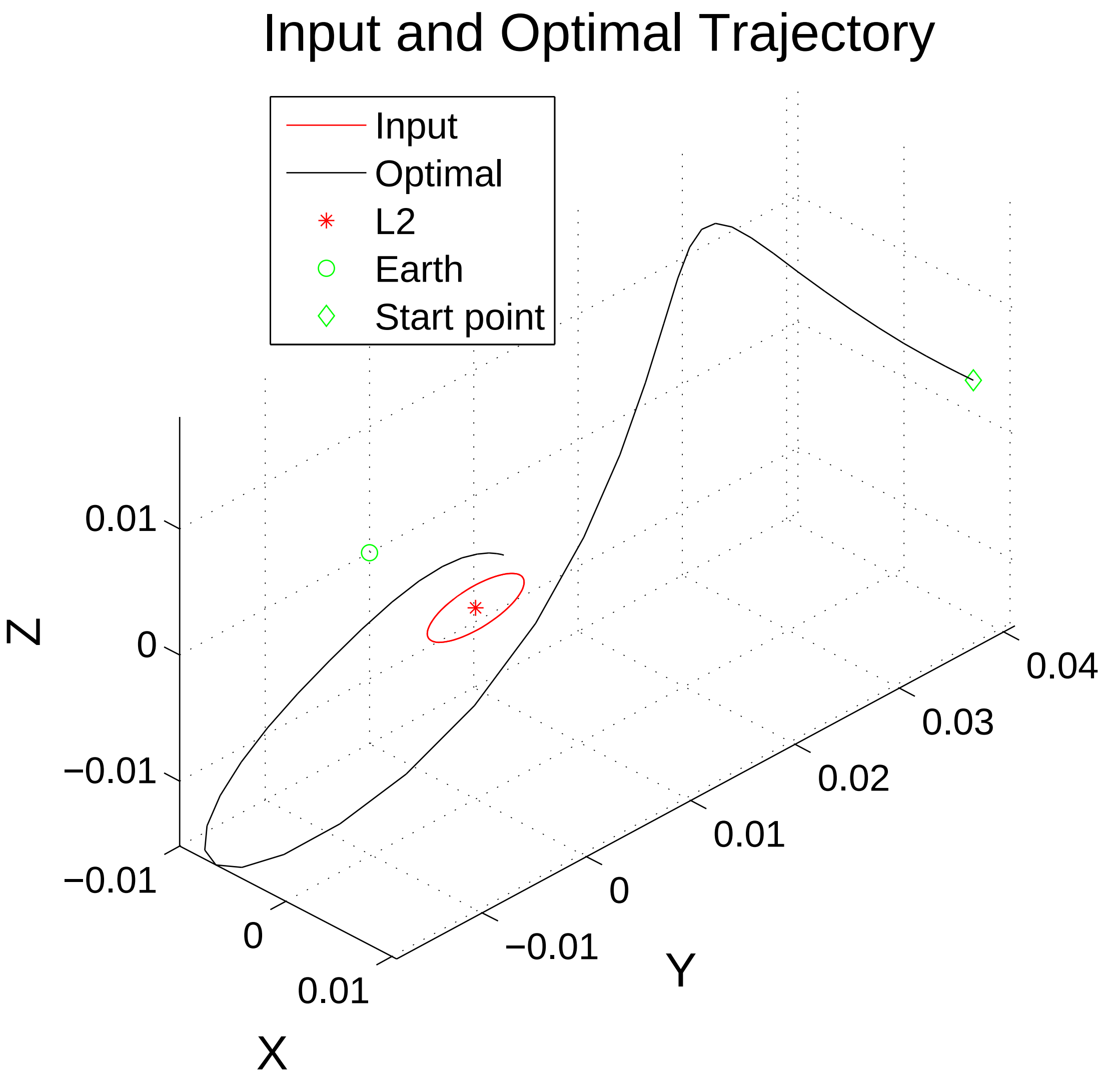

FIGURE 4.40 **Constrained Example 3:** *Optimal trajectory with constraint and states bound*

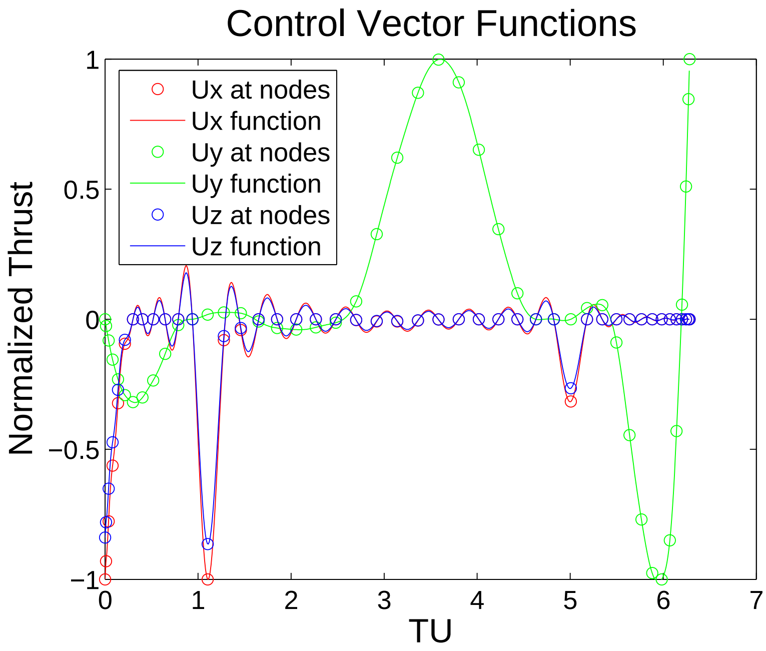

FIGURE 4.41 **Constrained Example 3:** *Thrust over time with constraint and states bound*

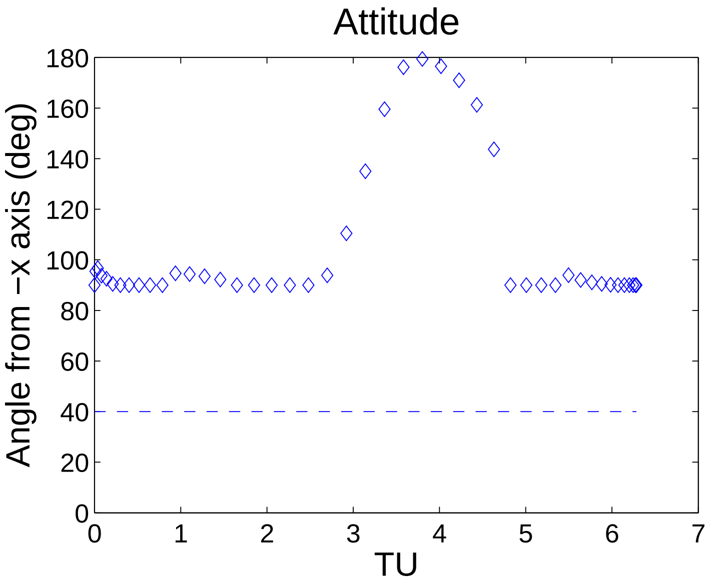

FIGURE 4.42 **Constrained Example 3:** *Attitude over time w/out constraint but states bound*

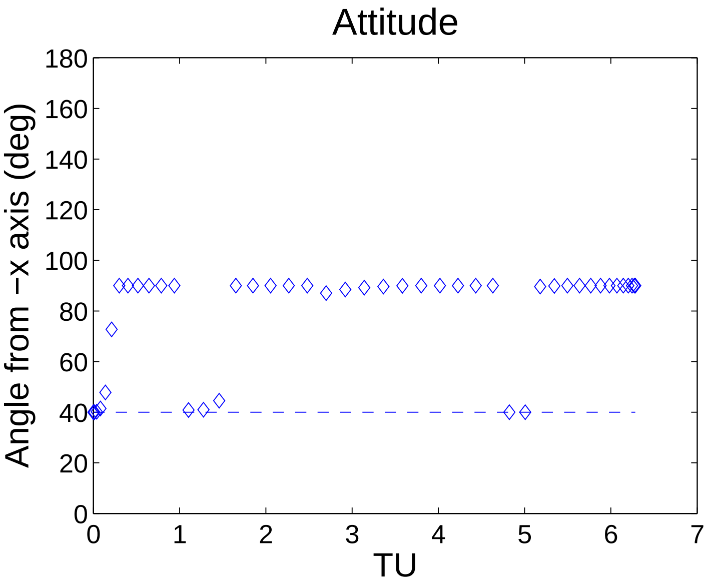

Figure 4.43 **Constrained Example 3:** *Attitude over time with constraint and states bound*

This example corresponds to Example 4 in the previous section, with the attitude constraint applied to the input of a stationary location at L2.

Example 4

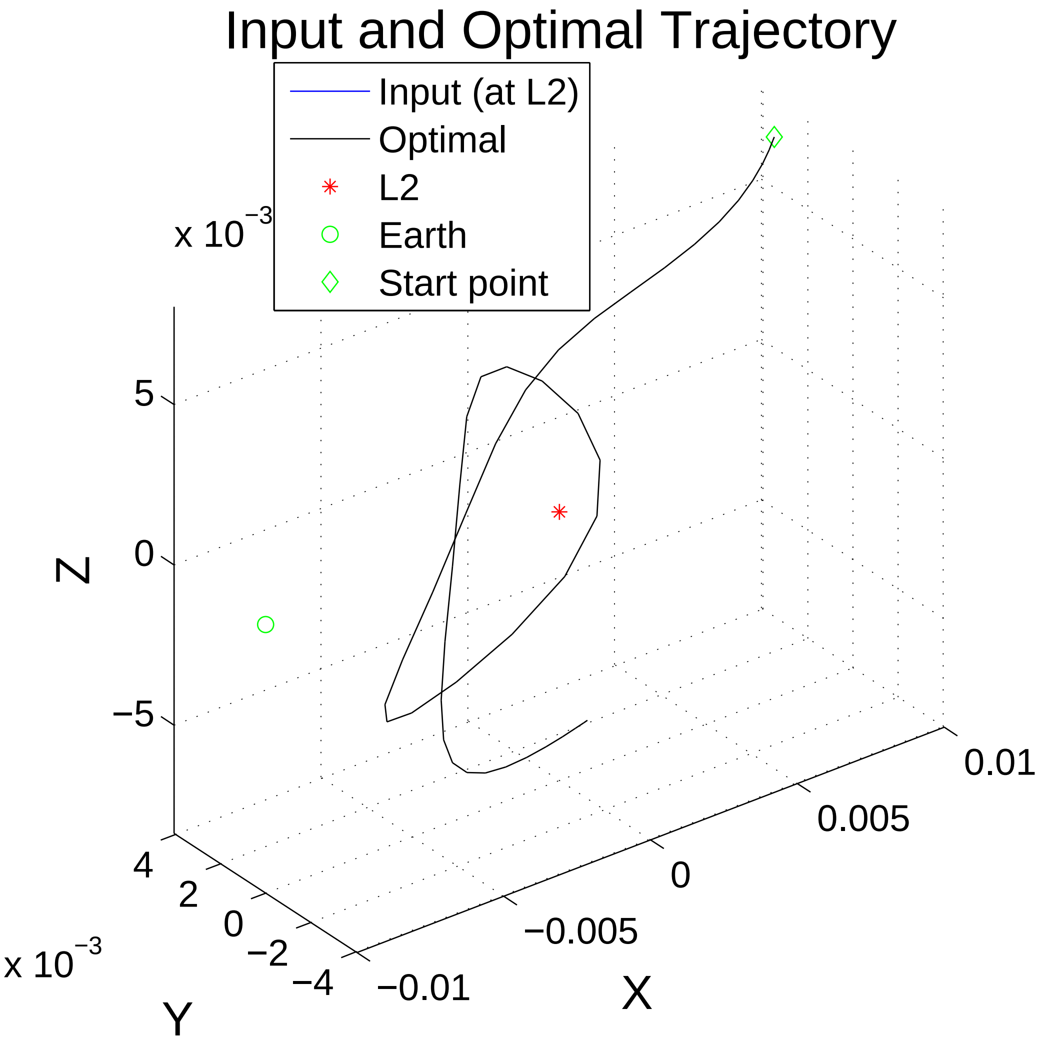

FIGURE 4.44 **Constrained Example 4:** *Optimal trajectory with constraint and states bound*

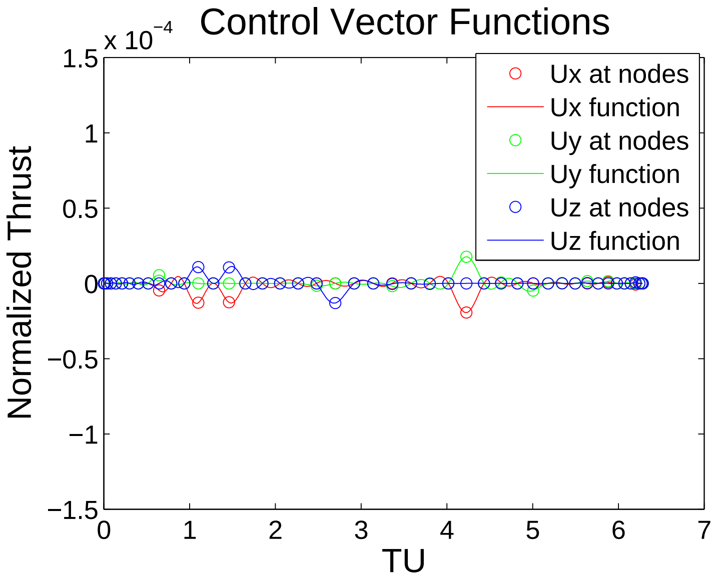

FIGURE 4.45 **Constrained Example 4:** *Thrust over time with constraint and states bound*

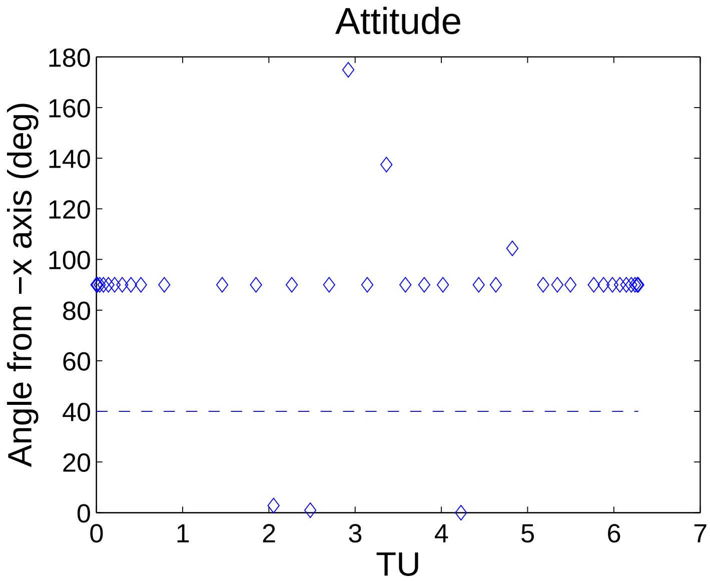

FIGURE 4.46 **Constrained Example 4:** *Attitude over time w/out constraint but states bound*

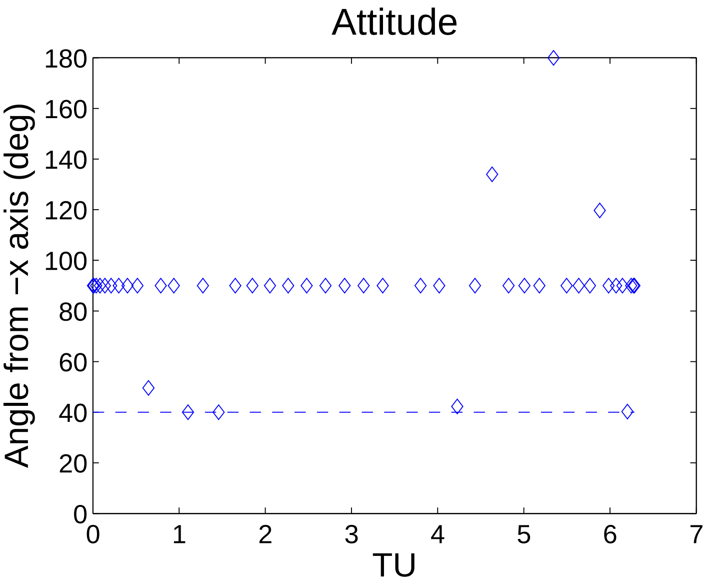

FIGURE 4.47 **Constrained Example 4:** *Attitude over time with constraint and states bound*

This example corresponds to Example 5 in the previous section, with the attitude constraint applied to the input of a stationary location halfway between the Earth and L2.

Example 5

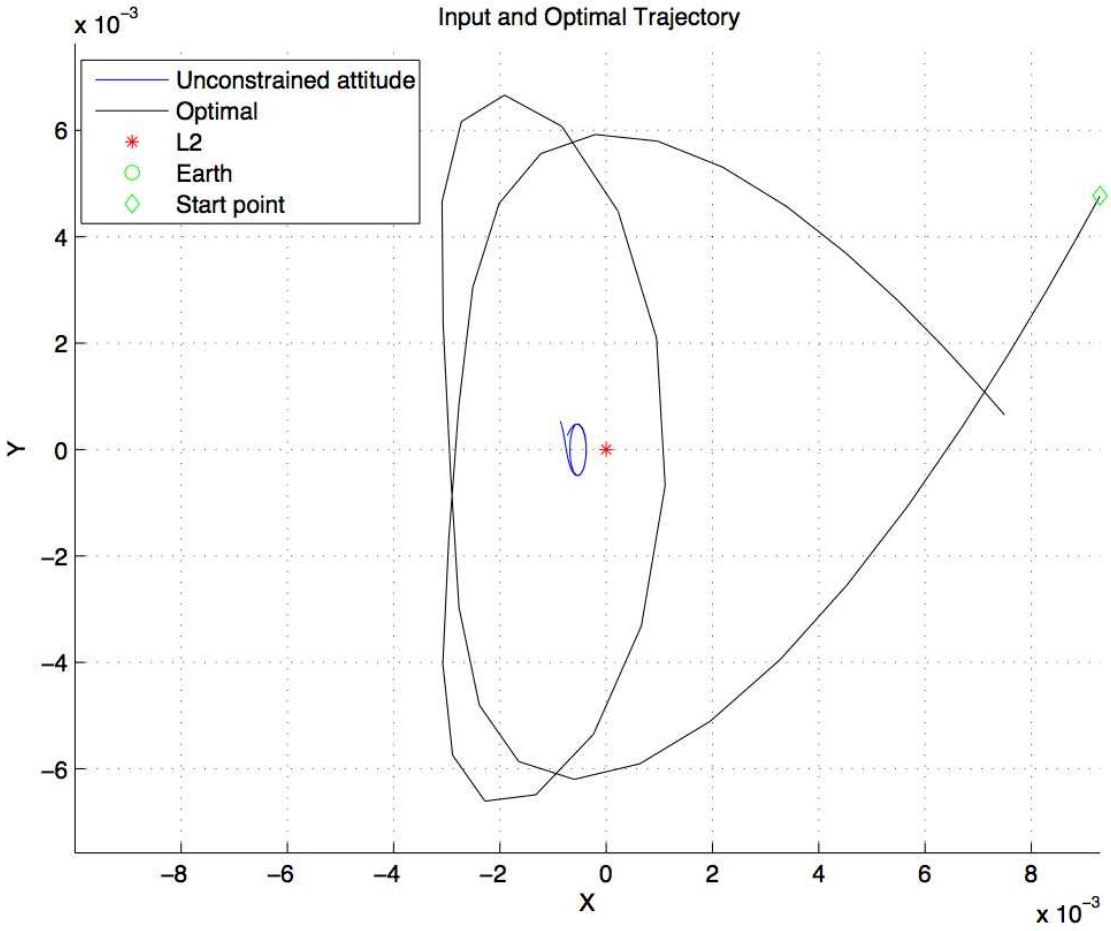

Figure 4.48 **Constrained Example 5:** *Optimal trajectory with constraint and states bound*

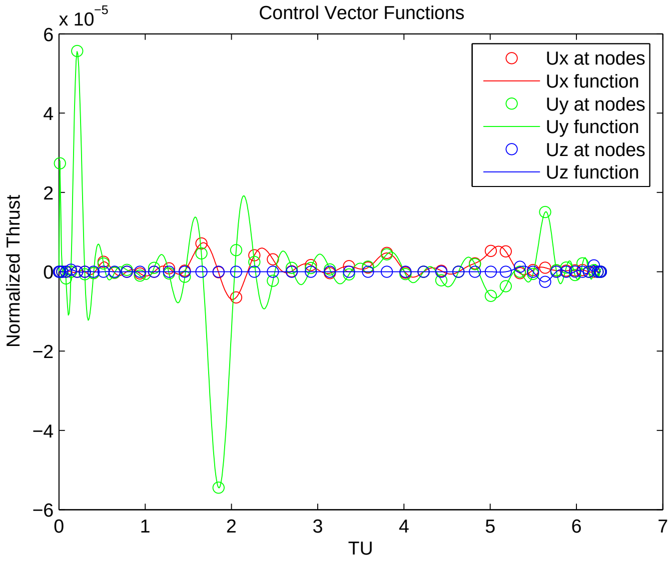

FIGURE 4.49 **Constrained Example 5:** *Thrust over time with constraint and states bound*

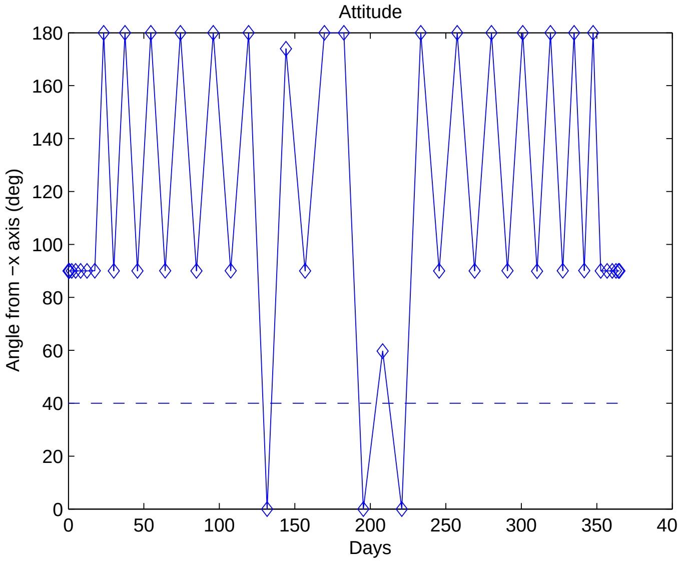

FIGURE 4.50 **Constrained Example 5:** *Attitude over time w/out constraint but states bound*

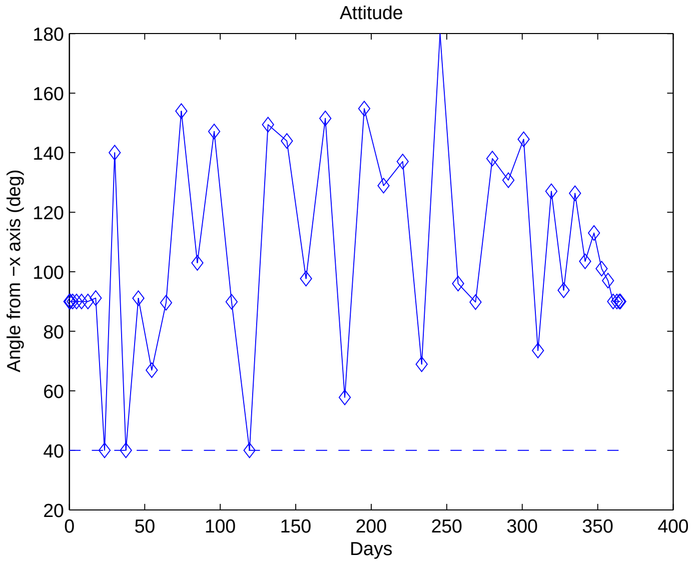

FIGURE 4.51 **Constrained Example 5:** *Attitude over time with constraint and states bound*

TABLE 4.3

Summary of Results: Constrained/Unconstrained Comparison. Cost in DU/TU

Ex.	Input	Min. angle (Unconstr.)	Min. angle (Constr.)	Cost (Unconstr.)	Cost (Constr.)
1	large halo	1°	44°	0.0035	0.0037
2	large halo	0	40	0.006	0.0056
3	large halo	90	40	0.36	0.48
4	L2 point	0	40	8.8×10^{-6}	2.3×10^{-6}
5	$x = L/2$	0	40	6.6×10^{-6}	6.1×10^{-6}

4.3 Comparison with Reference Orbit Approach

In order to make some comparison of these results with what is achieved by the general approach of first choosing a reference orbit and then designing the controls to match this path, the reference orbit approach is here approximated within the concurrent approach. An optimal solution from the simple model results is used as an input. The equation of motion constraints are defined as the perturbed model, and the angle constraint on the control variables is also used. Further path constraints limit the state variables to match that of the input (reference orbit) within a small margin. Constraining the trajectory to match exactly (within feasibility tolerance) would not let the optimization algorithm find a feasible solution, unless a very large number of nodes were used (probably 300 or more). With the margin, an solution within optimality tolerance still could not be found (with 100 nodes), but a 'near-optimal' solution was obtained. This solution matches the input states within the margin except for the x position which varies wildly, as seen in the trajectory in Figure 4.52 and in the x error in Figure 4.55.

The allowed margin is 1, and the error can be seen to jump back to this value for a few nodes at three regular intervals. This mission design problem cannot be solved with the reference orbit approach starting with a model more complex than the circular restricted three-body problem with no perturbations. To restrict the trajectory to match a reference orbit, the approach must be a multi-step process, rather than one concurrent optimization problem, (or take a very long computation time), so it is hard to optimize the whole mission design. For most types of missions, however, an exact path is not a mission requirement, so using a reference orbit approach is unnecessarily making the process longer and more difficult, and not finding the lowest fuel-use overall mission design.

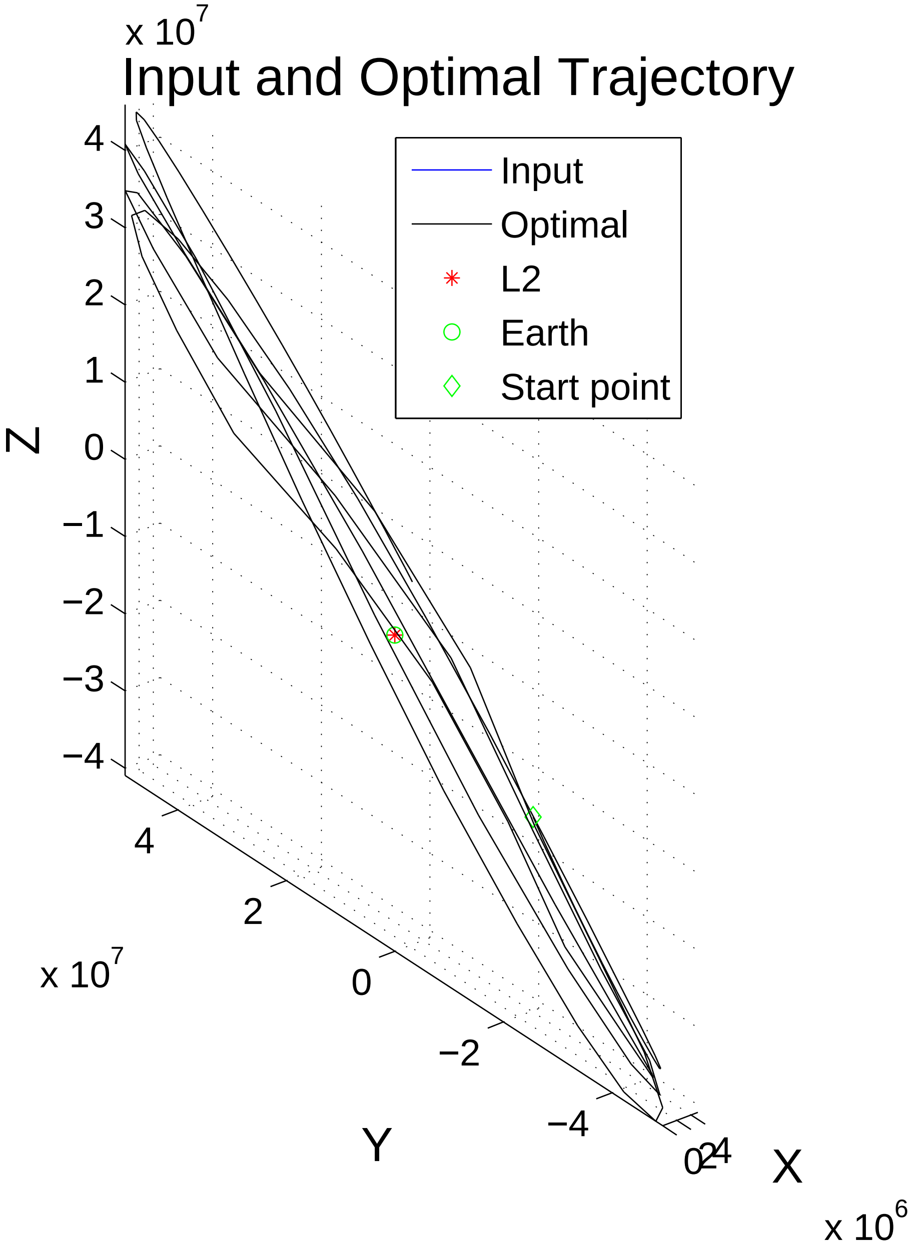

FIGURE 4.52 **Reference Orbit Approach:** *Near-Optimal Trajectory*

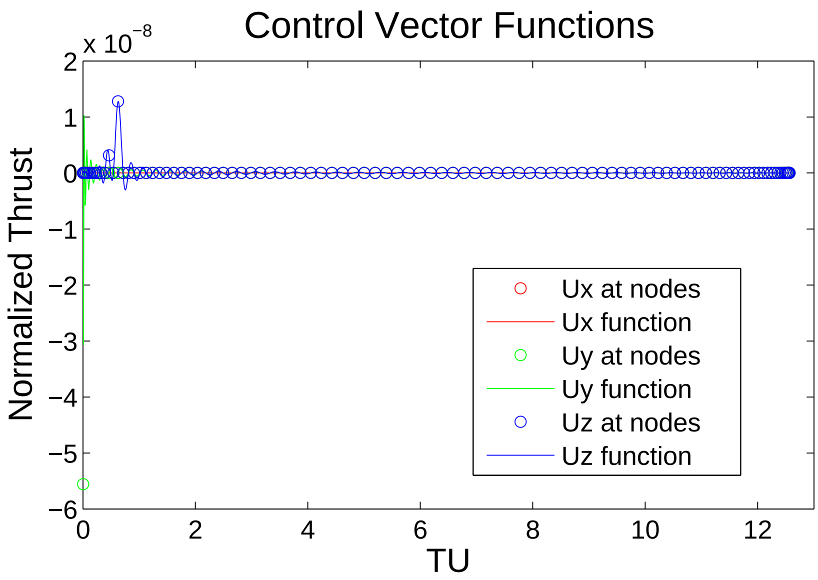

FIGURE 4.53 **Reference Orbit Approach:** *Thrust over time*

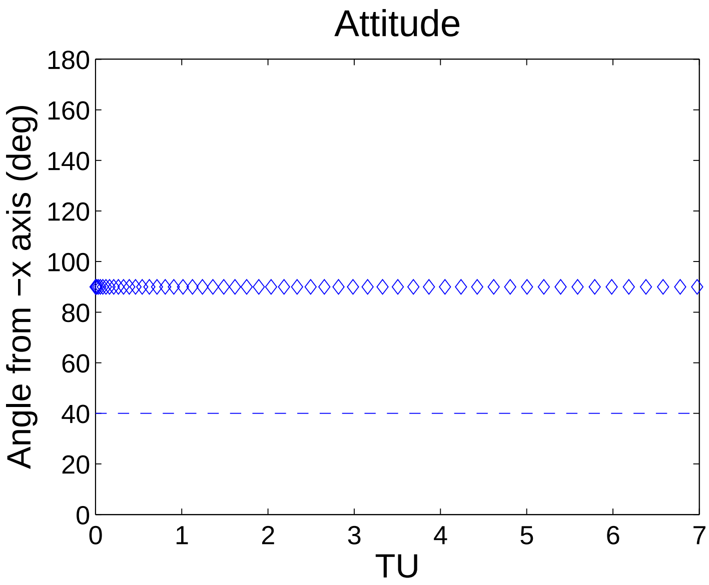

FIGURE 4.54 **Reference Orbit Approach:** *Attitude over time*

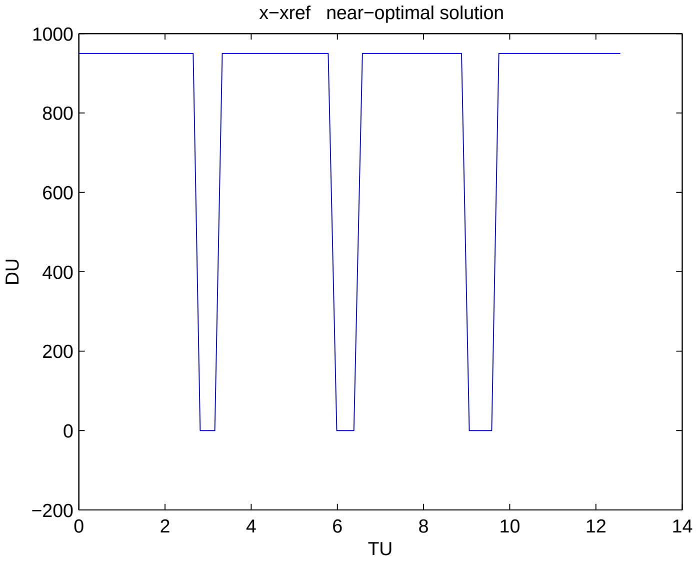

FIGURE 4.55 **Reference Orbit Approach:** *Error in x position state variable*

Chapter 5

Multiple Spacecraft: A Second Example Mission

This chapter shows how easily the design approach can be applied to a different type of mission. Here we look at formation flight in a multi-body system from the perspective of multi-agent control systems. The constraint that demonstrates the ability of the approach is now not the attitude but the distance between spacecraft. The strength of this approach in its ability to solve the design problem concurrently including multiple mission constraints still applies and is discussed.

A distributed space system (DSS) is a multi-agent control system and has long been recognized[36, 37, 38, 39] as a key technology area to enhance the scope of both military[36, 38] and civilian[37, 39] space applications. A particular type of DSS that is challenging to design[36, 37, 39, 38] is a collection of spacecraft in formation. Unlike other multi-agent systems, the design of a DSS has a specific unique requirement: the propellant consumption must be minimal[38, 39]. This requirement stems from the simple notion that if propellant consumption was not a prime driver, then any arbitrary configuration is possible, such as a circular 'halo orbit' whose center is not the gravitating body in an inverse-square gravity field. Thus, to explore various formation configurations, it is crucial to concurrently design the formation and the minimum-fuel control[8, 9]. In other words, we do not necessarily propose to control a particular formation configuration in minimum fuel (i.e. the problem of optimal formation keeping); rather, we follow Ross et al[8] and King[9], and propose that the more fundamental problem is to explore formation configurations (e.g. by varying initial estimates) that are minimum fuel solutions. Thus it is part of the method to find several locally optimal solutions, rather than looking for the one local optimal solution closest to an estimate of a particular formation configuration. Once this problem is solved, the next step would be to evaluate the formation configurations for science or military applications, modify the requirements if necessary, re-solve the problem and re-evaluate the result in conjunction with the propellant expenditures to determine its viability[8]. This approach, of telling agents what to do, rather than how to do it, has been successfully applied for the design and control of a variety of Earth-orbiting formations[8, 9] and station-keeping of libration-point missions[19]. In this paper, we extend the results of Infeld and Murray[19] by adopting the approach of Ross and King[8, 9].

Research on formation at libration points is motivated primarily by the opportunity to create the effect of larger telescopes with a precise formation of smaller telescopes. Currently in design are infrared interferometry missions NASA's Terrestrial Planet Finder[40] and ESA's Darwin[41], as well a NASA x-ray telescope formation mission, Constellation-X Observatory[42]. These are all located at the Sun-Earth L2 point. There are also ideas for formations spaced about a libration point orbit; more of a constellation around the point. An example of this idea is the two satellite constellation Solar Wind Satellite proposed at Sun-Earth L1 by the Department of Defense[43]. Similar to the extensive work on spacecraft formation in the two-body problem, much of the research on the three-plus-body problem is centered around linearization about a reference libration orbit[44, 45, 46, 47]. Thus, the problem is split into two problems: the design of a 'good' reference orbit and formation control around the reference orbit. There are number of procedures for finding a reference orbit[48, 49], many of them are based on a Lindstedt-Poincaré technique proposed by Richardson[50]. In this approach, the perturbation method of Lindstedt is applied to the circular restricted three-body problem with Legendre polynomials as expansion coefficients. The accuracy of this method is then judged by comparing the results to a direct numerical integration of the dynamical equations. This naturally leads to a procedure for improving the initial conditions by shooting methods[49, 51]. Junge et al[51] describe the issues and difficulties of this approach for real-life missions. Having determined the reference orbit in such a manner, formation keeping methodologies can be developed by applying linear control theory to the linearized equations of motion for a neighboring orbit[46, 47]. Many variants of this approach are actively being pursued by various researchers. While such a two-step approach may be viable for certain missions, a simple, unified, single-step approach to the design and control of spacecraft formations was proposed by Ross and King[8, 9]. In this approach, the orbits and the formation control strategies are designed concurrently using the framework of multi-agent optimal control theory. It will be apparent shortly that this framework, described Sec. II, is not the same as applying optimization techniques to compute the standard problem of impulsive trajectory correction maneuvers[52]. In any case, once the problem framework is set up, the optimal control problem it is solved by a Legendre pseudospectral method[12, 13, 14]. This method, summarized in Sec. III, essentially allows the state, control and costate variables to be represented as a series expansion of Legendre polynomials. Thus, although Legendre polynomials are also used, as in Richardson's method, the pseudospectral approach is fundamentally different and resembles a Galerkin method[53]. However, unlike a Galerkin method, all the computations in the pseudospectral method are performed in the time domain by an equivalent representation of the unknown variables in terms of Lagrange interpolating polynomials. The net result is that the semi-analytical framework of series expansion and the computational aspects of finding the coefficients are unified. The computational problem is reduced to a large nonlinear programming problem. Solving such large-scale problems are significantly easier today than ever before: thanks to major advances in practical algorithms pioneered by Betts[54] and Gill et al[16]; these algorithms promise global convergence under mild assumptions[55]. The results of this approach are reported in Sec. V. We briefly note that global convergence does not imply global optimality[55, 56]; we also present globally fuel-optimal solutions in the sense that the propellant expenditures are zero.

5.1 General Framework

Suppose that we have a collection of N_s spacecraft that constitute a DSS. Let $\mathbf{x}^i(t)$ denote the state of the i^{th} spacecraft at time t. This can be the usual 6-vector position-velocity state or any other set (e.g. orbital elements). We assume that the dynamics of the DSS is given in some coordinate system by a set of differential equations,

$$\dot{\mathbf{x}}^i = \mathbf{f}^i(\mathbf{x}^i, \mathbf{u}^i, t; \mathbf{p}^i) \quad i = 1 \ldots N_s, \tag{5.1}$$

where $\mathbf{f}^i$ is a given function, $\mathbf{u}^i$ is the control variable of the i^{th} spacecraft, and $\mathbf{p}^i$ is a vector of (constant) design parameters. In general, the dynamics need not be given in state-space form, as in Eq. (5.1), but for the purpose of brevity we limit our discussion to such a vector-field approach. By defining the state and control variables as,

$$\mathbf{x} = (\mathbf{x}^1, \ldots, \mathbf{x}^{N_s}) \quad \text{ and } \mathbf{u} = (\mathbf{u}^1, \ldots, \mathbf{u}^{N_s}),$$

the dynamics of the DSS may be represented quite succinctly as,

$$\dot{\mathbf{x}} = \mathbf{f}(\mathbf{x}, \mathbf{u}, t; \mathbf{p}). \tag{5.2}$$

Typically, the functions $\mathbf{f}^i$ are all the same so that $\mathbf{f}$ is simply N_s copies of $\mathbf{f}^1$. Let $d(\mathbf{x}^i, \mathbf{x}^j)$ be a generic distance metric (not necessarily Euclidean) between any two spacecraft. If $d(\mathbf{x}^i(t), \mathbf{x}^j(t))$ is a given constant in time, $c^{i,j}$, then we say we have a ***frozen formation***,

$$c^{i,j} \leq d(\mathbf{x}^i(t), \mathbf{x}^j(t)) \leq c^{i,j} \qquad \forall\ t, i, j. \tag{5.3}$$

By $\forall\ t$, we mean for all t associated with the finite lifetime of the DSS whereas by $\forall\ i, j$ we mean for all spacecraft in the system. Further, from the definition of a metric, $d(\mathbf{x}^i, \mathbf{x}^j) = 0\ \forall\ i = j$; hence, we must have $c^{i,j} = 0\ \forall\ i = j$ as a necessary condition for feasibility. Note that Eq.(5.3) is really an equality; the reason for masquerading it as an inequality is to define a ***relaxed formation*** as

$$c^{i,j} - \delta_l^{i,j} \leq d(\mathbf{x}^i(t), \mathbf{x}^j(t)) \leq c^{i,j} + \delta_u^{i,j} \qquad \forall\ t, i, j, \tag{5.4}$$

where $\delta_l^{i,j} \geq 0$ and $\delta_u^{i,j} \geq 0$ are lower and upper tolerances associated with the relaxation. When $i = j$, the tolerances must be zero in conformance with the definition of a metric. Equation (5.4) generalizes Eq.(5.3) since if $\delta_l^{i,j} = \delta_u^{i,j} = 0\ \forall\ i, j$, we recover the representation of the frozen formation defined by Eq.(5.3).

We can define and design various configurations based on various metrics. For example, in libration point missions, in order to generate halo orbits, there may be a forbidden zone such as a disk of radius R centered around the libration point, $\mathbf{y}$; in this case, we define an allowable region for $\mathbf{x}$ as,

$$d(\mathbf{x}^i(t), \mathbf{y}) \geq R \qquad \forall\ i, t.$$

See King[9] for an implementation of such constraints for a variety of Earth-orbiting missions. The requirement that no two spacecraft collide may be articulated as,

$$d(\mathbf{x}^i(t), \mathbf{x}^j(t)) \geq b^{i,j} > 0 \qquad \forall\ t \text{ and } i \neq j.$$

It is apparent that all these constraints (and many more that are specific to a particular mission) can be described in terms of a generic set of a possibly large number of inequality constraints that can be represented as,

$$\mathbf{h}_l \leq \mathbf{h}(\mathbf{x}, \mathbf{u}, t; \mathbf{p}) \leq \mathbf{h}_u. \tag{5.5}$$

In this description of a formation, there is no leader or follower; rather a system of multiple spacecraft. Thus, if any one spacecraft has an additional configuration constraint, it would automatically transfer in some fashion to the remainder of DSS by way of the couplings between the various equations. For example, if there was a mission requirement to designate a particular spacecraft as a leader and designate the others as followers, this can be easily accomplished by picking out the particular index, i, representing the leader. Then, when the leader moves along some trajectory, $t \mapsto \mathbf{x}^i$, the distance metrics along with any additional path constraints, Eq.(5.5), dictate how the remainder of the spacecraft must follow certain trajectories to meet the path constraints; i.e., a formation. Thus, although our framework is based on a collection of DSS, it does not exclude a leader-follower system.

As noted earlier, fuel consumption dominates any DSS design. Translating the fuel consumption cost we had with one spacecraft into the formation context gives

$$J_i = \int_{t_0}^{t_f} \left\| \mathbf{u}^i(t) \right\|_1 \, dt, \tag{5.6}$$

where $t_f - t_0$ is the time interval of interest and $\|\cdot\|_1$ is the usual l^1-norm. Treating the problem to be invariant under time translations allows us to set $t_0 = 0$. A critical modeling issue in the design and control of spacecraft formations is the treatment of the horizon, t_f, vis-à-vis the mission life time. Ideally, we would like to choose t_f to be equal to the mission life. Deferring a discussion of alternative choices for the horizon, we choose the cost functional for designing the DSS to be the total fuel consumption,

$$J = \sum_{i=1}^{N_s} J_i = \int_{t_0}^{t_f} \sum_{i=1}^{N_s} \left\| \mathbf{u}^i(t) \right\|_1 \, dt. \tag{5.7}$$

In certain applications, it may be necessary to require that each spacecraft in the DSS consume the same amount of propellant. This requirement can be stipulated as the so-called isoperimetric constraints,

$$J_i = J_k \quad \forall \; i, k. \tag{5.8}$$

If the equal-fuel requirement is ‘soft’ as in, $J_i \approx J_k$, it can be simply stipulated as an inequality with appropriate upper and lower bounds. Likewise, the allocation of fuel budgets can be similarly defined.

It will be apparent shortly that the problem formulation as posed so far is quite sufficient to handle Libration point formations in the Sun-Earth system if the spacecraft lifetime measured in terms of the duration of the formation is about a year or so as in the Genesis Mission.[57] This is because the number of halo orbits over this duration is about two. For a similar lifespan, the number of orbits in the two-body Earth system range from several hundred to thousands. To properly account for this periodicity, we adapt Bohr's notion of almost periodic functions[58, 59]. Under this framework[8, 60], periodicity may be exploited for an alternative problem formulation based on a modification to optimal periodic control theory. In this problem formulation, we write[8, 60]

$$J = \frac{1}{t_f - t_0} \int_{t_0}^{t_f} \sum_{i=1}^{N_s} \left\| \mathbf{u}^i(t) \right\|_1 \, dt, \tag{5.9}$$

which is a measure of fuel consumed by the DSS averaged over the time period, $(t_f - t_0)$. It is quite tempting to choose *a priori* this time period equal to the period of some appropriately chosen reference orbit; however, a far better option[8] is to let this period be free so that the problem formulation allows the determination of an optimal time period as well. In this case t_f is bound away from t_0 to prevent invalid function evaluations. As noted in Sec. I, this option tells the agents what to do rather than how to do it. In order to facilitate the existence of a solution for this scenario, it is now necessary to impose two additional constraints on the problem formulation:

1. The dynamical equations, Eq.(5.1), must be written in an appropriate coordinate system that facilitates a periodic or almost periodic solution, and
2. Boundary conditions representing the almost periodic structure of the desired solution must be included.

Thus, assuming that the the first condition is satisfied, the boundary conditions for strict periodicity of a ***periodic formation*** can be stipulated as,

$$\mathbf{x}^i(t_0) = \mathbf{x}^i(t_f) \quad \forall\ i. \tag{5.10}$$

Two points are worth noting at this juncture: first, these conditions are not the same as specifying standard boundary conditions because the values of $\mathbf{x}^i(t_0)$ and $\mathbf{x}^i(t_f)$ are unknown. Second, as briefly noted earlier, it is sufficient to stipulate all the constraints of Eq.(5.10) as a single constraint,

$$\mathbf{x}^i(t_0) = \mathbf{x}^i(t_f) \quad \text{for} \ \ i = 1 \tag{5.11}$$

or any other index. This is because, the path constraints will automatically enforce the remainder of the constraints. In this context, we may designate $i = 1$ as the leader, but it essentially reduces to semantics rather than a leader-follower architecture. By relaxing the constraint represented by Eq(5.10) to,

$$\varepsilon_l^i \le \mathbf{x}^i(t_0) - \mathbf{x}^i(t_f) \le \varepsilon_u^i \quad \forall\ i, \tag{5.12}$$

where ε_l^i and ε_u^i are formation design parameters, we easily stipulate a practical means to design and control almost periodic formations[9]. It is clear from these definitions that a frozen formation in the Euclidean metric is a periodic formation but not vice versa. The concept of almost periodicity is not only quite practical, it has significant theoretical advantages. See Fischer[58] for a quick review of almost periodic functions, and Junge et al[51] for practical demonstrations of possible contradictions in applying ordinary Floquet analysis. Deferring the details of applying this framework for Libration point missions to Sec. IV, we note that the problem of designing and controlling spacecraft formations can be summarized as a nonsmooth, nonlinear, multi-agent optimal control problem.

5.2 Libration Point Formations

Remember $\mathbf{r}^i = (x^i, y^i, z^i)$ denote the Cartesian components of a generic spacecraft in the barycentric frame (see Fig. 2.1) of the circular restricted three-body problem.

The spacecraft dynamical equations are well-known and given by,

$$\dot{\mathbf{r}}^i = \mathbf{v}^i \tag{5.13}$$

$$\dot{\mathbf{v}}^i = \mathbf{C}\mathbf{v}^i + \frac{\partial U^i}{\partial \mathbf{r}^i} + \mathbf{u}^i, \tag{5.14}$$

where

$$\begin{aligned}
\mathbf{C} &= \begin{pmatrix} 0 & -2 & 0 \\ 2 & 0 & 0 \end{pmatrix} \\
U^i &\equiv U(x^i, y^i, z^i) \\
U(x,y,z) &= \frac{x^2+y^2}{2} + \frac{1-\mu}{r_A(x,y,z)} + \frac{\mu}{r_B(x,y,z)} \\
r_A^2(x,y,z) &= (x+\mu)^2 + y^2 + z^2 \\
r_B^2(x,y,z) &= (x+\mu-1)^2 + y^2 + z^2.
\end{aligned}$$

The acceleration control $\mathbf{u}^i$ is norm-bounded,

$$\left\|\mathbf{u}^i\right\|_\infty \le u^i_{max}$$

and represents the thruster size of a particular configuration.[29] A multitude of formation options can be defined in various ways. For example, it may be necessary to keep the relative Euclidean distance (l^2-norm) bounded according to,

$$c_2^{i,j} - \delta_l^{i,j} \leq \left\|\mathbf{r}^i(t) - \mathbf{r}^j(t)\right\|_2 \leq c_2^{i,j} + \delta_u^{i,j} \qquad \forall\ t, i, j \tag{5.15}$$

Another option may require to bound the l^∞-norm,

$$c_\infty^{i,j} - \delta_l^{i,j} \leq \left\|\mathbf{r}^i(t) - \mathbf{r}^j(t)\right\|_\infty \leq c_\infty^{i,j} + \delta_u^{i,j} \qquad \forall\ t, i, j \tag{5.16}$$

as an alternative or additional requirement.

In some complex mission geometries, metrics not based on norms may also be used. All the conditions posed above apply to relative formation configurations. In order to design the ensemble about a generic Lagrange point, $L \in \{L1, \dots, L5\}$, an allowable zone can be defined as,

$$c_l^{i,L} \leq \left\|\mathbf{r}^i(t) - \mathbf{r}_L\right\|_2 \leq c_u^{i,L} \qquad \forall\ t, i,$$

where $\mathbf{r}_L$ is the position vector of L. Similar to the relative configuration metrics, other metrics or norms may also be chosen for the allowable zone.

All of the prior conditions apply to a design of the formation system. Thus there is no leader or follower system; rather a system of distributed spacecraft. As noted before, it is possible to transmit conditions to the entire system by stipulating conditions on any one spacecraft. For example, to create a formation along a halo orbit, it is necessary to specify the 'halo conditions' for just one spacecraft. This is also an orbit design problem and can be designed concurrently with the formation by imposing additional conditions. For example, if the formation system is required to be periodic, then it is necessary to impose the periodic conditions for just one spacecraft, say

$$\mathbf{r}^j(t_0) = \mathbf{r}^j(t_f) \tag{5.17}$$

$$\mathbf{v}^j(t_0) = \mathbf{v}^j(t_f) \quad \text{for } j = 1. \tag{5.18}$$

To generate almost periodic trajectories, these conditions

can be relaxed to give

$$\varepsilon_{r,l}^j \leq \mathbf{r}^j(t_0) - \mathbf{r}^j(t_f) \leq \varepsilon_{r,u}^j \tag{5.19}$$

$$\varepsilon_{v,l}^j \leq \mathbf{v}^j(t_0) - \mathbf{v}^j(t_f) \leq \varepsilon_{v,u}^j \quad \text{for} \quad j = 1. \tag{5.20}$$

Although the examples in the following section includes discussion of the actual constraints and values used in the formulation of each, the entire formulations can be seen in the Optimization Formulation chapter (Ch.3). Here it can be seen in the context of formulations for the major example mission, a single large telescope with large solar shield.

5.3 Numerical Examples

We demonstrate our ideas for a two spacecraft system ($N_s = 2$); the extension of this approach to three or more spacecraft is straightforward. Although our method can be applied to any libration point with similar results, we choose to design and control formations about the Sun-Earth $L2$ point because of the multitude of telescope formation missions proposed at this location; thus, we have,

$$\begin{aligned} \mu &= 2.448 \times 10^{-6} \\ \mathbf{r}_L &= (1 - \mu + 0.01, 0, 0)\ DU \end{aligned}$$

in the barycentric frame, where DU is the distance unit equal to the astronomical unit, AU. The origin in these examples is shifted to $L2$ to improve variable scaling, so $\mathbf{r}_L = (0, 0, 0)$. Also, we chose the Euclidean distance, the maximum acceleration and the allowable zone parameters as the design parameters. The separation parameter between the two spacecraft is chosen to reflect the spread of an interferometry mission. The TPF requirement is a 1km range[40]. The next generation of 'hypertelescopes' being explored by optical engineers[61] will use even larger baselines for resolution of smaller objects. At 150 km, characteristics of Earth-sized planets several parsecs away can be directly observed. At one million km, the hypertelescope will angularly resolve neutron stars, which are hundreds of parsecs away. We choose 15 km as the separation for our first two examples. In problem formulations with constraint dimensions this small in comparison to the state variable size (4 orders of magnitude difference), issues of scaling must be resolved in order to obtain optimal solutions. In the last example, the separation is much larger, approaching one million km, which reflects the design of a constellation of observers, similar to the SWS proposal[43], or the outer edges of the DSS neutron star observer of the distant future.

Example 1

In the first example, we consider a fixed-horizon problem, and set $t_f = 3.5\ timeunits(TU)$ (about 205 days). The time unit is equal to the period of the rotation system, which is the inverse of the frequency, 2π radians per year. In seeking a relaxed formation with a separation of 1×10^{-7} DU (about 15 km), we set the design parameters as,

$$
\begin{aligned}
c_2^{i,j} &= 1 \times 10^{-7}\ DU \quad \text{for } i \neq j && (5.21)\\
\delta_2^{i,j} &= 5 \times 10^{-6}\ DU \quad \text{for } i \neq j && (5.22)\\
u^i_{max} &= 0.001\ DU/TU^2\ \forall\ i && (5.23)\\
J_i &= J_k \quad \forall\ i,k, && (5.24)
\end{aligned}
$$

where TU, the time unit is $1/(2\pi)$ of the period of the of the primary system; i.e. a year for the Sun-Earth system. The input states and controls (the starting point for the optimization algorithm) were found by propagating an initial state and applying enough thrust along the x axis at the step closest to crossing the $x - z$ plane to make the x velocity zero at the next step. This was done for 3 maneuver and propagate cycles, producing a trajectory tracing a little further than one ‘orbit’, and a final time of 3.5 TU (thus the t_f defined above). This set of states and controls are the input for both spacecraft. This means the initial estimate of the solution is infeasible since the separation is below the minimum bound. The initial state that produced the input for this example is (in DU and DU/TU):

$$
\begin{aligned}
x(t_0) &= 0.0 \times 10^{-3}, & v_x(t_0) &= 1.0 \times 10^{-3}\\
y(t_0) &= 2.5 \times 10^{-3}, & v_y(t_0) &= -4.5 \times 10^{-3}\\
z(t_0) &= 1.0 \times 10^{-3}, & v_z(t_0) &= -1.0 \times 10^{-3}
\end{aligned}
$$

To reduce the computation time, the initial state of the solution was bound to a box of 0.001 DU on either side of the about input initial state. Periodic constraints are not imposed but the isoperimetric constraint of equal-fuel consumption is required (Cf. Eq. (5.24)).

As noted earlier, we used DIDO[15] with SNOPT[16] to solve the multi-agent optimal control design problem. A solution to the problem for a choice of 100 nodes (roughly, a 99th-order Legendre polynomial) is shown in Fig. 5.1. This solution is globally optimal because it has zero cost, i.e. $J = 0 \Leftrightarrow \mathbf{u} = \mathbf{0}$. The trajectories show that each of the two spacecraft appear to follow the same shaped halo-like orbit about L2, but parallel along the path, maintaining the tolerances on the specified separation distance as shown in Fig. 5.2. The relative orbit, i.e. the orbit of one of the spacecraft relative to the other, is shown in Fig. 5.3. The optimal controls are all zero at each node as shown in Fig. 5.4. The plots for the other thrusters are similar.

The claim of optimality is based on several tests[15]. One of these tests is the

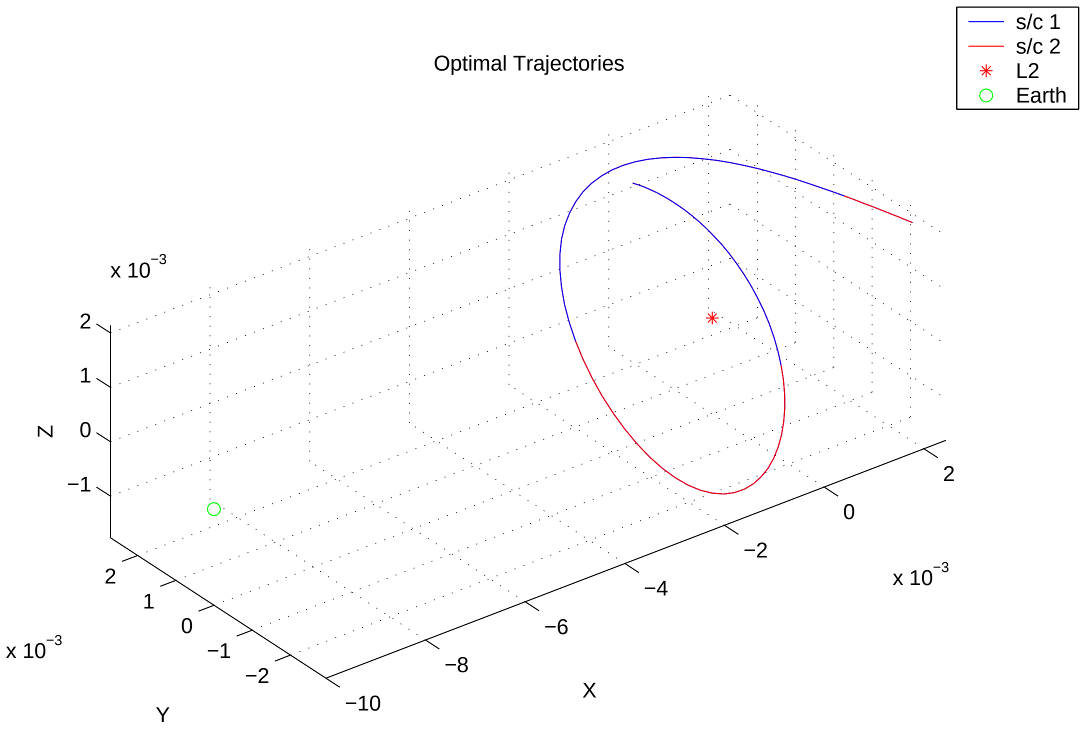

FIGURE 5.1 *Trajectories for a two-agent DSS*

approximate constancy of the Hamiltonian with an average value equal to zero.[13] The non-zero values of the Hamiltonian for this example are trivially small as shown in Fig. 5.5. In order to practically demonstrate the convergence of the solution, we use the optimal initial conditions (in DU and DU/TU),

$$\begin{aligned} x^1(t_0) &= -0.43 \times 10^{-3}, & v_x^1(t_0) &= 2.00 \times 10^{-3} \\ y^1(t_0) &= 1.52 \times 10^{-3}, & v_y^1(t_0) &= -4.30 \times 10^{-3} \\ z^1(t_0) &= 1.93 \times 10^{-3}, & v_z^1(t_0) &= -0.15 \times 10^{-3} \end{aligned}$$

($\mathbf{x}^2(t_0)$ is the required $1 \times 10^{-7} DU$ away in position, and has similarly small differences in velocity) to propagate the solutions using ode45 in Matlab. Fig. 5.6 shows a comparison of the optimized states to the propagated states of one of the spacecraft. It is apparent that the propagated states track fairly well to the optimized ones indicating that the 100 node solution is a good solution over this time period for preliminary design considerations. The timestep at which the solution diverges from the propagated

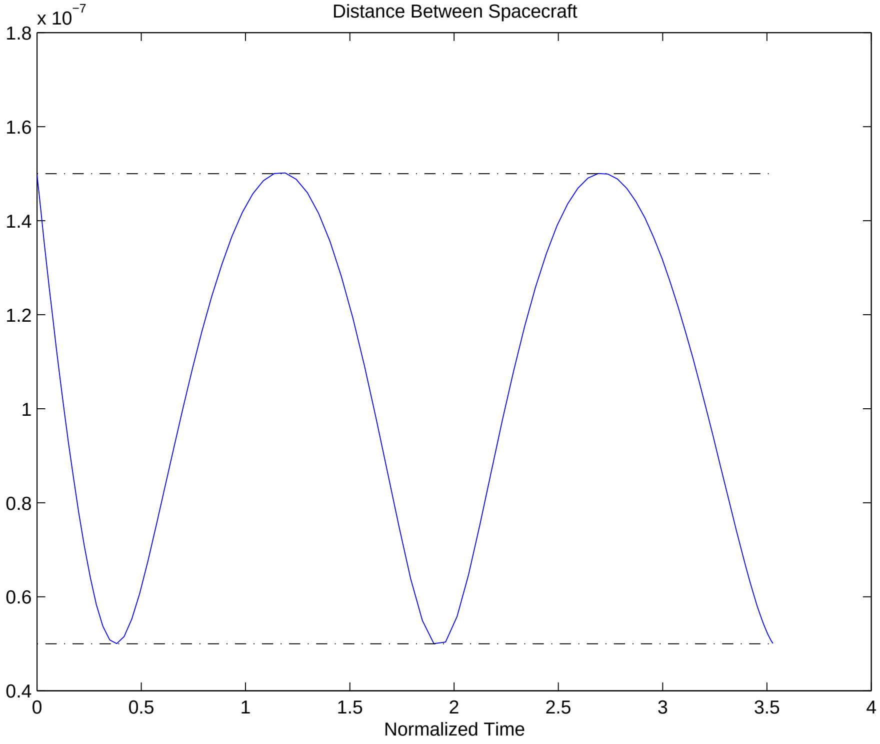

FIGURE 5.2 *Separation between the two spacecraft over time*

trajectory increases proportionally to the number of nodes.

Example 2

Having obtained a zero-cost solution in Example 1, we now consider the same problem with the addition of periodicity constraints. As explained in Sec. II, perodicity in the states is imposed under a free horizon, t_f; thus, we now have,

$$c_2^{i,j} = 1 \times 10^{-7}\ DU \quad \text{for } i \neq j \tag{5.25}$$

$$\delta_2^{i,j} = 5 \times 10^{-6}\ DU \quad \text{for } i \neq j \tag{5.26}$$

$$u_{max}^i = 0.001\ DU/TU^2\ \forall\ i \tag{5.27}$$

$$J_i = J_k \quad \forall\ i,k \tag{5.28}$$

$$\mathbf{x}^i(t_0) = \mathbf{x}^i(t_f) \quad \text{for} \quad i = 1. \tag{5.29}$$

The input states and controls for this example were the optimal states and controls of the first example. The initial state of the solution was again bound to a box of

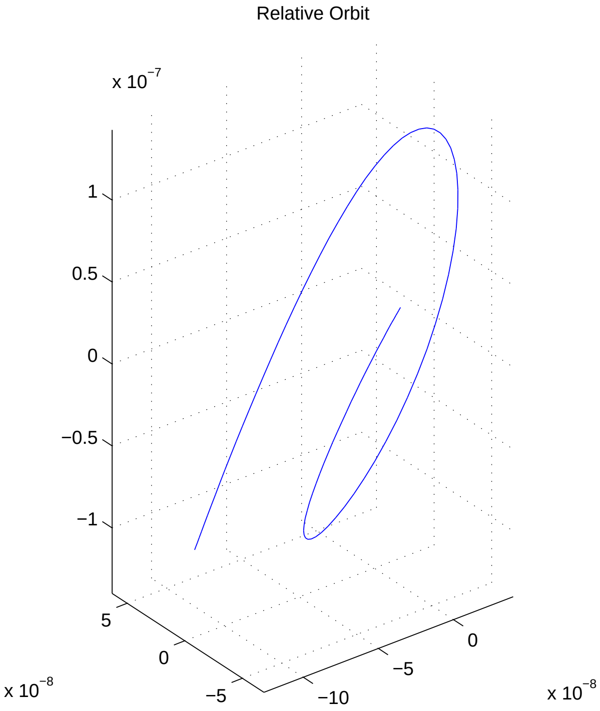

FIGURE 5.3 *Relative orbit for the two-agent DSS*

0.001 *DU* on either side, but only the positions were bound so that the initial velocities were totally free variables. This input trajectory is shown along with the optimal trajectories in Fig. 5.8, which is a zoomed in and stetched view of Fig. 5.7 Nevertheless, the trajectory plots illustrate that the solution to this problem is substantially different from that of Example 1. To properly illustrate the shape of this orbit, the trajectory in y-z plane is plotted in Fig. 5.9 with y-axis stretched appropriately. The optimal period, t_f, for this design configuration was 3.18 TU, or 185 days. This solution is also globally optimal because $J \approx 0$. That $\mathbf{u}$ is almost zero (well within numerical tolerances) is shown in Fig. 5.10 for one of the thrusters. The plots for the other thrusters are similar.

The trajectories show that each of the two spacecraft appear to follow the same orbit about L2, but parallel along the path, maintaining the tolerances on the specified separation distance as shown in Fig. 5.11. The relative orbit is shown in Fig. 5.12. A clearer picture of the satisfaction of the periodicity constraints is illustrated in Fig.s 5.13 and 5.14. The circles in Fig. 5.13 are the initial and final (x, y, z). In Fig. 5.14 they mark the initial and final (v_x, v_y, v_z). The velocity plot shows only the data for spacecraft one for clarity. Of course, $\mathbf{x}^i(t_0)$ does not exactly equal $\mathbf{x}^i(t_f)$, but the differences are all around 1×10^{-7} DU, with the largest difference occurring in the z velocities of 2×10^{-6} DU. These are physically small enough compared to the orbital dimension of about

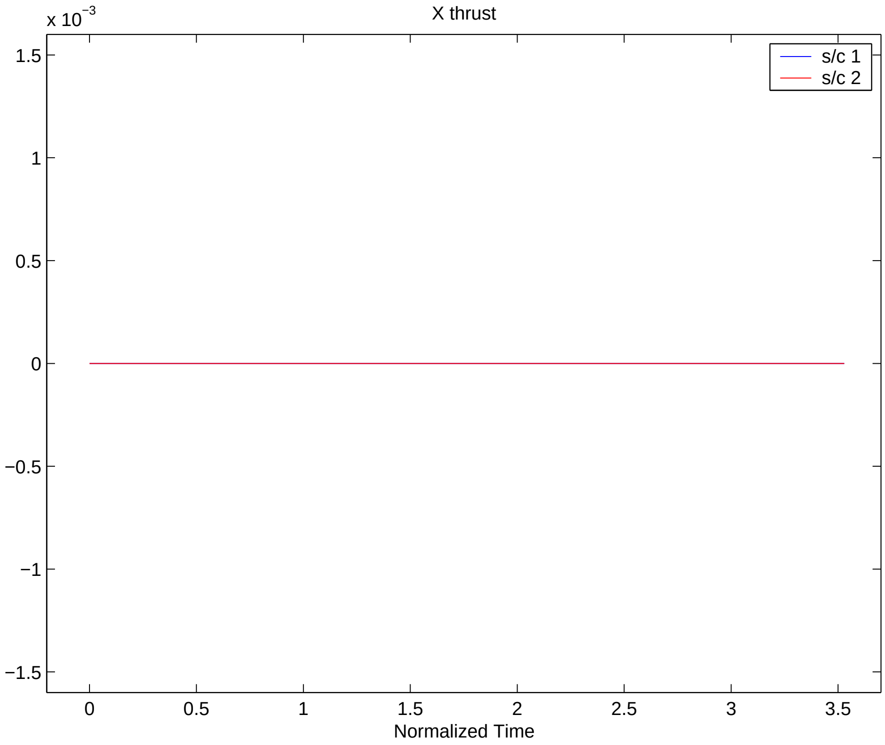

FIGURE 5.4 *Thrust along the x axis for the two-agent DSS*

0.002 DU to confirm that the set feasibility tolerances for the optimization algorithm make sense.

The Hamiltonian plot in Fig. 5.15 shows that this is an optimal solution because of its average value of zero.

We demonstrate the convergence of this large-baseline solution by propagating a trajectory from the optimal initial conditions (in DU and DU/TU),

$$\begin{aligned} x^1(t_0) &= -0.78 \times 10^{-3}, & v_x^1(t_0) &= 0.23 \times 10^{-3} \\ y^1(t_0) &= 0.03 \times 10^{-3}, & v_y^1(t_0) &= 0.05 \times 10^{-3} \\ z^1(t_0) &= 1.86 \times 10^{-3}, & v_z^1(t_0) &= -2.53 \times 10^{-3} \end{aligned}$$

($\mathbf{x}^2(t_0)$ is the required $1 \times 10^{-7} DU$ away in position, and has similarly small differences in velocity), using ode45 in Matlab. Fig. 5.16 shows a comparison of the optimized states to the propagated states of one of the spacecraft. It is apparent that the propagated states track fairly well to the optimized ones indicated that the 100 node solution is a

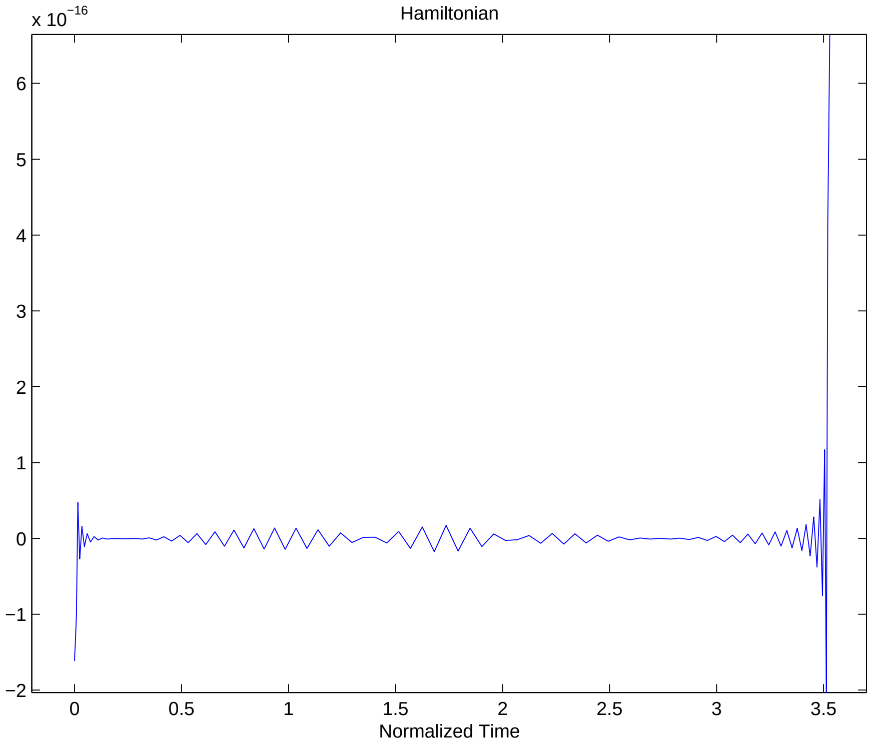

FIGURE 5.5 *Evolution of the Hamiltonian for the two-agent DSS; note the scale on the ordinate*

good solution for preliminary design considerations.

Example 3

In this example, we are looking for a large baseline formation, with spacecraft spread out over the libration point orbital space. This kind of formation would be used for the constellation type of mission, like the Solar Wind Satellite mentioned in Section I. Thus we want a separation of about one third to one half of the 'diameter' of the orbit, which from previous experiments with orbits found using the same input is about .005 DU; around 750,000 km. The nominal values of the design parameters for the third example are,

$$c_2^{i,j} = 0.002 \; DU \quad \text{for } i \neq j \tag{5.30}$$

$$\delta_2^{i,j} = 0.0015 \; DU \quad \text{for } i \neq j \tag{5.31}$$

$$u_{max}^i = 0.001 \; DU/TU^2 \; \forall \; i. \tag{5.32}$$

The input states and controls are those of the first example, a propagation and maneuver schedule starting from the same initial state. The horizon, t_f was fixed then at 3.5 TU

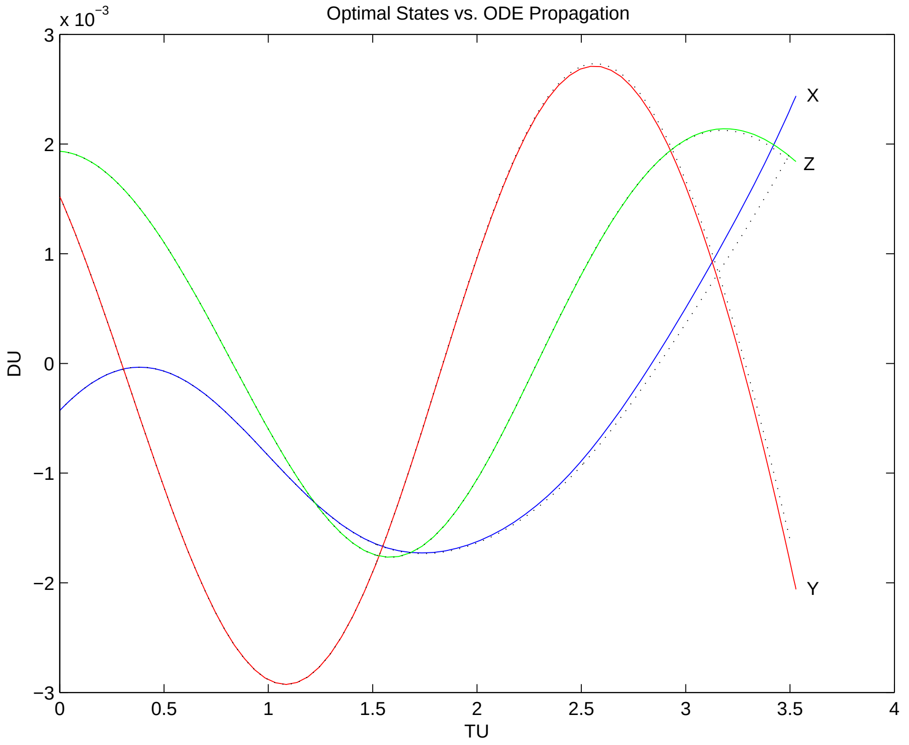

FIGURE 5.6 *Comparison of the position states of spacecraft one (solid) to those propagated by ODE45 in Matlab (dotted)*

. No periodicity constraints were imposed, and the initial states were all free with no bounds, however there were bounds on the positions of $\pm 5 \times 10^{-3}$, which was an active constraint at a few time steps for the x coordinate.

A solution to the problem for the choice of parameters listed above is shown in Fig. 5.17. This solution again is globally optimal because it has zero cost, i.e. $J = 0 \Leftrightarrow \mathbf{u} = \mathbf{0}$. The trajectories show that each of the two spacecraft appear to follow distinct halo-like orbits about L2 maintaining the tolerances on the specified separation distance as shown in Fig. 5.19. The relative orbit, i.e. the orbit of one of the spacecraft relative to the other, is more illustrative of the configuration and is shown in Fig. 5.20.

The Hamiltonian plot in Fig. 5.21 shows that this is an optimal solution because of its average value of zero. We demonstrate the convergence of this large-baseline solution

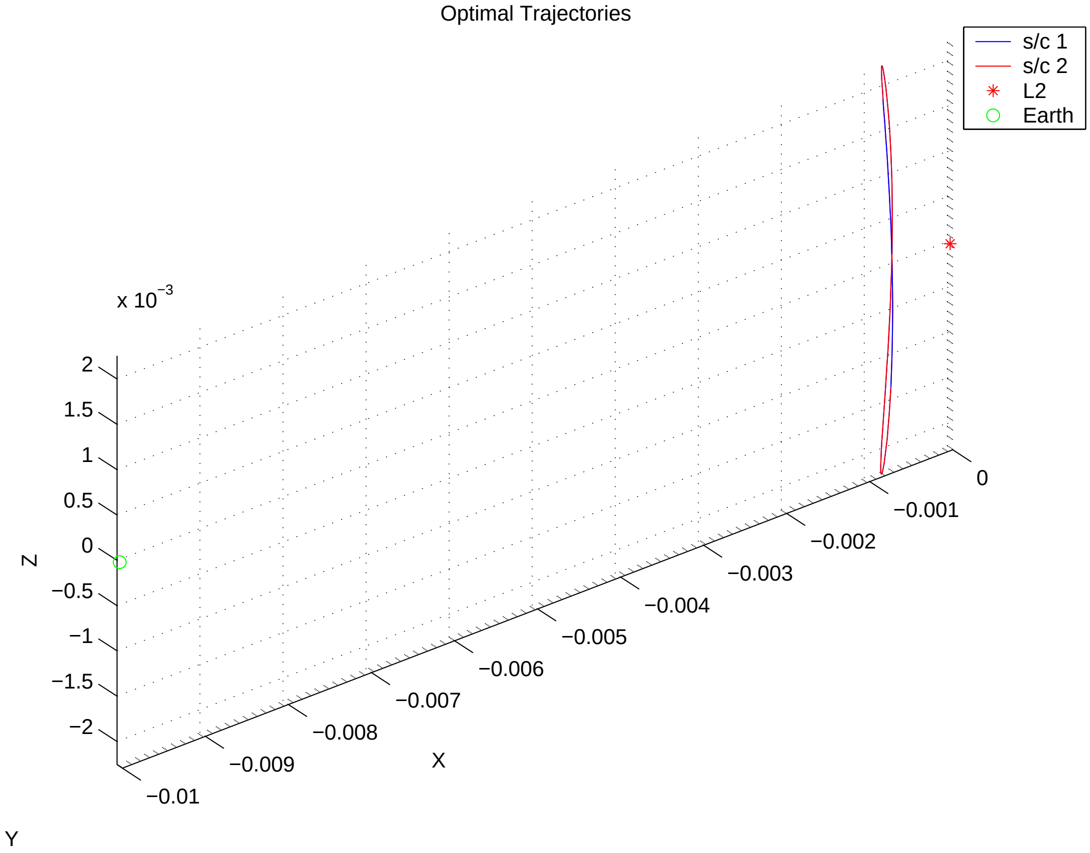

Figure 5.7 *Trajectories for a two-agent DSS with periodicity constraints*

by propagating a trajectory from the optimal initial conditions (in DU and DU/TU),

$$
\begin{aligned}
x^1(t_0) &= -5.00 \times 10^{-3}, & x^2(t_0) &= -3.94 \times 10^{-3}\\
y^1(t_0) &= 1.94 \times 10^{-3}, & y^2(t_0) &= 0.71 \times 10^{-3}\\
z^1(t_0) &= 2.72 \times 10^{-3}, & z^2(t_0) &= 2.09 \times 10^{-3}\\
v_x^1(t_0) &= 12.74 \times 10^{-3}, & v_x^2(t_0) &= 10.55 \times 10^{-3}\\
v_y^1(t_0) &= 3.50 \times 10^{-3}, & v_y^2(t_0) &= -2.30 \times 10^{-3}\\
v_z^1(t_0) &= 7.88 \times 10^{-3}, & v_z^2(t_0) &= 10.54 \times 10^{-3}
\end{aligned}
$$

(note $\mathbf{x}^2(t_0)$ is the required distance away from $\mathbf{x}^1(t_0)$ of 0.002) using ode45 in Matlab. Fig. 5.22 shows a comparison of the optimized states to the propagated states of one of the spacecraft. It is apparent that the propagated states track fairly well to the optimized ones indicated that the 100 node solution is a good solution for preliminary design considerations.

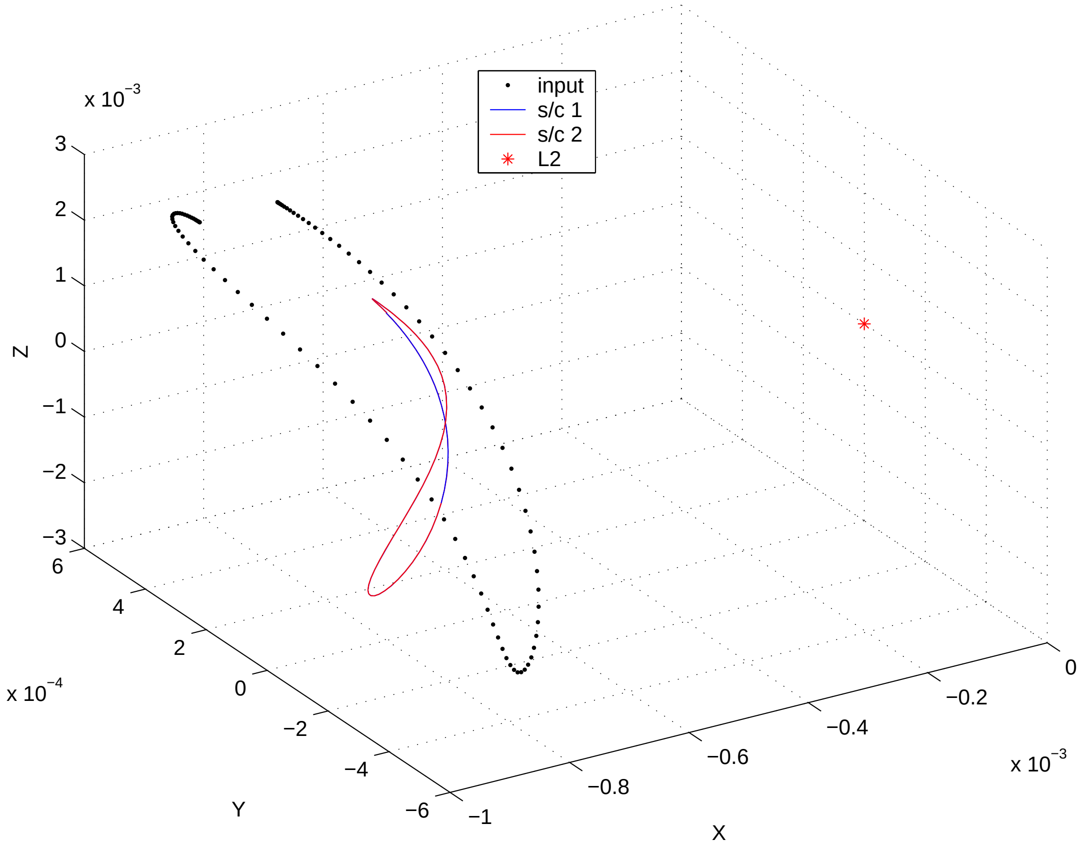

FIGURE 5.8 *Input and Optimal Trajectories for a two-agent DSS with periodicity constraints. NOT TO SCALE: stretched to show orbit shape*

5.4 Framework for Spacecraft Formations

Because there is no linearization in this framework, we can use the same technique and inputs for both small and large baseline formations, and find globally optimal (zero-cost) solutions for both with entirely different trajectories. We can limit our results as needed to find specific types of formations by including different constraints (e.g. periodic conditions). This framework has this flexibility in applications with a simple consistent problem formation process because the design and control are approached concurrently.

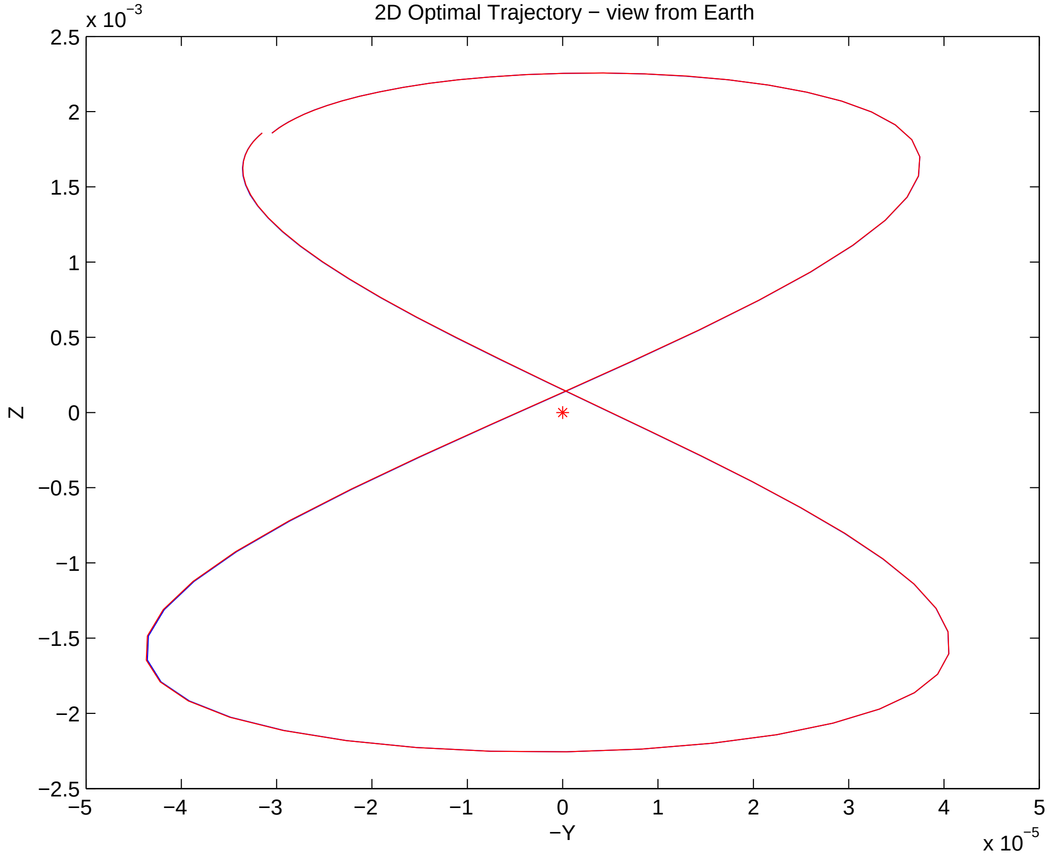

FIGURE 5.9 *Trajectories on the y-z plane for a two-agent DSS with periodicity constraints. NOT TO SCALE: stretched along the y axis*

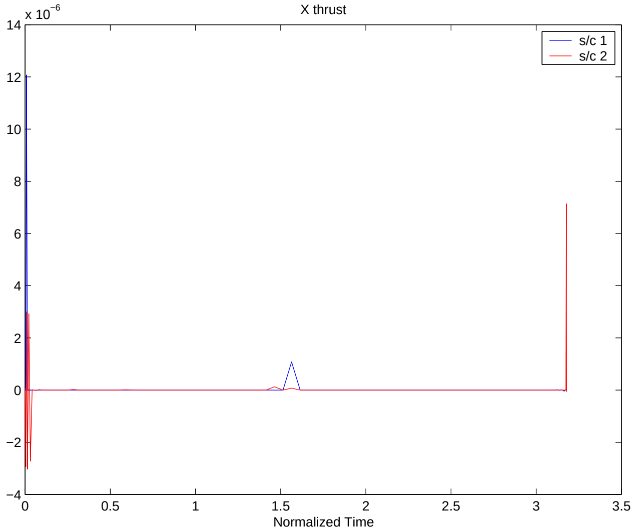

FIGURE 5.10 *Thrust along the x axis for the periodic two-agent DSS.*

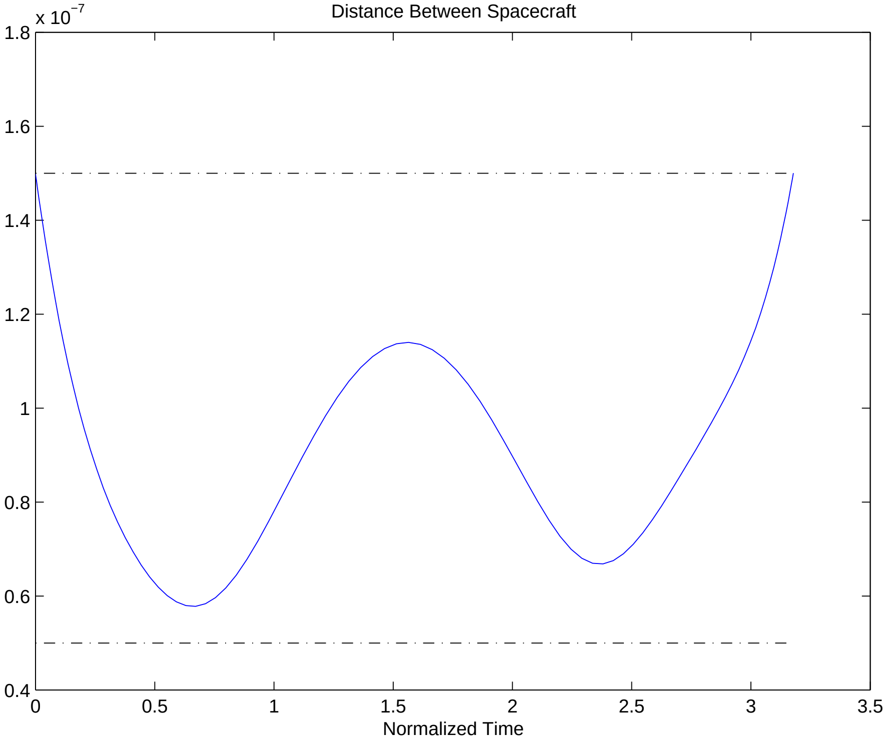

FIGURE 5.11 *Separation between the two spacecraft over time*

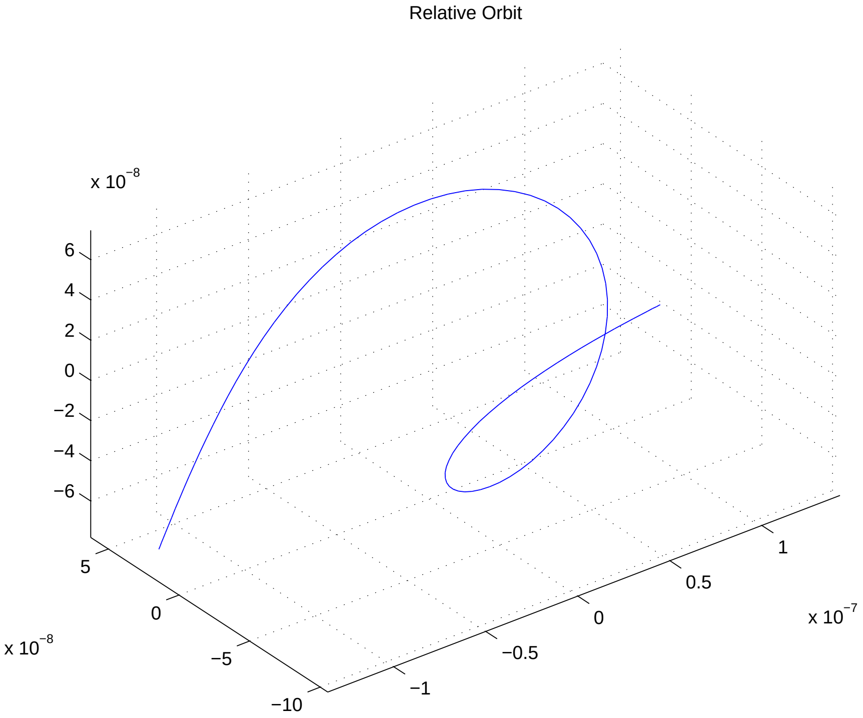

FIGURE 5.12 *Relative orbit for the periodic two-agent DSS*

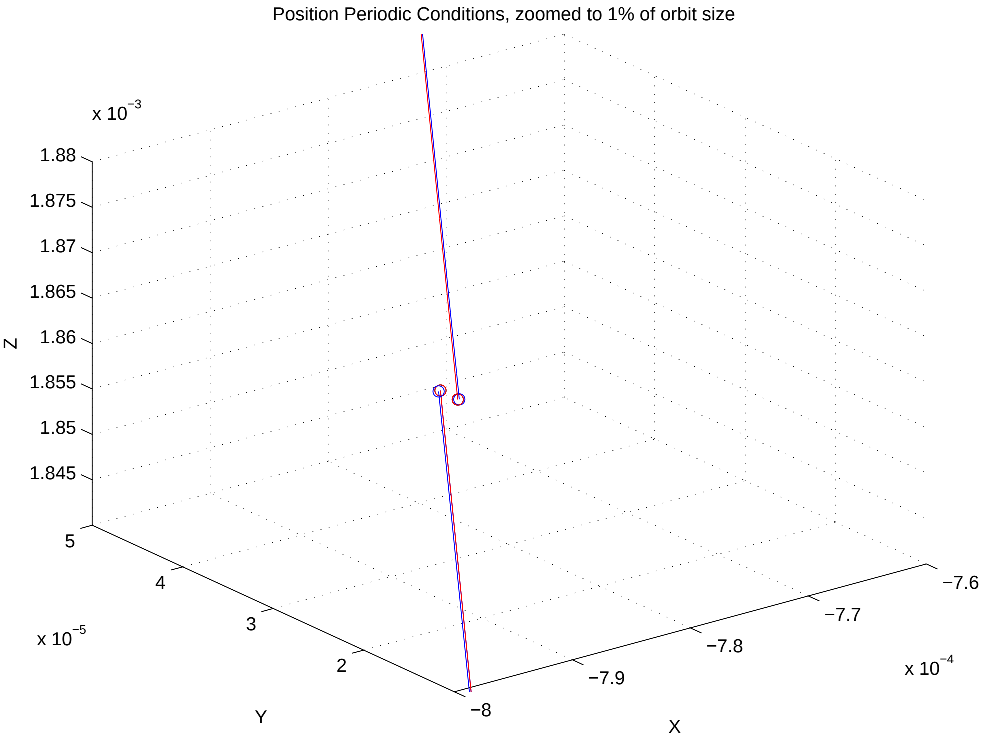

FIGURE 5.13 *The values of the position half of* $\mathbf{x}^i(t_0)$ *and* $\mathbf{x}^i(t_f)$ *for* $i = 1, 2$ *are marked with circles on this close-up view of the trajectory where it starts and ends.*

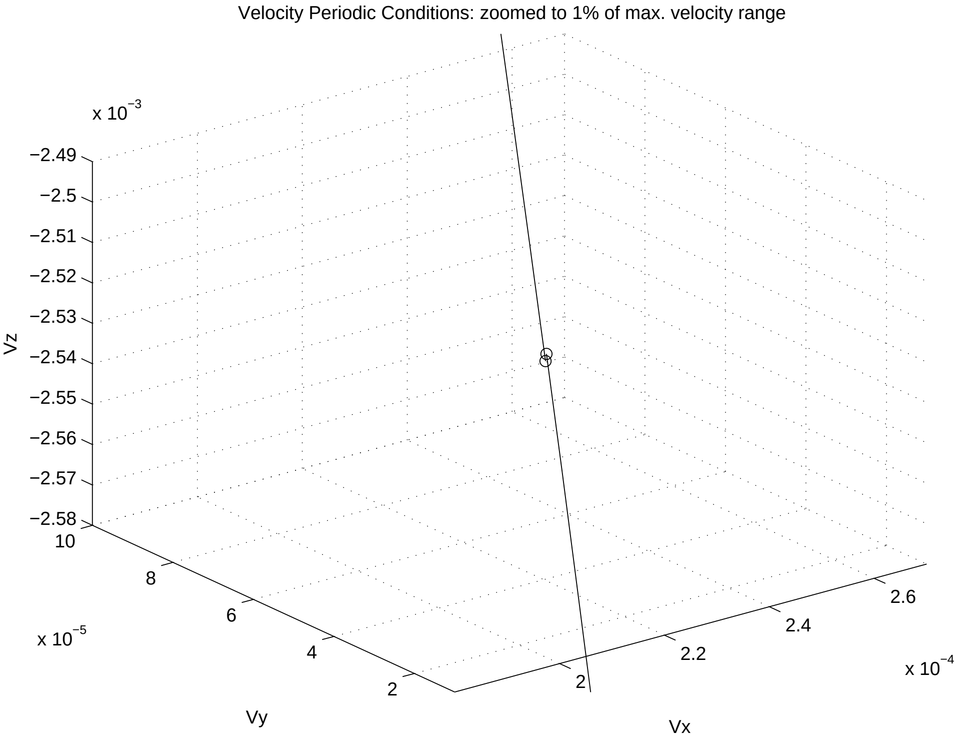

FIGURE 5.14 *The values of the velocity half* $\mathbf{x}^i(t_0)$ *and* $\mathbf{x}^i(t_f)$ *for* $i = 1$ *are marked with circles on this close-up view of the velocity trajectory start and end.*

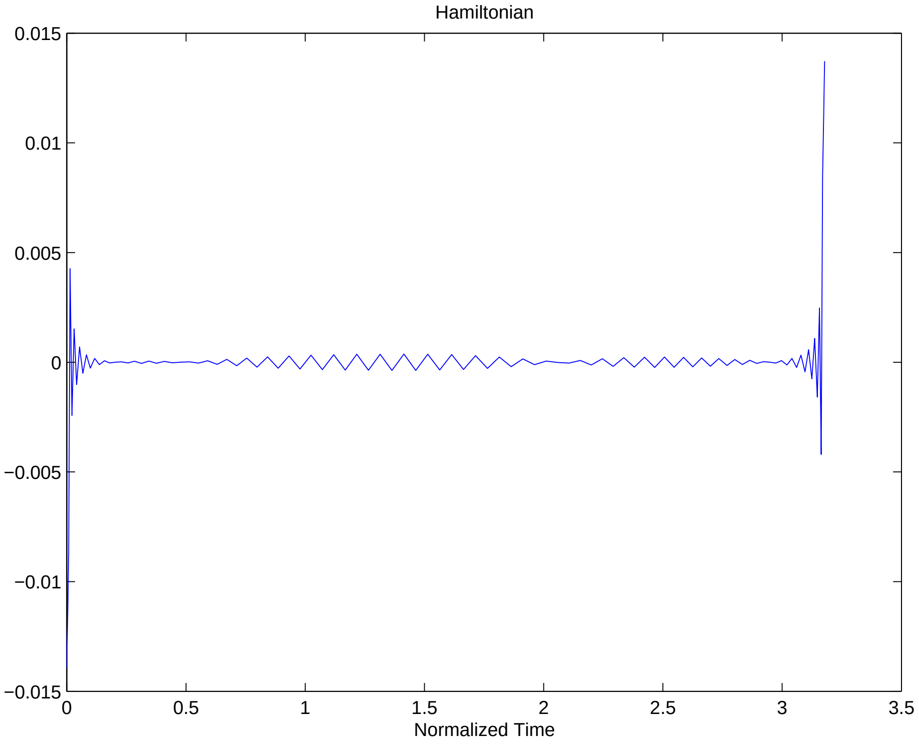

Figure 5.15 *Evolution of the Hamiltonian for the periodic two-agent DSS*

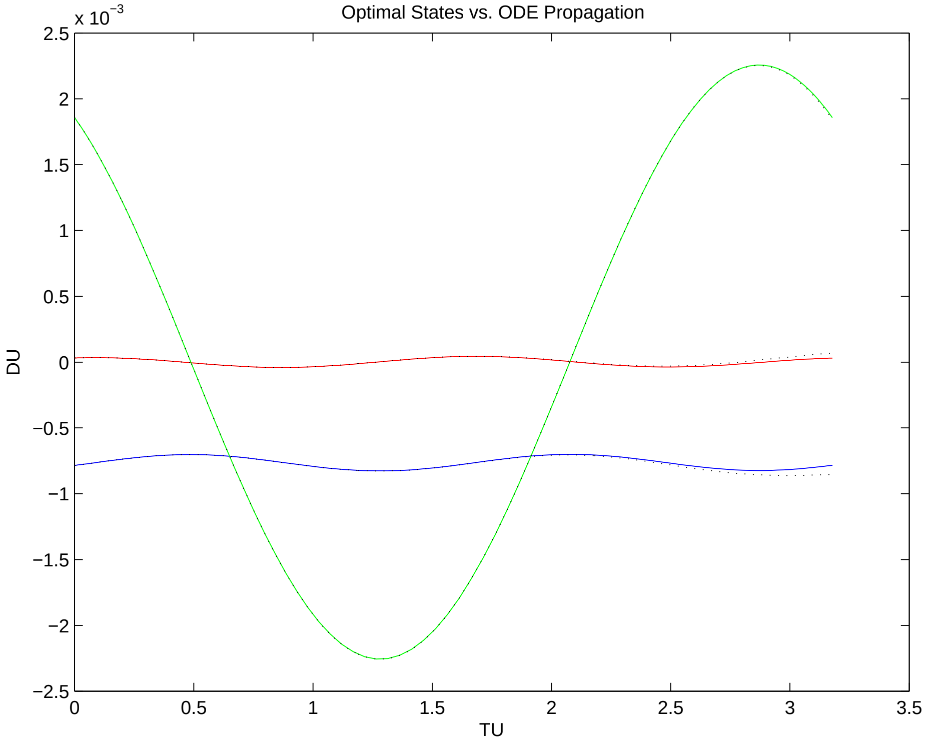

Figure 5.16 *Comparison of the position states of spacecraft one (solid) to those propagated by ODE45 in Matlab(dotted)*

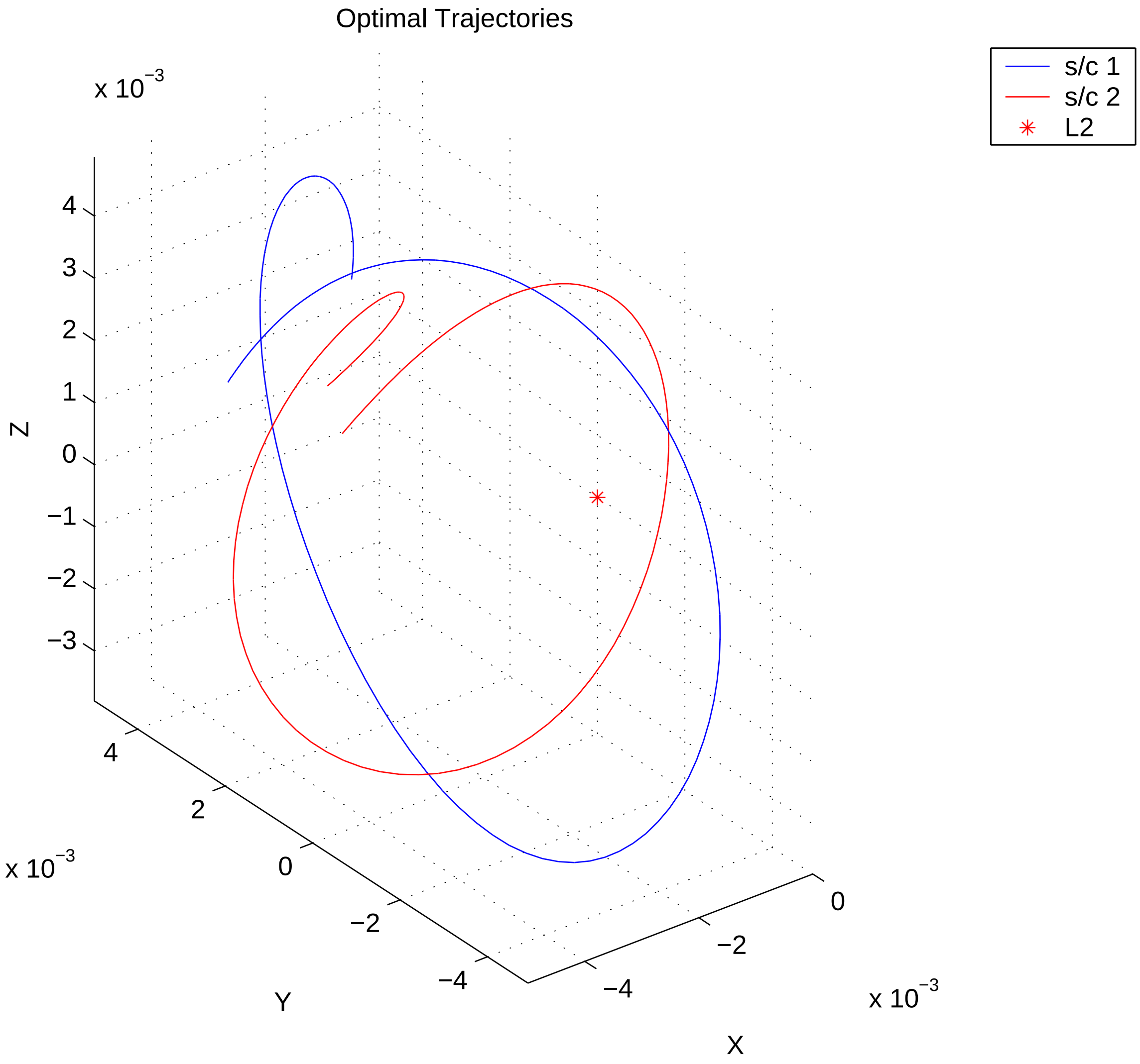

FIGURE 5.17 *Trajectories for a large-baseline two-agent DSS*

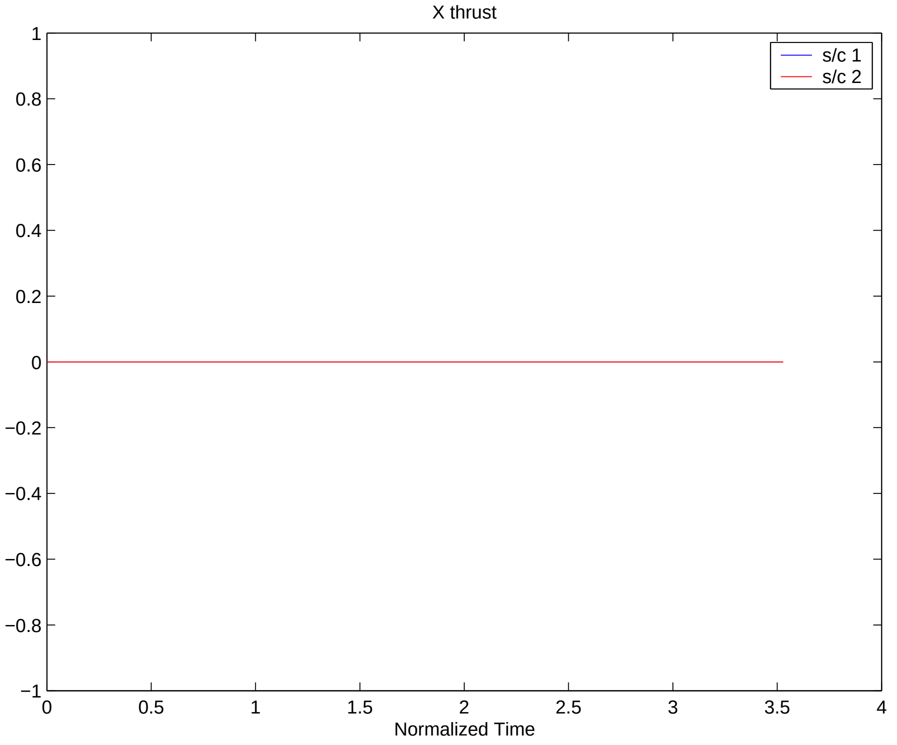

FIGURE 5.18 *Thrust along the x axis for the large-baseline two-agent DSS; note the scale on the ordinate*

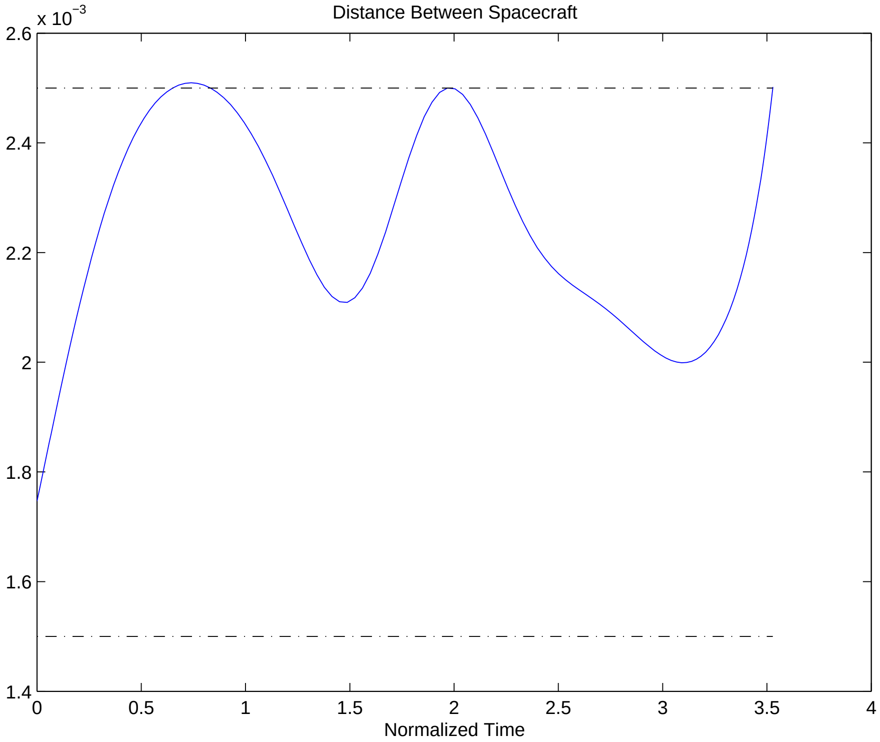

FIGURE 5.19 *Separation between the two spacecraft over time*

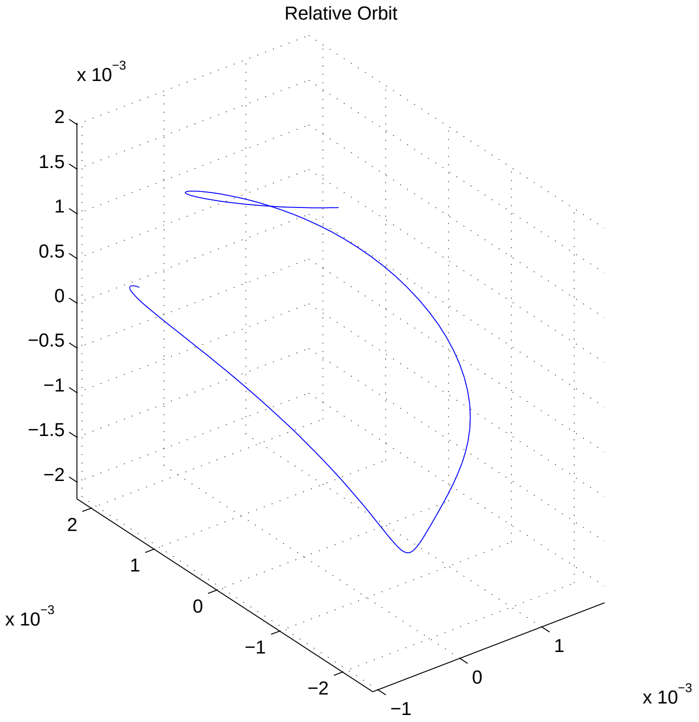

FIGURE 5.20 *Relative orbit for the large-baseline two-agent DSS*

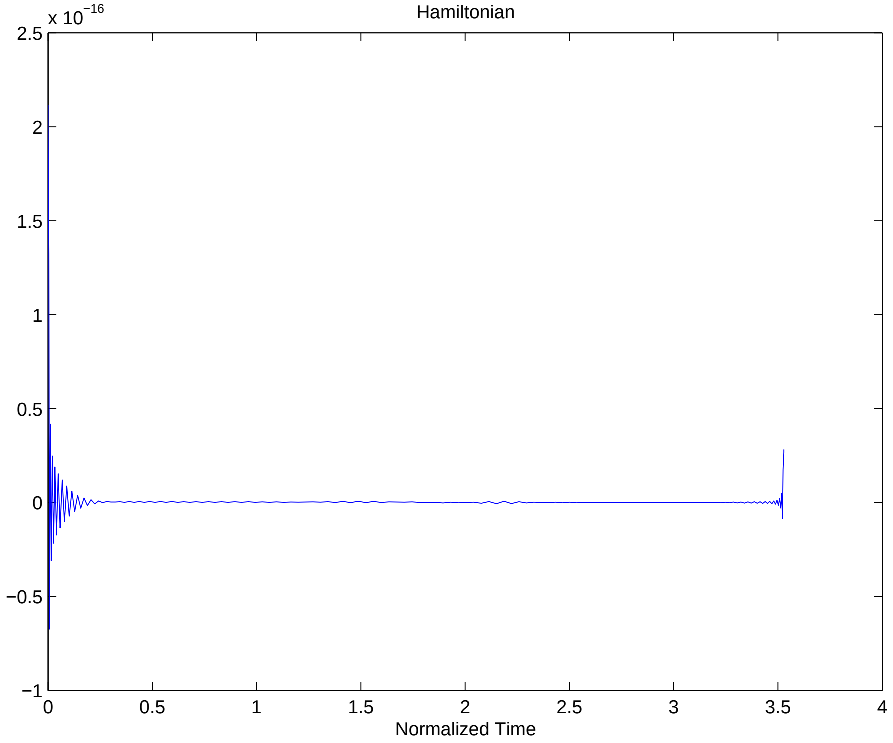

FIGURE 5.21 *Evolution of the Hamiltonian for the large-baseline two-agent DSS; note the scale on the ordinate*

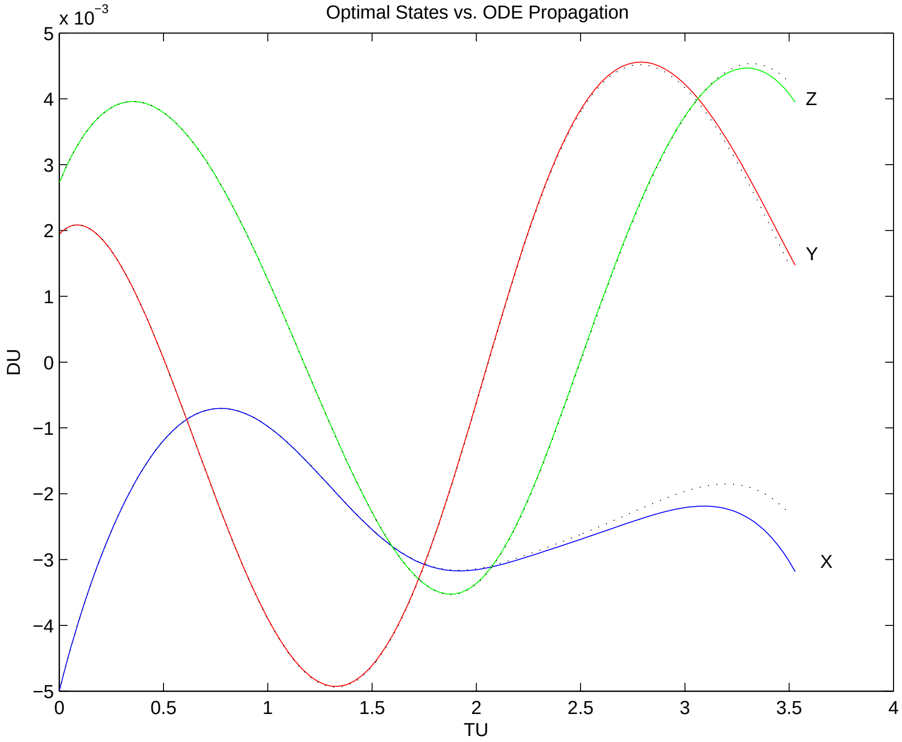

Figure 5.22 *Comparison of the position states of spacecraft one (solid) to those propagated by ODE45 in Matlab (dotted)*

Chapter 6

Conclusions and Future Work

This thesis showed that a systems engineering approach for space mission design of concurrently choosing the orbit and controls, and satisfying the mission constraints, is possible with a reasonable computation time and a relatively simple process. Changing the mission constraints, spacecraft or force models, or type of mission is also easy, and trivial to the solving of the problem. This is a flexible approach in that the search space for minimum-fuel trajectories is not confined to be close to a reference orbit. This design approach brings the more sophisticated process of concurrent engineering to entire mission design. By incorporating optimization from the beginning of the design process we will find total designs with lower fuel requirements because of the elimination of unnecessary assumptions about the orbit or control design. Design approaches which make these assumptions do not find fuel-optimal designs (only fuel-optimal maneuvers given a set orbit).

The approach was illustrated on a libration point mission because the unstable dynamics make this a more challenging optimal control problem than Earth orbit or interplanetary trajectory missions. Future missions at libration points will carry more complicated and sensitive spacecraft structure and on-board instruments, and consequently will require more constraints on the stationkeeping plan, as well as being more affected by solar radiation pressure (Chapter 2). This situation illustrated the strength of the single optimization problem approach as the complicated dynamics and sample constraints were easily added and only improved the performance of the optimization algorithm, due to the choice of discretization and optimization methods (Chapter 3).

Methods of optimizing mission design using existing commercial software packages work well enough for libration point mission design optimization if the design is sequential; first finding a reference trajectory that will work and then optimizing the maneuver (controls) history to maintain this given constraints and perturbations. Using the concurrent trajectory control design and open design space, the standard methods would result in a discrete problem too large computationally to be of use during a mission, and may not be solvable. For example, the collocation discretization requires a very fine grid to find an minimum-fuel mission design for a significant mission length (Section 3.1.2).

The approach presented here can be applied in the future to all types of space missions, rather than just the libration point example, to introduce the expanded optimization capability to general use in mission design. The current process could be more efficiently applied to long mission lengths by subdividing the mission timeline and having a higher level optimization problem to ensure smooth transitions between subdivisions; a bi-level optimization framework. For other types of missions, or even for a similar example, the cost functional may be differently formulated. An exponential form may allow an even larger set of constraints and inputs to result in a good solution. To apply this approach to later steps in the design process, one can replace the equations of motion that describe a simple model with a more sophisticated model, even including ephemeris data, and including error probabilities. This does not change the basic problem formulation or the ease of solving the design problem with the algorithms. Finally, the algorithms used at this time may be improved for mission design application to increase their efficiency. Possibilities include reformulating the differentiation matrix to make it full rank, and allowing user- defined first and second derivatives of the functions as part of the input of the continuous problem.

Bibliography

[1] Richard H. Battin, *An Introduction to the Mathematics and Methods of Astrodynamics*, AIAA Education Series, 1987, p.385-6.

[2] Robert W. Farquhar, "The Control and use of Libration-Point Satellites," Ph.D. Dissertation, Department of Aeronautics and Astronautics, Stanford University, Stanford, CA, July 1968.

[3] K.C. Howell and H.J. Pernicka, "Stationkeeping Method for Libration Point Trajectories," *Journal of Guidance, Control, and Dynamics*, Vol. 16, No. 1, January-February 1993, pp. 151-159.

[4] C. Sim, G. Gmez, J. Llibre, R. Martnez, and R. Rodrquez, "On the Optimal Station Keeping Control of Halo Orbits," *Acta Astronautica*, Vol. 15, No 6/7, 1987, pp. 391-397.

[5] G. Gmez, W.S. Koon, M.W. Lo, J.E. Marsden, J. Masdemont, and S.D. Ross, "INVARIANT MANIFOLDS, THE SPATIAL THREE-BODY PROBLEM AND SPACE MISSION DESIGN", AAS 01-301.

[6] Steven W. Evans, Editor, "NATURAL ENVIRONMENT NEAR THE SUN/EARTH-MOON L2 LIBRATION POINT", Marshall Space Flight Center.

[7] Bryson, A. and Ho, Y., *Applied Optimal Control*, Hemisphere/Wiley, 1975.

[8] Ross, I. M., King, J. T. and Fahroo, F., "Designing Optimal Spacecraft Formations," *Proceedings of the AIAA/AAS Astrodynamics Conference*, AIAA-2002-4635, Monterey, CA, 5-8 August 2002.

[9] King, J. T., "A Framework for Designing Optimal Spacecraft Formations," M. S. Thesis, Department of Aeronautical and Astronautical Engineering, Naval Postgraduate School, Monterey, CA, September 2002.

[10] Infeld, S., Josselyn, S., Murray, W., and Ross, I. M., "Design and Control of Libration Point Spacecraft Formations," *AIAA Guidance, Navigation, and Control Conference and Exhibit*, Providence, RI, August 2004. AIAA2004–4786.

[11] Bryson, Jr., A. E., *Dynamic Optimization*. Addison-Wesley, 1999.

[12] Elnagar, J., Kazemi, M. A. and Razzaghi, M., "The Pseudospectral Legendre Method for Discretizing Optimal Control Problems," *IEEE Transactions on Automatic Control,* Vol. 40, No. 10, 1995, pp. 1793-1796.

[13] Ross, I. M., and Fahroo, F., "Legendre Pseudospectral Approximations of Optimal Control Problems," *Lecture Notes in Control and Information Sciences*, Vol.295, Springer-Verlag, New York, 2003.

[14] Ross, I. M. and Fahroo, F., "Pseudospectral Knotting Methods for Solving Optimal Control Problems," *Journal of Guidance, Control and Dynamics*, Vol.27, No.3, pp.397-405, 2004.

[15] Ross, I. M. and Fahroo, F. , "User's Manual for DIDO 2002: A MATLAB Application Package for Dynamic Optimization," *NPS Technical Report, AA-02-002*, Department of Aeronautics and Astronautics, Naval Postgraduate School, Monterey, CA, June 2002.

[16] Gill, Murray, and Saunders, "SNOPT: An SQP Algorithm for Large-Scale Constrained Optimization", SIAM Journal of Optimization, Vol. 12, No. 4, pp. 979-1006.

[17] Holmström, K., Göran, A. O. and Edvall, M. M., "User's Guide for Tomlab 4.0.6," Tomlab Optimization, Sweden, August 2003. http://www.tomlab.biz

[18] Analytical Graphics' Satellite Tool Kit homepage http://www.stk.com

[19] Infeld, S. I. and Murray, W., "Optimization of Stationkeeping for a Libration Point Mission," *AAS Space Flight Mechanics Meeting*, Maui, HI, February 2004. AAS 04-150.

[20] Howell, K.C., B.T. Barden, and M.W. Lo, "Application of Dynamical Systems Theory to Trajectory Design for a Libration Point Mission," The Journal of Astronautical Sciences, Vol. 45, No. 2, April-June, 1997, pp.161-178.

[21] Strizzi, J. D., Kutrieb, J. M., Damphousse, P.E., Carrico, J. P., "Sun-Mars Libration Points and Mars Mission Simulations," *AAS* , 2001. AAS 01-159.

[22] Wilson, R. S., "Trajectory Design in the Sun-Earth-Moon Four Body Problem," Ph.D. Dissertation, Department of Aeronautics and Astronautics, Purdue University, West Lafayette, IN, December 1998.

[23] Folta, D. and Beckman, M., "Libration Orbit Mission Design: Applications Of Numerical And Dynamical Methods," *Libration Point Orbits and Applications*, Girona, Spain, June 2002.

[24] D.L. Richardson and N.D. Cary, "A Uniformly Valid Solution for Motion About the Interior Libration Point of the Perturbed Elliptic-Restricted Problem," *AIAA/AAS Astrodynamics Specialists Conference*, Nassau, Bahamas, July 1975. AAS 75-021.

[25] K. C. Howell and H. J. Pernicka, "Numerical Determination of Lissajous Trajectories in the Restricted Three-Body Problem," Celestial Mechanics, Vol. 41, 1988, pp. 107-124.

[26] Beckman, M., "James Webb Space Telescope Flight Dynamics Analysis Report," Flight Dynamics Analysis Branch, NASA Goddard Space Flight Center, May 2004.

[27] Barden, B. T., Wilson, R. S., Howell, K. C., and Marchand, B. G., "Summer Launch Options for the Genesis Mission,"*AAS/AIAA Astrodynamics Specialist Conference*, Quebec City, Canada, August 2001. AAS 01-306.

[28] Whiffen, G. J., "An Investigation of a Jupiter Galilean Moon Orbiter Trajectory," AAS 03-544.

[29] Ross, I. M., "How to Find Minimum-Fuel Controllers," *Proceedings of the AIAA Guidance, Navigation and Control Conference*, Providence, RI, August 2004. AIAA Paper No. 2004-5346.

[30] Williams, P., "A Comparison of Differentiation and Integration Based Direct Transcription Methods,"*AAS/AIAA Space Flight Mechanics Conference*, Copper Mountain, CO, January 2005. AAS 05-128.

[31] De Miguel, V., "The Solution of Optimal Control Problems by Discretization Methods," Qualifying Tutorial Report, Department of Engineering Economic Systems and Operations Research, Stanford University, 2000.

[32] Stanford Business Software Inc., distributor of software produced by Systems Optimization Laboratory, Stanford University, Stanford, CA and University of California at San Diego, La Jolla, CA. http://www.sbsi-sol-optimize.com/

[33] Gill, Murray, and Wright, *Practical Optimization*, Academic Press, 1986, p. 54.

[34] *GESOP – Software User Manual*, 2002, Institute of Flight Mechanics and Control, University of Stuttgart, 70550 Stuttgart, Germany. http://gesop.de

[35] I. M. Ross and F. Fahroo, "Legendre Pseudospectral Approximations of Optimal Control Problems," *Lecture Notes in Control and Information Sciences, Springer-Verlag*, 2003.

[36] *New World Vistas*, Summary Volume, USAF Scientific Advisory Board, December 1995.

[37] Vincent, M. A. and Bender, P. L., "The Orbital Mechanics of a Space-Borne Gravitational Wave Experiment," *Advances in the Astronautical Sciences, Astrodynamics*, 1987, Vol. 65, Part II, Pg. 1346. Edited by Soldner, J.K. et al. Paper AAS 87-523. Full paper in AAS Microfiche Series, Vol.55.

[38] Ross, I. M., "A Mechanism for Precision Orbit Control With Applications to Formation Keeping," *Journal of Guidance, Control and Dynamics*, Vol.25, No. 4, 2002, pp. 818-820.

[39] Carpenter, R. J., Leitner, J. A., Folta, D. C. and Burns, R. D., "Benchmark Problems for Spacecraft Formation Flying Missions," *Proceedings of the AIAA Guidance, Navigation and Control Conference*, Austin, TX, August 2003, AIAA 2003-5364.

[40] Lindensmith, C. A., editor, "Technology Plan for the Terrestrial Planet Finder ", *JPL Publication 03-007*, 2003

[41] Fridlund, C.V.M., "Darwin - The Infrared Space Interferometry Mission," *ESA Bulletin*, 01 Aug 2000, Vol. 103, pp. 20-25

[42] Constellation X homepage http://constellation.gsfc.nasa.gov/

[43] National Security Space Road Map http://www.wslfweb.org/docs/roadmap/spacroad.htm

[44] Marchand, B. G. and Howell, K. C., "Formation Flight Near L_1 and L_2 in the Sun-Earth/Moon Epheremis System Including Solar Radiation Pressure," *AAS/AIAA Astrodynamics Specialist Conference*, Big Sky, MT, August 2003. AAS 03-596.

[45] Hsiao, F. Y. and Scheeres, D. J., "Design of Spacecraft Formation Orbits Relative to a Stabilized Trajectory," AAS 03-175.

[46] Hamilton, N. H., Folta, D. and Carpenter, R., "Formation Flying Satellite Control Around the L2 Sun-Earth Libration Point," *AIAA/AAS Astrodynamics Specialist Conference*, Monterey, CA, August 2002, AIAA 2002-4528.

[47] Gurfil, P. and Kasdin, N. J., "Dynamics and Control of Relative Motion in an Unstable Orbit," *AIAA/AAS Astrodynamics Conference*, Denver, CO, August 2000, AIAA 2000-4135.

[48] Gomez, G. Masdeont, J. and Simo, C., "Quasihalo Orbits Associated with Libration Points," *Journal of the Astronautical Sciences*, Vol.46, 1998, pp.135-176.

[49] Kim, M. and Hall, C. D., "Lyapunov and Halo Orbits about L_2," AAS 01-324.

[50] Richardson, D. L., "Analytic Construction of Periodic Orbits About the Collinear Points," *Celestial Mechanics*, Vol. 22, 1980, pp. 241253.

[51] Junge, O., Levenhagen, J. Seifried, A. and Dellnitz, M., "Identification of Halo Orbits for Energy Efficient Formation Flying," *Proceedings of the International Symposium on Formation Flying*, Toulouse, France, 2002.

[52] Serban, R., Koon, W. S., Lo, M. Marsden, J. E., Petzold, L. R., Ross, S. D. and Wilson, R. S., "Halo Orbit Mission Correction Maneuvers Using Optimal Control," *Automatica*, **38**, 2002, pp.571-583.

[53] Canuto, C., Hussaini, M. Y., Quarteroni, A., and Zang, T.A., *Spectral Methods in Fluid Dynamics,* Springer Verlag, New York, 1988.

[54] Betts, J. T., *Practical Methods for Optimal Control Using Nonlinear Programming,* SIAM: Advances in Control and Design Series, Philadelphia, PA, 2001.

[55] Boggs, P. T. and Tolle, J. W., "Sequential Quadratic Programming," *Acta Numerica*, 1995, Cambridge University Press, Cambridge, UK, 1995, pp. 151.

[56] Ross, I. M., and Fahroo, F., "A Perspective on Methods for Trajectory Optimization," *Proceedings of the AIAA/AAS Astrodynamics Conference*, Monterey, CA, August 2002. AIAA Paper No. 2002-4727.

[57] Lo, M., B. G. Williams, W. E. Bollman, D. Han, Y. Hahn, J. L. Bell, E. A. Hirst, R. A. Corwin, P. E. Hong, K. C. Howell, B. Barden, and R. Wilson, "Genesis Mission Design," Paper No. AIAA 98-4468.

[58] Fischer, A., "Structure of Fourier Exponents of Almost Periodic Functions and Periodicity of Almost Periodic Functions," *Mathematical Bohemica*, No. 3, 1996, pp. 249-262.

[59] Corduneanu, C., *Almost Periodic Functions*, John Wiley, New York, 1968.

[60] Ross, I. M., Yan, H. and Fahroo, F., "A Curiously Outlandish Problem in Orbital Mechanics," *AAS/AIAA Astrodynamics Specialist Conference*, Quebec City, Canada, July 2001, AAS-01-430.

[61] Labeyrie, A., Le Coroller, H., Dejonghe, J. , Martinache, F., Borkowski, V., Lardire, O., Koechlin, L., "Hypertelescope imaging: from exo-planets to neutron stars," *Proceedings of SPIE conference*, vol. 4852, Hawaii, 2002.

[62] Carlson, B., Pernicka, H., and Balakrishnan, S., "Spacecraft Formation Flight About Libration Points," AIAA-2004-4737.

[63] Pernicka, H., Carlson, B., and Balakrishnan, S., "Discrete Maneuver Formation-keeping at Libration Points L1 and L2," *AAS/AIAA Spaceflight Mechanics Conference*, Copper Mountain, CO, January 2005. AAS 05-194.

[64] McLoughlin, T. and Campbell, M., "Hybrid Leader Follower and Sensor Scheduling for Large Spacecraft Networks," AIAA-2004-5022.

[65] Howell, K.C. and Marchand, B.G., "Design and Control of Formations Near the Libration Points of the Sun-Earth/Moon Ephemeris System," *GSFC Flight Mechanics Symposium*, Greenbelt, MD, October 2003.

[66] Marchand, B.G. and Howell, K.C., "Aspherical Formations near the Libration Points in the Sun-Earth/Moon Ephemeris System," *AAS/AIAA Space Flight Mechanics Meeting*, Maui, HI, February 2004. AAS 04-157.

[67] Folta, D., Hartman, K., Howell, K., Marchand, B., "Formation Control of the MAXIM L2 Libration Orbit Mission," *AIAA/AAS Astrodynamics Specialist Conference*, Providence, RI, August 2004.

[68] Howell, K.C. and Marchand, B.G., "Formations Near the Libration points: Design Strategies Using Natural and Non-Natural Arcs," *GSFC 2nd International Symposium on Formation Flying Missions and Technologies*, Greenbelt, MD, September 2004.

[69] Hussein, I.I., Scheeres, D.J., and Hyland, D.C., "Optimal Formation Control for Imaging and Fuel Usage," *AAS/AIAA Spaceflight Mechanics Conference*, Copper Mountain, CO, January 2005. AAS 05-160.

[70] Luquette, R., J., and Sanner, R. M., "A non-linear approach to spacecraft formation control in the vicinity of a collinear libration point," *AAS/AIAA Astrodynamics Specialist Conference*, Quebec City, Canada, August 2001. AAS 01-330.

[71] Gurfil, P., and Kasdin, N.J., "Dynamics and Controls of Spacecraft Formation Flying in Three-Body Trajectories", *AIAA Guidance Navigation, and Control Conference and Exhibit*, Montreal, Canada, August 2001, AIAA-2001-4026

[72] Gurfil, P., Idan, M., and Kasdin, N. J., "Adaptive neural control of deep-space formation flying," *American Control Conference*, Anchorage, AK, May 2002

[73] Li, H. and Williams, T., "Formationkeeping for Sun-Earth Libration Point Formations by Using Solar Radiation Pressure," *AAS/AIAA Spaceflight Mechanics Conference*, Copper Mountain, CO, January 2005. AAS 05-195.

[74] Bryson, A. E. and Ho, Y.-C., *Applied Optimal Control*, Hemisphere Publishing Corporation, Chapter 7, 1975.

[75] Gong, Q., Ross, I. M., Kang, W., and Fahroo, F., "Convergence of Pseudospectral Methods for Constrained Nonlinear Optimal Control Problems," *Intelligent Systems and Control*, Series on Modelling, Identification and Control, Acta Press, Calgary, Canada, 2004.

[76] Strizzi, J. Ross, I. M and Fahroo, F., "Towards real-time computation of optimal controls for nonlinear systems," *Proceedings of the AIAA Guidance, Navigation, and Control Conference,* Monterey, CA, August 2002, AIAA Paper No. 2002-4945.